Assembly of Membrane-deforming Objects in Tubular and Vesicular Membranes Theory and Simulations

Vahid Belarghou, Afshin

DOI
10.4233/uuid:e6df2051-7db1-4316-9867-c800be313c13

Publication date
2018

Document Version
Final published version

Citation (APA)
Vahid Belarghou, A. (2018). *Assembly of Membrane-deforming Objects in Tubular and Vesicular Membranes: Theory and Simulations*. [Dissertation (TU Delft), Delft University of Technology]. https://doi.org/10.4233/uuid:e6df2051-7db1-4316-9867-c800be313c13

Assembly of Membrane-deforming Objects in Tubular and Vesicular Membranes

Theory and Simulations

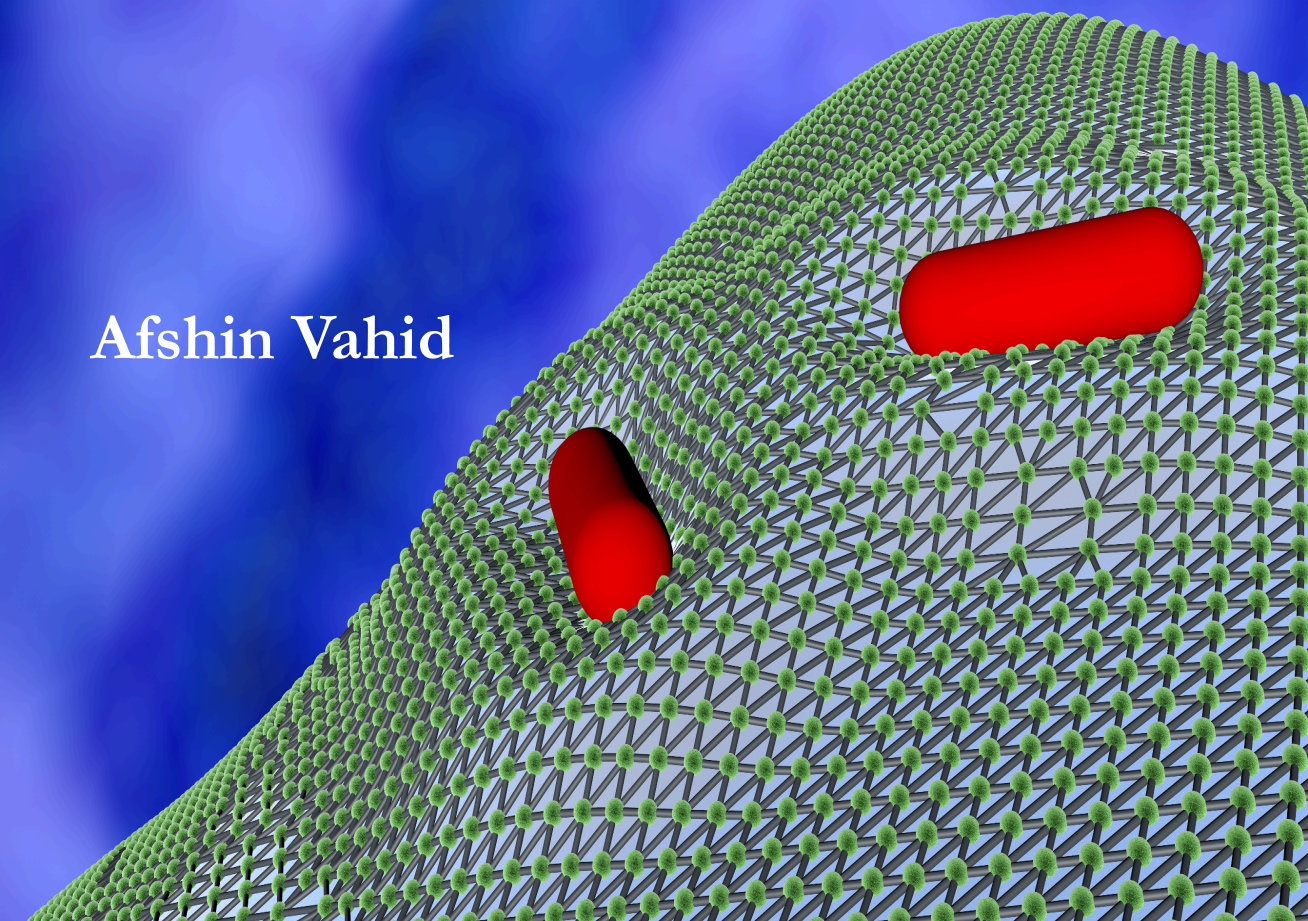

Afshin Vahid

Assembly of Membrane-deforming Objects in Tubular and Vesicular Membranes

Theory and Simulations

Assembly of Membrane-deforming Objects in Tubular and Vesicular Membranes

Theory and Simulations

Proefschrift

ter verkrijging van de graad van doctor
aan de Technische Universiteit Delft,
op gezag van de Rector Magnificus prof.dr. ir. T.H.J.J. van der Hagen,
voorzitter van het College voor Promoties,
in het openbaar te verdedigen op
woensdag 17 oktober 2018 om 12:30 uur

door

Afshin VAHID

Master of Science in de Werktuigbouwkunde,
Sharif University of Technology, Iran
geboren te Urmia, Iran.

Dit proefschrift is goedgekeurd door de

promotor: Prof. dr. M. Dogterom
copromotor: Dr. T. Idema

Samenstelling promotiecommissie:

Rector Magnificus,	voorzitter
Prof. dr. M. Dogterom	TU Delft
Dr. T. Idema	TU Delft
Onafhankelijke leden:	
Prof. dr. C. Storm	TU Eindhoven
Prof. dr. F. H. J. Redig	TU Delft
Prof. B. Mulder	U-Wageningen
Dr. M. E. Aubin-Tam	TU Delft
Dr. A. Šarić	UC London
Prof. dr. C. Dekker	TU Delft, reserve member

Cover Image: Afshin Vahid

Printed by:

Casimir PhD series: 2018-36
ISBN: 978-90-8593-365-6

An electronic version of this dissertation is available at http://repository.tudelft.nl/.

To my beloved parents
and siblings,

Contents

1

Cellular Shapes and Curvature

Living cells are out of equilibrium systems. Cellular structures are endowed with special mechanical properties, enabling them to cope with non-equilibrium conditions. A prominent example of such structure is the lipid bilayer. Biological membranes are dynamic entities and equipped with both elastic and fluid properties. Both the plasma membrane on the outside of a cell and the many surrounding organelles inside a cell constantly remodel, forming wide range of sometimes peculiar shapes. Membranes are clearly not detached from other key machines in the cell. For example, numerous inclusions like proteins are either embedded in or bound to membranes in order to carry out diverse functions. The interaction of the plasma membrane of a cell with its internal dynamic cytoskeleton is another example. Physical principles underlie the interplay between the characteristic shape of membranes and the behavior of attached proteins and cytosekeletal filaments. Using physical and mathematical tools, we study membrane mediated interactions between both lipid associated proteins and microtubule-driven protrusions, in order to understand such phenomena in the realm of membrane biophysics.

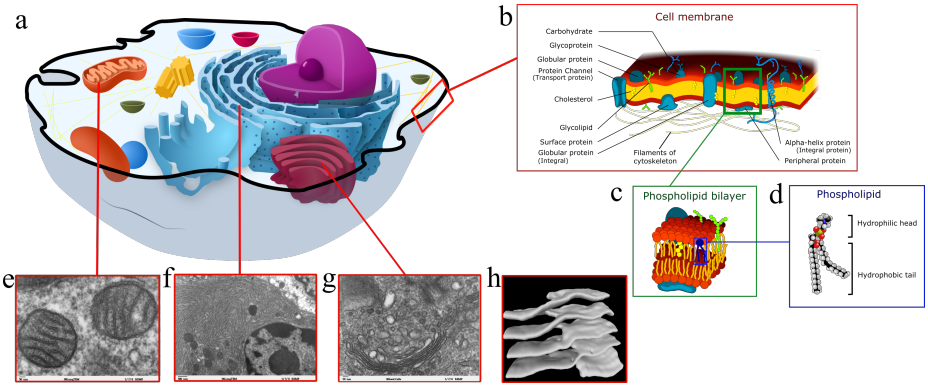

Figure 1.1: (a) Schematic shape of a cell containing membranous organelles. These membranes consist of lipid bilayers. They also host numerous inclusions like proteins. (b-d) The main building blocks of a membrane are phosphlipids with amphiphilic properties. (e-h) Many internal cellular compartments are also enclosed by membranes. These organelles constantly remodel and adapt various shapes in, for example, mitochodria (e), the endoplasmic reticulum (f and h) and the Golgi apparatus (g). Transmission electron microscope images (e-g) by Louisa Howard and Miguel Marin-Padilla, public domain. Images (a-d) and (h) are reproduced from [1, 2]

1.1. Membranes

Living cells are isolated from their external environment by a soft selective barrier called the plasma membrane (see Fig. 1.1). Lots of other organelles within the cell are also bound by their own membranes. Membranes exhibit a large variety of shapes, ranging from a simple spherical lysosome to bewildering complex structures like connected stacks of perforated membrane sheets in the Golgi apparatus to a highly branched network of tubes in the endoplasmic reticulum (ER). In the ER, for example, Terasaki et al.[1] have recently shown that the 3D structure of membrane sheets in neuronal cells and secretory salivary gland cells of mice resembles a parking garage with helical ramps connecting the different membrane levels (Fig. 1.1h). Having such structure enables the ER, the protein-making factory of a cell, to maximize the space for protein synthesis within a limited volume. In general, membranous boundaries enable a cell to maintain its integrity and host proteins to be served as gatekeepers and energy transducers.

The predominant constituents of a biological membrane are phospholipid molecules (Figs. 1.1b-d). These molecules are amphiphilic, containing both hydrophilic (polar heads) and hydrophobic (nonpolar tails) regions. As such, when immersed in an aqueous solution, depending on their shape, lipid molecules may self-organize themselves into either a mono-layer or a bilayer with the hydrocarbon chains of each layer pointing toward each other. For example, lipids that are conical form micelles and those with a cylindrical shape construct a bilayer. The hydrophobic and hydrophilic properties of lipids enable the solution to minimize the contact between hydrophobic tails and polar molecules, hence reducing the total energy of the system. This scheme of a cell envelope was depicted for the first time by Gorter and Grendel, the “pioneers” of modern membrane theories, in 1925 [3]. The model lacked any explanations for embedded proteins inside the membrane. To rectify this deficiency, pulling all the findings of more than a

decade together, Singer and Nicholson in 1972 drew a new scheme called the “fluid mosaic model” to describe the structure of a lipid bilayer [4]. Their model suggests that the cell’s membrane is a mosaic of proteins (solute) embedded in a fluid bilayer of lipids (solvent). Although the mosaic model has generally been accepted as a reasonable paradigm for the structure of cell membranes, recently it has been challenged in some aspects, hence amended models are suggested. For example, the existence of different regions of lipids that are distinct in size and composition necessitates equipping the previous model with variable patchiness, variable membrane thickness and a higher occupancy of proteins as they are of central importance in lipid-lipid and lipid-proteins interactions [5]. The flexible surface model is another alternative suggested for the mosaic model. It considers both the membrane and the collection of floating proteins as complex fluids. Resultantly, the properties and shape of the lipid bilayer can possibly govern the structure and function of the embedded proteins [6].

Membrane shape is deformed by various actors, the most important of which are proteins and cytoskeletal filaments [7–10]. Proteins deform the membrane through three major mechanisms (Fig. 1.2). Firstly, molecular motors walking on a microtubule convert chemical energy to pushing/pulling forces that can be harnessed to deform a membrane (Fig. 1.2g). Secondly, integral proteins that are much larger than lipids in size, can induce local curvature on the membrane (Fig. 1.2c). Attachment of proteins to the membrane by either insertion of an active amphipathic helix into one leaflet of the bilayer or anchoring to the lipid heads can also distort a membrane (Fig. 1.2b). Epsin proteins, for instance, utilize a wedging mechanism to drive membrane curvature during the formation of clathrin coated pits [7] and tubular networks [11]. Finally, oligomerization and scaffolding of proteins at the surface of a membrane can dictate the shape of a protein motif on the lipids (Figs. 1.2d and e). A Bin/Amphiphysin/Rvs (BAR) domain is a

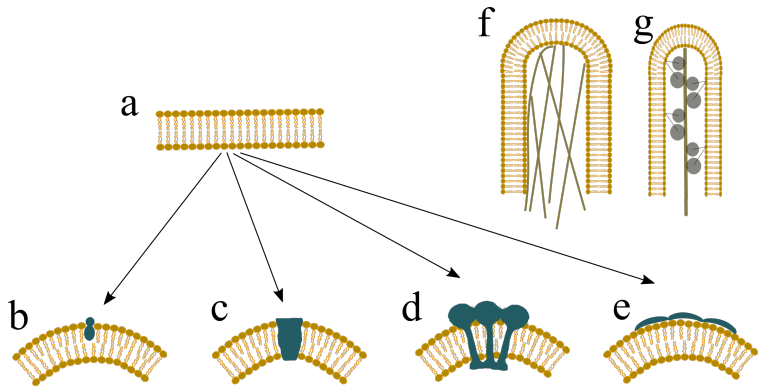

Figure 1.2: Some direct mechanisms of shaping a piece of undisturbed lipid bilayer (a). (b) When interacting with a membrane, some proteins self-organize themselves into α-helices, called amphipathic helices. Proteins with amphipathic helices penetrates like a wedge into the bilayers to induce positive curvature. (c) Some integral proteins are nearly rigid and can induce different types of deformation. (d,e) Oligomerization and scaffolding of proteins create a structure that can induce curvature on the membrane. (f,g) The force generated either by specialized motor proteins or by polymerization of acting/tubular filaments is capable of pulling/pushing tube-like deformations.

well-known example that bends the membrane via scaffolding. BAR domains commonly emerge in crescent-shaped (or banana-shaped) dimers like F-BAR, I-BAR and N-BAR [12, 13]. The curved region of these dimers is positively charged and interacts with the head groups of the lipids, via which BAR proteins impose their concave/convex shape on the lipid bilayer.

The interaction between proteins and membrane shape is bilateral: while the proteins with a fairly rigid structure deform the membrane, they can also sense and respond to the curved regions. For example, the insertion mechanism usually happens in highly curved regions. Some BAR domains may exist in the shape of oligomers. These oligomers can discern the curved geometries on the membrane to use as a platform to assemble on. It is worth mentioning that sensory behavior of proteins often takes place in the regime of weak interactions with the membrane [14]. All the proteins that act as a sensor can become curvature inducers at high concentration. Septins, a conserved family of cytoskeletal GTP-binding proteins at the cell cortex, are an example of such factors that are known to recognize shallow curved regions of a membrane and in high concentration can drive curvature [10, 15].

Mechanical deformations of the membrane create a type of interaction between proteins on top of other possible direct interactions like electrostatic or Van der Waals forces. The interplay between membrane shape and such cooperative interactions between curvature inducers/sensors (of different type) is crucial for driving myriad phenomena in biology. Examples include the tubulation process during the internalization of virus particles, clathrin mediated endocytosis and the process of releasing mechanical stress in the tubular network of mitochondria (see Fig. 1.3). Ewers et al. [16] have studied the process of cell infection by simian virus 40 (SV40), which is a colloid-like particle. Particularly, they suggest that SV40 particles bind to the plasma membrane of a cell via specific ligand-receptor interactions and generate indentations on the membrane. A few minutes after binding to the membrane, SV40 particles were observed in virus-induced invaginations and formed tightly-fitted vesicles. For both virus-like and SV40 particles (if no scission of the vesicle occurs), the membrane promotes tubule formation via aggregation of SV40 particles in order to collectively minimize the deformation energy at the neck, both in the cellular and reconstituted membranes. In **Chapter 5**, we will reveal how similar patterns emerge through introducing membrane mediated interactions between colloids.
Clathrin-mediated endocytosis (CME) is one of the most extensively studied mechanisms by which cells absorb nutrients and signaling molecules [7]. During this process, first a membrane invagination is formed via an array of accessory proteins using the insertion mechanism to deform the membrane. In the next step, coated proteins are recruited (via specific binding interactions) to construct a cargo that is necessary for stabilization and driving the budding process. In the end, dynamin proteins that have preference for the curvature of the neck are employed to drive the nascent vesicle scission (see Fig. 1.3).
On subcellular scales, despite having very limited space and a very complicated network of membranous tubes, mitochondria do not suffer any tubular entanglement or dras-

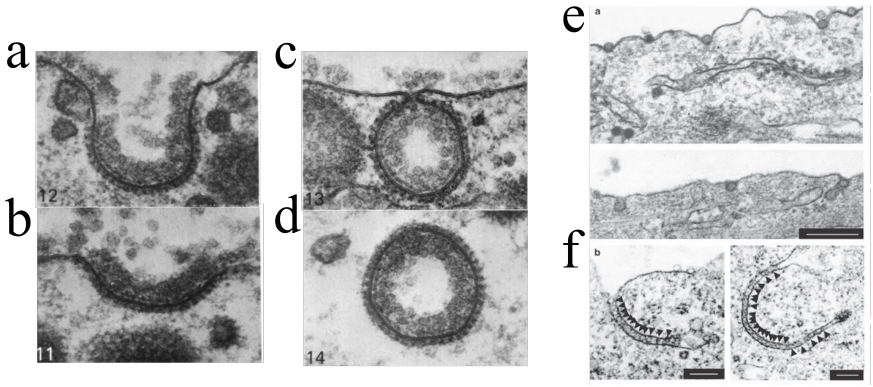

Figure 1.3: (a-d) Different stages of clathrin mediated endocytosis in immature chicken egg cells show the continuation of vesicle invagination and the scission of the the completed vesicle. From [18]. (e-f) Membrane tube formation induced by binding of SV40 virus particles. Figure (e) depicts electron micrographs of cells that were incubated for 7 min with SV40. Note the tight-fitting membrane under SV40 particles. (f) Electron micrographs of virus-like particles after 30 min incubation with cells. The virus-like particles assembled inside tubular membrane invaginations are shown by arrowheads. Reprinted from [16].

tic collisions. It has recently been shown [17] that mitochondrial fission factors (MFF) act as both detectors (in low concentration) and inducers (in high concentration) of the curvature which is key for the relaxation of such a network. As soon as two tubes collide, MFF proteins detect the mechanically stressed areas and recruit fission machinery to cut those regions. On a larger scale, the collective interaction between FtsZ proteins during cell division is another example of the coordination between inducing/sensing proteins. **Chapters 2-4** explain how this phenomenon and other similar membrane remodeling processes in a tubular network can be induced only via introducing membrane mediated interactions.

In addition to proteins, cytoskeletal architecture is also strongly coupled to the shape of a cell (Fig. 1.2f). The cytoskeleton (do not get misled by the word “skeleton”, they are very soft) of a cell mainly consists of actin filaments, composed of actin monomers, intermediated filaments, and microtubules that are composed of tubulin dimers. These structures provide mechanical support to stabilize the shape of a cell. They also play an important role in the adhesion and motility of cells. They are involved in crucial processes during cell migration. For example in filopodia, which cells use to recognize chemical gradients and make a move correspondingly, both microtubules and actin filaments contribute to provide the driving force. The foremost feature of coupling between the shape of a cell and the internal filaments are membrane protrusions. Deforming a membrane costs energy. Therefore, the plasma membrane in turn can participate in the rearrangement of filaments. For example, the presence of a lipid membrane introduces an effective attractive interaction between protrusions; hence it influences the spatial rearrangements of membrane-anchored filaments [19]. **Chapter 7** suggests that having membrane mediated interactions is already sufficient for the microtubules in order to form the structures commonly found in cells.

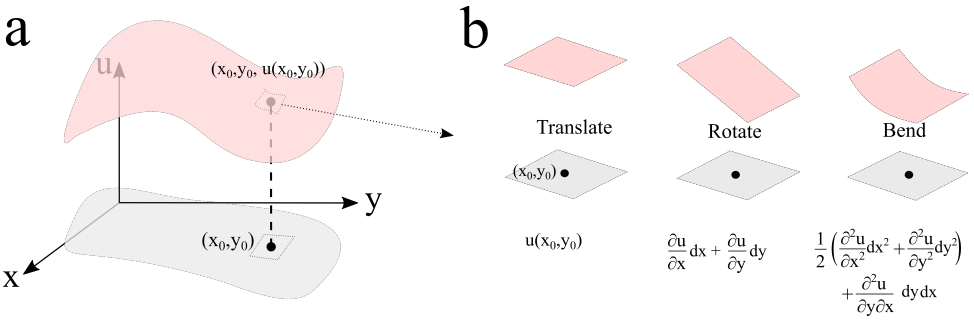

Figure 1.4: (a) Schematic representation of the Monge parametrization. (b) Taylor expansion of the surface $u(x, y)$ around an arbitrary point (From [20]).

1.2. When physics meets biology

1.2.1. Theory of membrane curvature

As mentioned in the previous section, the variety in the range of shapes that membranes adopt is very broad. To physically understand membrane reshaping, we first need to identify the relevant parameters. Having these parameters enables us to associate an energy functional with the lipid bilayer, the minimization of which would naturally gives the geometrical shapes consistent with experimental observations.

For now let us assume that a membrane can be considered as a two dimensional surface (we will see later that this is actually a very good approximation). As such, we can associate a height function $u(x, y)$ to any point on the membrane (with no overhangs) to describe its position with respect to a reference plane, where x and y are the Cartesian coordinates on the reference plane (see Fig. 1.4). As depicted in Fig. 1.4b, we simply use a Taylor expansion at any arbitrary point $u(x_0, y_0)$ inside a segment with size $dx \times dy$ to approximately describe the shape around it. Such an expansion reads [20]:

$$u(x,y) = u(x_0,y_0) + \frac{\partial u}{\partial x}\mathrm{d}x + \frac{\partial u}{\partial y}\mathrm{d}y + \frac{1}{2}\left[\frac{\partial^2 u}{\partial x^2}\mathrm{d}x^2 + \frac{\partial^2 u}{\partial y^2}\mathrm{d}y^2 + \frac{\partial^2 u}{\partial x \partial y}\mathrm{d}x\mathrm{d}y\right] + \ldots \tag{1.1}$$

The first and second terms in the expansion simply relate to the height and slope of the surface at that point. These two terms therefore do not really capture the shape. It is the second order derivatives that measure how bent the surface is. These terms can be rewritten in the following fashion: $\frac{1}{2}\mathbf{dx}^T C\mathbf{dx}$, where C is a symmetric matrix of second order partial derivatives called the curvature matrix or Hessian and is defined as :

$$\mathbf{dx} = \begin{pmatrix} \mathrm{d}x \\ \mathrm{d}y \end{pmatrix} \text{ and } C = \begin{pmatrix} \partial_{xx} u & \partial_{xy} u \\ \partial_{xy} u & \partial_{yy} u \end{pmatrix} \tag{1.2}$$

The curvature matrix at each point reasonably determines the concavity of the surface and hence the local shape. When dealing with curves we can osculate circles at each point, from which we can obtain the curvature at that point. It is possible to do this for a curve because there is only one direction for the curvature. In contrast, at each point on a 2D surface there exits a countless number of directions along which we can define the

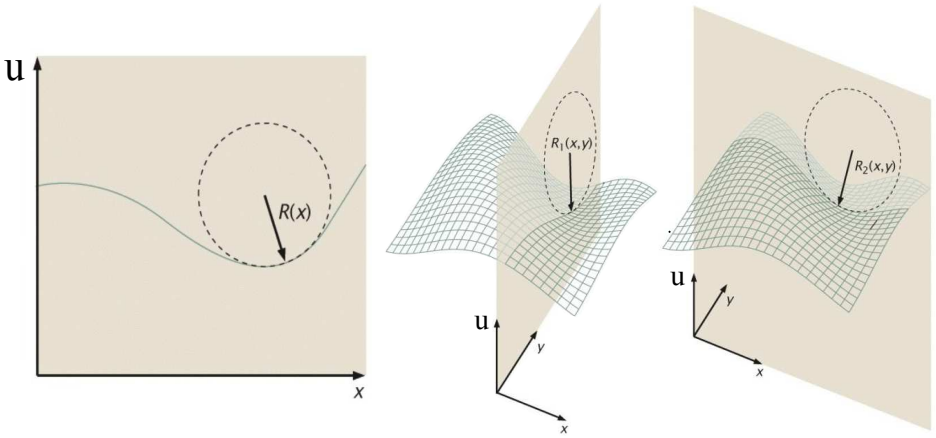

Figure 1.5: The curvature of spatial curves and two dimensional surfaces (From [20]).

curvature matrix. Among all the possible directions, however, there are two directions that correspond to maximum and minimum curvature at the tangent plane with a normal vector perpendicular to the surface. These directions are called principal directions and the corresponding curvatures are called the principal curvatures. The principal curvatures and directions are the eigenvalues and eigenvectors of the curvature matrix C, respectively. One of the characteristic properties of the principal curvatures is that they are independent of our choice of spatial coordinates. Therefore, we can construct two quantities out of them, namely, mean and Gaussian curvature:

$$H = (C_1 + C_2)/2 \tag{1.3}$$

$$K = C_1 C_2 \tag{1.4}$$

It's worth noting that these two numbers are the invariants of the curvature matrix C, namely its trace and determinant. If C_1 and C_2 have the same sign and value the resultant shape would correspond to a sphere of radius $R = 1/C_1$; if the signs are opposite, the corresponding local shape would resemble a saddle-like geometry.
Regardless of the exact form, the curvature energy of a membrane can be expanded in terms of its principal curvatures. Using symmetry consideration, up to quadratic order in the two principal curvatures, the energy density reads:

$$f_c = f_0 + \frac{\kappa}{2}(2H)^2 + \kappa_g K \tag{1.5}$$

where f_0 is the energy of the ground state and the rest accounts for the membrane distortion. The expansion coefficients κ and κ_g are the bending rigidity and the elastic modulus of the Gaussian curvature. The Gaussian modulus is a measure of the energy penalty associated with changing the topology (from a vesicle to a donut, for example) of the membrane which can occur when we have drastic deformations. The total excess

bending energy ΔF is often more relevant and given by:

$$\Delta F = \oint_S \left(\frac{\kappa}{2} (2H - C_0)^2 + \kappa_g K + \sigma \right) dA \tag{1.6}$$

This energy, which will be used many times throughout this thesis, is called the Canham-Helfrich energy functional [21]. The last term in the equation is introduced to penalize any changes in the number of lipids in the lipid bilayer, hence in the total surface area of the membrane. C_0 is the spontaneous curvature of the membrane and σ is sadly (the reason becomes clear shortly) called the surface tension of the bilayer[1]. In bulk fluids the interface is a result of inhomogeneity in the force acting on the molecules. In the center of a full bucket of water, for example, molecules attract each other from every direction, resulting in a zero total force. Surface molecules, however, feel this force only from the neighboring molecules beneath the surface. Consequently, the surface of the water behaves as if it is made of an elastic membrane, contracting toward the bulk flow. This elastic tendency of the surface is called surface tension. Similarly treating lipid bilayers, the surface tension of a membrane is zero(!) because the stretching energy of a membrane is humongous compared to the amount of energy required for its bending ($\sim 10^5$ times larger, as we will discuss later). In addition, in the case of a lipid bilayer the situation is somewhat contrasting. They form an interface even without having a bulk of lipids. The surface tension that we have in Eq. 1.6 is more like a chemical potential associated to including/excluding lipids to the bilayer (correspondingly changing the surface area). When having a fluctuating membrane, the surface tension (or more precisely, the membrane frame tension) is connected to the surface of projected area and not that of the membrane itself [22–24].
As the natural way towards explaining the shape transformations in cellular membranes, we need to minimize the total energy of the membrane. So far, we have been trying to physically make an intuitive connection between the equilibrium shapes of membranes and the relevant parameters. However, it is worth providing the mathematical descriptions of both the curvature and the surface area in an arbitrary framework.

1.2.2. Differential geometry of surfaces

Differential geometry is a mathematical discipline that studies geometrical entities like curves and surfaces using differential calculus. It is closely related to other fields of mathematics including differential equations or topology. Its results have a very broad range of applications from biologically inspired problems to general relativity. As the geometrical object of our interest, we deal with differential geometry of surfaces here to understand how we can describe its properties. Our goal is not to dive deeply into the framework and concepts of differential geometry, but is rather modest (and sometimes not really mathematically true!). We simply introduce the tools and important geometric objects that can be utilized to grasp the notion of Gaussian curvature, mean curvature and principal curvatures. To know more about the concepts please consult the relevant lecture notes and books like Refs. [25–28].

[1] When discussing numerical simulations, we show the surface tension with the letter γ

As will be justified later in this chapter, lipid membranes can be considered as two dimensional surfaces embedded in 3-D space. All the characteristic geometries like a cylinder, sphere or ellipsoid can be described in different ways, depending on the coordinate system we are using. Imagine that we have a surface of an arbitrary shape in space. We can then generalize the parametrization systems we know from before like the equation of a sphere or the Monge gauge parametrization introduced in the previous section. We describe such a surface in a general coordinate system (v^1, v^2) as:

$$\mathbf{r}(v^1, v^2) = \begin{pmatrix} X(v^1, v^2) \\ Y(v^1, v^2) \\ Z(v^1, v^2) \end{pmatrix} \tag{1.7}$$

When introducing the general geometrical objects we will also apply it to a special case in Cartesian Coordinates System (CCS). The parametrization in CCS reads: $\mathbf{r}(x, y) = (x, y, u(x, y))$. Having defined the general position vector $\mathbf{r}(v^1, v^2)$, we can construct perpendicular tangent vectors and the normal vector at each point on the surface, from which we can basically derive the intrinsic and extrinsic properties of the surface! These vectors are defined as:

$$\mathbf{e}_i = \frac{\partial \mathbf{r}(v^1, v^2)}{\partial v^i} \text{ where } i \epsilon \{1, 2\} \text{ , and } \mathbf{n} = \frac{\mathbf{e}_1 \times \mathbf{e}_2}{||\mathbf{e}_1 \times \mathbf{e}_2||} \tag{1.8}$$

with $\mathbf{e}_i$ and $\mathbf{n}$ the tangent and normal vectors, respectively. Only the latter has to be normalized. Continuing with our simple example in CCS, we obtain $\mathbf{e}_x = (1, 0, u_x)$, $\mathbf{e}_y = (0, 1, e_y)$ and $\mathbf{n} = (-u_x, -u_y, 1)/\sqrt{1 + u_x^2 + u_y^2}$. We can characterize the intrinsic geometry of the surface in the neighborhood of any point by using the tangent vectors. For example, the distance between two infinitesimally close points on the surface (S) can be approximated from the differential of the position vector $d\mathbf{r} = \mathbf{r}_{v^1} dv^1 + \mathbf{r}_{v^2} dv^2$ as:

$$\begin{aligned} ds^2 &= \mathrm{d}\mathbf{r}.\mathrm{d}\mathbf{r} \\ &= \mathbf{e}_1.\mathbf{e}_1(\mathrm{d}v^1)^2 + \mathbf{e}_1.\mathbf{e}_2(\mathrm{d}v^1)(dv^2) + \mathbf{e}_2.\mathbf{e}_2(\mathrm{d}v^2)^2 \\ &= g_{ij}\mathrm{d}v^i\mathrm{d}v^j \end{aligned} \tag{1.9}$$

where $g_{ij} = \mathbf{e}_i.\mathbf{e}_j$ are the elements of a tensor called the metric, or first fundamental form. Note that we have approximated the actual distance with the corresponding one on a tangent plane spanned by the two tangent vectors (which are also referred as Gauss normal coordinates). It can also easily be shown that in general coordinate system the area elements equals: $\mathrm{d}A = |e_1 \times e_2|\mathrm{d}v^1\mathrm{d}v^2 = \sqrt{g}dv^1dv^2$,where g is the determinant of the metric tensor. For our problem in CCS, the surface element becomes: $\mathrm{d}A = \sqrt{(1 + u_x^2 + u_y^2)}\mathrm{d}x\mathrm{d}y$.

Now let us see how the surface is embedded in the ambient space. To do so we again look at the same infinitesimally close points and see how much we have deviated from the actual distance on the surface S (mathematically speaking, $|S(o) - S(o')| - ds$) . This quantity, which provides some information about the extrinsic properties of the surface,

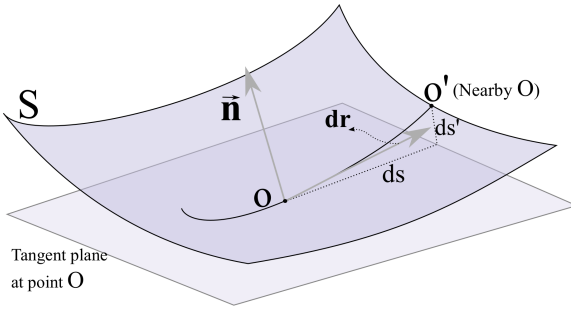

Figure 1.6: The second fundamental form locally characterizes the shape of a surface (S) around a point (O).

can be written as:

$$\begin{aligned} 2\mathrm{d}s' &= -\mathrm{d}\mathbf{r}.\mathrm{d}\mathbf{n} \\ &= \mathbf{r}_{v^1 v^1}.\mathbf{n}(\mathrm{d}v^1)^2 + \mathbf{r}_{v^1 v^2}.\mathbf{n}(\mathrm{d}v^1)(\mathrm{d}v^2) + \mathbf{r}_{v^2 v^2}.\mathbf{n}(\mathrm{d}v^2)^2 \\ &= b_{ij}\mathrm{d}v^i\mathrm{d}v^j \end{aligned} \tag{1.10}$$

where the tensor with coefficients $b_{ij} = (\partial_{v^i v^j}\mathbf{r}).\mathbf{n}$ is called the second fundamental form of the surface, or the extrinsic curvature tensor, as it determines how the surface is embedded in 3-D. Following our example in CCS, we get:

$$\mathbf{b} = \frac{-1}{\sqrt{g}}\begin{pmatrix} u_{xx} & u_{xy} \\ u_{xy} & u_{yy} \end{pmatrix} \tag{1.11}$$

The resultant curvature tensor basically contains all the information we are looking for. To extract this information we should look for the invariants of such a tensor, which are the determinant and the trace of $\mathbf{b}$. Indeed it turns out that the mean and Gaussian curvatures can be written as:

$$H = \frac{\text{trace}\,(\mathbf{g}^{-1}\mathbf{b})}{2} \quad \text{and} \quad K = \frac{\det(\mathbf{b})}{g} \tag{1.12}$$

Finally for our example in CCS, we obtain: $H = (u_{xx}(1+u_y^2) + u_{yy}(1+u_x^2) - 2u_{xy}u_x u_y)/g^3$, $K = (u_{xx}u_{yy} - u_{xy}^2)/g^2$ and $dA = \sqrt{g}dxdy$, where $g = \sqrt{1+u_x^2+u_y^2}$.
Now for any given parametrization we can easily derive the mean and Gaussian curvatures as well as the surface element.

1.2.3. Membrane mediated interactions

Thus far we have clarified how to get the energy functional associated to the shape of a membrane (Eq. 1.6). To get the shape equation we need to minimize the energy functional. At the moment let us apply the formalism on a flat membrane. Plugging the differential objects for the Cartesian coordinates system from the previous section into Eq. 1.6, we obtain the following expressions for the energy and shape of the membrane

to the second and first order, respectively:

$$\begin{aligned} \Delta F &= \frac{1}{2}\oint_S \left[\kappa(\nabla^2 u)^2 \sigma |\nabla u|^2\right] \mathrm{d}x\mathrm{d}y \\ \kappa\nabla^4 u - \sigma\nabla^2 u &= 0 \end{aligned} \tag{1.13}$$

where for the sake of simplicity we have ignored the Gaussian and intrinsic curvatures' contribution here. The resultant shape equation minimizes the energy associated with the surface tension and bending energies for any arbitrary set of boundary conditions. Specifically, these boundary conditions can be the deformation field induced by the shape of proteins. Exploiting the tendency of the membrane to minimize its distortions induced on its shape, one can determine protein-proteins communication by changing their positions and calculating the total energy corresponding to that. Proteins can either attract or repel each other in order to minimize the membrane perturbation. In addition to boundary conditions, the nature of interaction between proteins depends on the intrinsic lenghth scale of the membrane $\lambda^{-1} = \sqrt{\kappa/\sigma}$. For example, while the membrane mediated interaction for two identical isotropic proteins changes as $\Delta E \propto 1/d^4$ for a flat elastic membrane, in case of a fluid membrane (with non-zero surface tension) the leading order term in the interaction energy goes as $\Delta E \propto \log(d)$ with d the separation between the proteins. Since the 1990s, a large amount of research has been dedicated to this process in order to understand the nature of such interactions on cellular scales. In the introduction of each chapter we have provided a brief literature review corresponding to the biological process investigated in that chapter.

In contrast to electrostatic and van der Waals interactions, the interaction energy between deformation inducing proteins is non-additive. This complicates the analysis of the shape equation enormously, because adding any proteins or changing the boundary conditions equals to having a completely new system. Therefore, many models have been proposed and developed to solve the shape equation for fluid surfaces on different length scales. The Canham-Helfrich formalism for example describes the membrane as a continuous surface and looks for a shape that minimizes the total energy. It is a course-grained method and does not account for the atomistic structure of the lipid bilayer. We can also numerically solve the corresponding energy functional. Such methods are usually called particle-based models, among which we will use the triangulated network. The triangulated model, as will be explained in detail later, assumes that the membrane is made of many beads forming a triangular network. Regardless of the molecular properties of such triangular patches, the model tries to minimize the bending energy between triangles and in our case the free energy associated with the change in the surface area by randomly moving the beads around. A full description of the method will be provided in the corresponding chapters. In this thesis we these two models to study our research problems. There are, however, many other deterministic and molecular-based models which are not really suitable for our purposes.

1.3. Membrane numbers

It is helpful to characterize membranes by providing and comparing some of the parameters that are relevant to this research. It also helps to clarify some of the implicit

assumptions we took in the two previous sections (and for the later assumptions in this thesis). Depending on the type of a cell and subcellular organelles we can have membranes (in the shape of enclosed vesicles or tubes) of different sizes. For example, the size of a cell can vary in a range of ~ 10-100 μm. For intracellular organelles we can have a vesicle size of ~ 25-30 nm. The diameter of tubules in the ER is ~ 60 nm. The thickness of a typical membrane in the other hand is in the order of ~ 4 nm. Comparing these numbers and the fact that membrane mediated interactions have long range effects, for inclusions that are much larger than the size of lipids, membranes to a good approximation can be considered as two dimensional surfaces embedded in three dimensional space. Thus far, we have assumed only that membranes can get bent, but one may argue that such a material can undergo other modes of deformation like shearing or stretching. The first assumption is actually related to one of the basics properties of membranes. Lipids in a biological membrane freely diffuse around and are fluid in the plane of the membrane and therefore cannot withstand shearing (so we don't need any number for that). Stretching of a membrane does indeed cost energy and appears as the change in the surface area of the membrane. Using micropipette pressurization technique, it has been shown [29] that the area-stretch modulus of the membrane is in the order of $\sim 50\,\mathrm{kT/nm^2}$. During the experiments, membranes from one side sucked into a pipette in order to put the other side under lateral tension and increase the area. It turned out that even for the small tension values of about $\sim 2\,\mathrm{kT/nm^2}$ the membrane underwent rupture, confirming that under smaller tensions it is a reasonable approximation to consider the area constant. Therefore, membranes favor the bending modes of deformations which are less costly. The bending rigidity of biological membranes is in the range of $\sim 10-25\,\mathrm{kT}$ and the surface tension values are about $10^{-2}-1\,\mathrm{kT/nm^2}$ [30], indicating a characteristic length scale $\lambda^{-1} \approx 3-50$ nm.

1.4. Brief outline of this research

In the previous sections, we mentioned that the membrane shape is regulated by protein inclusions, which can act both as curvature sensors and curvature inducers. The background shape of the membrane on the other hand can control the interaction between such objects. A concise investigation of these phenomena is the core of this thesis.

In contrast to previous works, most of which assume membranes as a flat surface, in **Part I** we investigate the interaction between membrane deforming objects in highly curved regimes. We particularly show that the curved and closed nature of cellular membranes has a significant effect on the self organization of embedded inclusions. With the help of Monte Carlo simulations, we further show that curvature sensing proteins in high densities can constrict tubular membranes and facilitate their splitting. This chapter also provides some recent experimental evidences confirming that these interactions are essential for tubular networks in the cell to avoid entanglement.

In **Part II**, we study the interaction between colloidal-shaped proteins bound to closed vesicles. First, through a numerical approach, we demonstrate that fully wrapped colloids on a spherical membrane attract each other in order to minimize the curvature energy of the membrane. We then elucidate how the curvature variation controls particle aggregation on fluid membrane vesicles. We particularly find that particles adhered to an ellipsoidal vesicle exploit the curvature variation to self-assemble and form a ring

at the mid-plane of an ellipsoid.
Last but not least, **chapter 7** reveals the role of membrane shape on the rearrangement of cytoskeletal filaments like microtubules. Our results explain the possible effective mechanism underlying the preference of filaments for having parallel configurations.

1

References

[1] M. Terasaki, T. Shemesh, N. Kasthuri, R. W. Klemm, R. Schalek, K. J. Hayworth, A. R. Hand, M. Yankova, G. Huber, J. W. Lichtman, *et al.*, *Stacked endoplasmic reticulum sheets are connected by helicoidal membrane motifs,* Cell **154**, 285 (2013).

[2] Wikipedia, *Endoplasmic reticulum — Wikipedia, the free encyclopedia,* (2004), [Online; accessed 22-July-2004].

[3] E. Gorter and F. Grendel, *On bimolecular layers of lipoids on the chromocytes of the blood,* Journal of Experimental Medicine **41**, 439 (1925).

[4] S. J. Singer and G. L. Nicolson, *The fluid mosaic model of the structure of cell membranes,* Science **175**, 720 (1972).

[5] D. M. Engelman, *Membranes are more mosaic than fluid,* Nature **438**, 578 (2005).

[6] M. F. Brown, *Soft matter in lipid-protein interactions,* Annual Review of Biophysics **46**, 379 (2017).

[7] H. T. McMahon and J. L. Gallop, *Membrane curvature and mechanisms of dynamic cell membrane remodelling,* Nature **438**, 590 (2005).

[8] H. T. McMahon and E. Boucrot, *Membrane curvature at a glance,* J Cell Sci **128**, 1065 (2015).

[9] T. Baumgart, B. R. Capraro, C. Zhu, and S. L. Das, *Thermodynamics and mechanics of membrane curvature generation and sensing by proteins and lipids,* Annual review of physical chemistry **62**, 483 (2011).

[10] Y. Shibata, J. Hu, M. M. Kozlov, and T. A. Rapoport, *Mechanisms shaping the membranes of cellular organelles,* Annual Review of Cell and Developmental **25**, 329 (2009).

[11] F. Campelo, H. T. McMahon, and M. M. Kozlov, *The hydrophobic insertion mechanism of membrane curvature generation by proteins,* Biophysical journal **95**, 2325 (2008).

[12] B. J. Peter, H. M. Kent, I. G. Mills, Y. Vallis, P. J. G. Butler, P. R. Evans, and H. T. McMahon, *Bar domains as sensors of membrane curvature: the amphiphysin bar structure,* Science **303**, 495 (2004).

[13] M. Simunovic, G. A. Voth, A. Callan-Jones, and P. Bassereau, *When physics takes over: Bar proteins and membrane curvature,* Trends in cell biology **25**, 780 (2015).

[14] G. Guigas and M. Weiss, *Effects of protein crowding on membrane systems,* Biochimica et Biophysica Acta (BBA)-Biomembranes **1858**, 2441 (2016).

[15] K. S. Cannon, B. L. Woods, and A. S. Gladfelter, *The unsolved problem of how cells sense micron-scale curvature,* Trends in Biochemical Sciences (2017).

[16] H. Ewers, W. Römer, A. E. Smith, K. Bacia, S. Dmitrieff, W. Chai, R. Mancini, J. Kartenbeck, V. Chambon, L. Berland, *et al.*, *Gm1 structure determines sv40-induced membrane invagination and infection,* Nature cell biology **12**, 11 (2010).

[17] S. C. J. Helle, Q. Feng, M. J. Aebersold, L. Hirt, R. R. Grüter, A. Vahid, A. Sirianni, S. Mostowy, J. G. Snedeker, A. Šarić, *et al.*, *Mechanical force induces mitochondrial fission,* eLife **6** (2017).

[18] M. Perry and A. B. Gilbert, *Yolk transport in the ovarian follicle of the hen (gallus domesticus): lipoprotein-like particles at the periphery of the oocyte in the rapid growth phase,* Journal of cell science **39**, 257 (1979).

[19] A. P. Liu, D. L. Richmond, L. Maibaum, S. Pronk, P. L. Geissler, and D. A. Fletcher, *Membrane-induced bundling of actin filaments,* Nature physics **4**, 789 (2008).

[20] R. Phillips, J. Kondev, J. Theriot, and H. Garcia, *Physical biology of the cell* (Garland Science, 2012).

[21] W. Helfrich, *Elastic properties of lipid bilayers: theory and possible experiments,* Zeitschrift für Naturforschung C **28**, 693 (1973).

[22] O. Farago and P. Pincus, *Statistical mechanics of bilayer membrane with a fixed projected area,* The Journal of chemical physics **120**, 2934 (2004).

[23] J.-B. Fournier and C. Barbetta, *Direct calculation from the stress tensor of the lateral surface tension of fluctuating fluid membranes,* Physical review letters **100**, 078103 (2008).

[24] H. Shiba, H. Noguchi, and J.-B. Fournier, *Monte carlo study of the frame, fluctuation and internal tensions of fluctuating membranes with fixed area,* Soft matter **12**, 2373 (2016).

[25] B. F. Schutz, *Geometrical methods of mathematical physics* (Cambridge university press, 1980).

[26] M. Deserno, *Notes on differential geometry,* (2004).

[27] M. Deserno, *Fluid lipid membranes: From differential geometry to curvature stresses,* Chemistry and physics of lipids **185**, 11 (2015).

[28] S. Kobayashi and K. Nomizu, *Foundations of differential geometry*, Vol. 2 (Interscience publishers New York, 1969).

[29] W. Rawicz, K. Olbrich, T. McIntosh, D. Needham, and E. Evans, *Effect of chain length and unsaturation on elasticity of lipid bilayers,* Biophysical journal **79**, 328 (2000).

[30] A. Evans, M. Turner, and P. Sens, *Interactions between proteins bound to biomembranes,* Physical Review E **67**, 041907 (2003).

I

Tubular Membranes

2

Pointlike inclusion interactions in tubular membranes

Membrane tubes and tubular networks are ubiquitous in living cells. Inclusions like proteins are vital for both the stability and the dynamics of such networks. These inclusions interact via the curvature deformations they impose on the membrane. We analytically study the resulting membrane mediated interactions in strongly curved tubular membranes. We model inclusions as constraints coupled to the curvature tensor of the membrane tube. First, as special test cases, we analyze the interaction between ring and rod-shaped inclusions. Using Monte Carlo simulations, we further show how pointlike inclusions interact to form linear aggregates. To minimize the curvature energy of the membrane, inclusions self-assemble into either line- or ringlike patterns. Our results show that the global curvature of the membrane strongly affects the interactions between proteins embedded in it, and can lead to the spontaneous formation of biologically relevant structures.

A version of this chapter has been published as: A. Vahid and T. Idema, *Pointlike inclusion interactions in tubular membrane*, Phys. Rev. Lett. **117**,138102 (2016).

2.1. Introduction

Membrane nanotubes can be extracted experimentally from 'giant' unilamellar vesicles (GUVs) by different techniques like optical tweezers [1] or micropipettes [2–4]. In vivo, for example in the endoplasmic reticulum, these membrane tubes are generated either by being pulled out by molecular motors [5] or pushed out by polymerizing cytoskeletal filaments [6]. The formation mechanism and the stability of tubular membranes have been extensively studied both theoretically [7–10] and experimentally [1–3, 11].

In addition to direct interactions like electrostatic forces, inclusions (like proteins) embedded in biological membranes experience interactions mediated by the elastic deformation of that membrane. Inclusions create these deformations by imposing a curvature field in the lipid bilayer when they are bound to or embedded in a membrane. Despite the presence of a repulsive pair potential between such inclusions in a flat membrane [12, 13], because of the non-pairwise additive nature of many-body interactions, they collectively attract each other and form stable spatial patterns [14]. Numerous analytical investigations [15, 16] and computer simulations [17, 18] have been done to show that this non-additivity drives vesiculation and budding in biological membranes. In contrast to flat membranes, membrane-mediated interactions between inclusions embedded in tubular membranes are not well understood. These interactions can be found, for example, in the last step of exocytosis and in cell division, where some specific proteins make energy-favorable structures to facilitate membrane scission [19]. Compared to the scale of the plasma membrane which can be approximately considered as a flat surface, the curved nature of such a tubular membrane can significantly affect these interactions. Recently, it has been revealed that hard particles and semi flexible polymers absorbed to soft elastic shells, collectively induce aggregates and produce a rich variety of aggregation patterns [18, 20–26]. Particularly, Pàmies and Cacciuto showed that spherical nanoparticles adhering to the outer surface of an elastic nanotube can self-assemble into diverse aggregates [22]. They considered elastic nanotubes as stretchable and bendable structures; in contrast biological membranes cannot withstand shearing forces and are stretch free interfaces. Therefore, an obvious question to ask is what kinds of structure inclusions might induce in a cylindrical fluid surface.

The aim of this paper is to analytically study the interactions between inclusions embedded in a membrane tube. We treat inclusions as point-like constraints imposing local curvature on the membrane. Previous work done by Dommersnes and Fournier [27, 28] already suggested a methodology to derive inclusion interactions mediated by membrane deformations in planar geometries. Using this framework, one can easily calculate the interaction of many point-like inclusions in a non-additive way. Here, we apply that framework to a membrane tube containing an arbitrary number of inclusions. For simplicity we assume that inclusions do not undergo any conformational changes, though these could also be accounted for using the same formalism [29]. After giving a brief outline of the model, first we look at some specific shapes like rings and rods, and afterwards we will study interactions between point-like inclusions. Using Monte Carlo simulations, we investigate the effects of different parameters like the density and the size of inclusions on their final equilibrium configuration.

Our results reveal that in contrast to the interaction of two rings, two infinite rods em-

bedded in a membrane tube behave completely different from the same inclusions in a flat membrane. While two identical inclusions always repel each other in a flat membrane, in a cylindrical membrane they can also attract. We find a similar behavior for identical point-like particles, which can also attract and repel on the tube, depending on their separation and relative orientation. Consequently, for many inclusions, and depending on their hard-core radius, they form either ring or line like structures. We conclude that rings of membrane inclusions, such as the dynamin rings found in endocytosis, or the FtsZ rings found in bacterial cytokinesis [30], can thus spontaneously form on tubular membranes, due to membrane-mediated interactions alone.

2.2. Model

As mentioned earlier, we use the theoretical framework introduced in ref. [28]. We apply this method to membranes with a cylindrical topology. The unperturbed system is a perfect cylinder, parametrized by angular (θ) and longitudinal ($\zeta = Z/R$, with R the radius of the cylinder) coordinates. We describe deviations from the perfect cylindrical shape using the Monge gauge (see Fig. 1.4):

$$\mathbf{r}(\theta,\zeta) = R\begin{pmatrix}(1+u(\theta,\zeta))\cos(\theta)\\(1+u(\theta,\zeta))\sin(\theta)\\\zeta\end{pmatrix}, \tag{2.1}$$

where $u(\theta,\zeta) << 1$. Using Canham-Helfrich model explained in chapter 1, the bending energy of the membrane reads:

$$E = \int_S \mathrm{d}A\left(2\kappa H^2 + \sigma\right), \tag{2.2}$$

It is well known that, under the application of a constant force $f = 2\pi\sqrt{2\kappa\sigma}$ to the membrane, a cylindrical tube of radius $R = \sqrt{\kappa/2\sigma}$ is an equilibrium shape minimizing the energy functional given by Eq. 2.2 [2, 8].

Following the construction by Dommersnes and Fournier, we put N inclusions in the membrane at positions $\left(\mathbf{r}_1, \mathbf{r}_2, ..., \mathbf{r}_p, ..., \mathbf{r}_N\right)$ imposing the curvature matrix $\mathbf{C} = (..., C^p_{\theta\theta}, C^p_{\zeta\theta}, C^p_{\zeta\zeta}, ...)$, where $C^p_{ij} = \partial_{ij}u(\theta,\zeta)\delta(\theta-\theta_p, \zeta-\zeta_p)$. To get the deformation field of the tube, $u(\theta,\zeta)$, we minimize the energy functional (Eq. 2.2) given that we have imposed the curvature constraints. For the details of solving the resulting Euler-Lagrange equations please see the *Model* section in the Supplemental Material for the derivation. In the case of self-interactions, we need to take the actual size of the inclusions into account, and should therefore introduce two cutoff wave vectors (we cannot have fluctuations with wavelength smaller than the size of the lipids): $\Lambda_\zeta = 1/a$ and $\Lambda_\theta = 2\pi R/a$, where the cutoff radius a is chosen such that $\Lambda^{-1}_{\theta(\zeta)}$ is in the order of the membrane thickness [33].

Using this formalism, we can get an analytical expression for the elastic energy and the shape of the deformed membrane for any arbitrary number of inclusions. The nondimensionalized components of the curvature tensor $\mathbf{C}$, for a tube with a thickness of $\simeq 5$ nm and radius $\simeq 20-50$ nm, are in the order of $c^{-1} \simeq 0.1-0.25$. In the following, we measure the energy in units of $2\pi\kappa c^2$, which, for the standard values of $\kappa = 30k_BT$ and $c = 10$, equals $2\pi\kappa c^2 \simeq 20\times10^3 k_BT$.

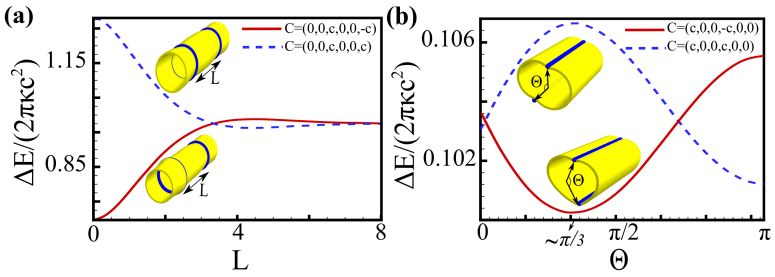

Figure 2.1: The calculated energy cost of having two inclusions (as compared to none) for a membrane tube as a function of the distance between (a) two rings and (b) two rods. Inclusions impose either the same (dashed line) or opposite (solid line) curvatures.

2.3. Special test cases

To show the difference between planar and highly curved regimes, we study two special shapes of inclusions using the described formalism. First, we look at the interaction between two rings, separated by a distance L, in a cylindrical membrane (Fig. 2.1a). Second, we analyze the energy favorable configuration of rod-like inclusions embedded in a membrane tube (Fig. 2.1b). By considering ring shaped constraints, recent studies have constructed a variational framework to model the constriction process during cytokinesis [34, 35]. Also, using an analytical approach, the wrapping process of a rod like particle by a tubular membrane has been studied via minimization of bending and adhesion energies [36].

The energy dependence on inclusion separation between two rings is shown in Fig. 2.1a. We find that two identical rings ($\mathbf{C} = (0,0,c,0,0,c)$) have strong short range repulsion and weak long range attraction; this behavior causes two rings imposing equal curvature to not coalesce, but equilibrate at a certain distance from each other. The long-range attraction originates from the fact that the membrane's size is finite in the angular direction, resulting in a reduction in the total energy of two overlapping tails when distant rings move closer together. For different radii of the tube, we get different equilibrium separations for the rings; the larger the radius is, the further the rings are away from each other (See Fig. S1 in the Supplemental Material). The situation for rings imposing opposite curvature will be reversed. The membrane, to globally minimize its curvature energy, favors two rings to coalesce despite having a local minimum for larger separations.

In contrast to rings, two rods interact completely differently. Depending on their angular separation (Θ), two identical rods ($\mathbf{C} = (c,0,0,c,0,0)$) can either attract or repel each other (Fig. 2.1b). One clear difference with both flat membranes and the previous test case is that the tails of deformations in the angular direction are limited to a confined space and overlap. Consequently, there are two contributions to the total energy of the tube: one is due to the membrane deformation between two rods and the other one originates from the overlapping tails. For small distances, these two interactions add to a net attraction between identical rods, as this minimizes the overlap between their tails. For larger separations, the effect of the deformed membrane between the inclusions becomes dominant, and in order to minimize the bending energy of the sys-

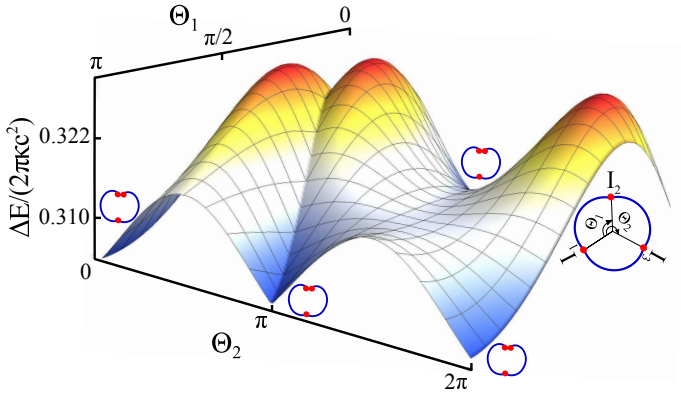

Figure 2.2: The energy landscape for a membrane tube containing three rod like inclusions I1, I2 and I3.

tem, they sit on the opposite poles. Similar to rings, the location and the strength of the energy barrier depends on the radius of the tube. In the limit of very large R, the interaction between two rods imposing the same curvature is purely repulsive (see Fig. S2 in the Supplemental Material), like in a flat membrane [37]. Since membrane mediated interactions, in contrast to for example electrostatic interactions, behave in a non-additive way, it is interesting to look at a system with more than two inclusions. Particularly, we find that adding a third rod into the previous system makes the repulsion between the first two attractive. The global minimum of the three dimensional energy landscape, as illustrated in Fig. 2.2, corresponds to the situation that two rods are on top of each other and the third one is on the opposite pole. Similarly, for more than three inclusions, we find that for an even number of rods the global minimum occurs when they equally distribute between the two poles; and in case of having an odd number of inclusions, one of the poles will have one more rod than the other.

2.4. Point-like inclusions

Before focusing on many body interactions between point-like inclusions, let us first consider a tubular membrane containing two identical inclusions imposing the same curvature, so $\mathbf{C} = (c, 0, c, c, 0, c)$ (similar to rods and rings, the behavior for inclusions inducing opposite curvature will be reversed). Fig. 2.3a depicts the excess curvature energy of the membrane as a function of both angular and longitudinal distances between two inclusions. At small distances there are two different kinds of behavior corresponding to two distinct directions: along the tube axis two inclusions strongly repel each other at short distances and attract each other at longer distances (Fig. 2.3d), while in the transversal direction the two-body interaction is purely attractive (Fig. 2.3c). When two identical point-like inclusions have the same transversal coordinates ($\Theta = 0$), they behave like rings, although the long-range attraction becomes very weak (see inset in Fig. 2.3d). However, when these inclusions have the same longitudinal coordinates ($L = 0$), their behavior differs from that of the infinite rods. While for the rods we find both short-range attraction and long-range repulsion, identical point-like inclusions at

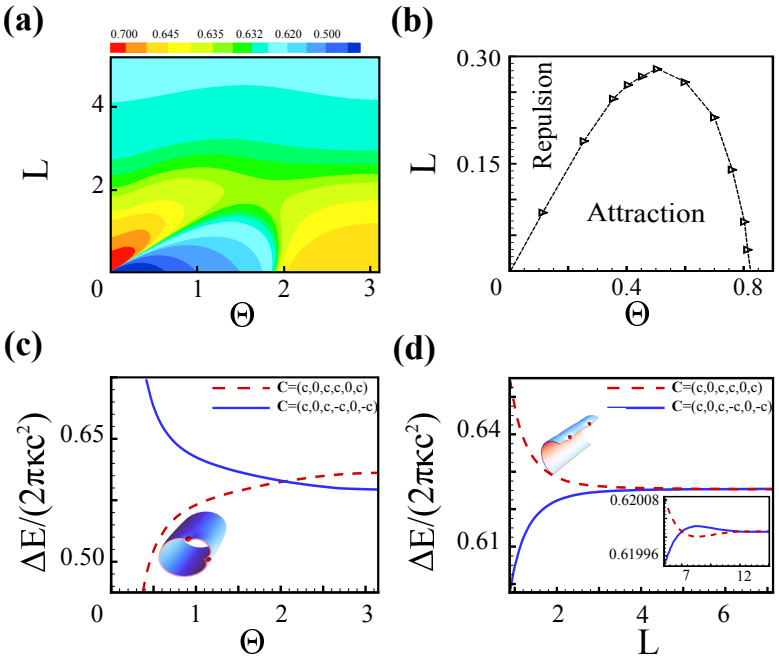

Figure 2.3: (a) The curvature energy ($\frac{\Delta E}{2\pi\kappa c^2}$) of a membrane containing two inclusions, as a function of their angular (Θ) and longitudinal (L) separation, with L in units of the tube radius R. (b) The line around the global minimum at which the energy equals the local minimum at large separations. For particles whose diameter exceeds the size of this region, the overall behavior is repulsive (settling in the local minimum at large separations). Smaller particles globally attract, but have a high energy barrier separating the attractive and repulsive regime. (c) Two identical inclusions placed at the same longitudinal coordinates ($L = 0$) attract each other. (d) Point-like inclusions behave like rings when they are situated on the same transversal coordinates ($\Theta = 0$); the inset shows the weak long-rage attraction.

the same longitudinal coordinate always attract. The global energy minimum of the system corresponds to the two inclusions sitting next to each other in the angular direction (see Fig. 2.3a). However, if the inclusions are initially separated, there is a large energy barrier (on the order of $\sim 100 k_B T$) that the inclusions have to overcome to reach this global minimum state. Moreover, the region around the global minimum where the energy is less than that at the local minimum at large separations (see inset in Fig. 2.3d) is only very small, as shown in Fig. 2.3b. Consequently, small inclusions globally attract, but may not find each other due to the large barrier; particles with a diameter larger than the size of the attractive basin in Fig. 2.3b have a global minimum at large but finite separation, also separated from the (now local) minimum close together by a large barrier.

Like for rods, adding more inclusions changes the energy landscape. For point-like inclusions the net effect is a lowering of the barrier between the energy minima at small and large separations. Consequently, the presence of other inclusions can allow two inclusions to reach their global equilibrium state, which could potentially take very long if those other inclusions were absent.

To elucidate the collective behavior of multiple inclusions packed in the system, we perform Monte Carlo (MC) simulations on a membrane tube containing inclusions with different hard-core radii (which are introduced to take into account the finite size of the particles). During the simulations, we consider periodic boundary conditions in the longitudinal direction. The only effect of a non-zero hard-core radius of inclusions is the transition from the short-range attractive-dominated regime to the repulsion dominated area. In all cases the tube's reduced length is $\zeta = 10\pi$ and correspondingly, the cut-off wave vectors are $\Lambda_\zeta = 314$ and $\Lambda_\theta = 62$ for the cutoff radius of $a = 0.1$. During MC simulations we use the Metropolis algorithm [38] with parallel tempering [39]. As membrane mediated interactions between inclusions originate from both the average deformation of the membrane and the constraints imposed on its shape fluctuation, one may be concerned about the Casimir interactions. In our system, the thermal fluctuation effects nicely decouple from the elastic ones [40], and it is straightforward to show that their effects are relatively small, quickly fading out with the distance between inclusions [41] (see Fig. S3 in the Supplemental Material). We find that for an arbitrary number of inclusions with a hardcore radius $a_0 = 0.2$, they will attract each other in the angular direction and self-assemble into ring like configurations (Figs. 2.4a and 2.4b). Because of having a rough energy landscape, including many barriers like the one shown in Fig. 2.3a, inclusions could not always completely merge and reach the global energy minimum. However, we can certainly conclude that in order to minimize the curvature energy of the membrane, such identical inclusions will assemble into rings. This process is reminiscent of recruiting dynamin proteins during exocytosis, during which they self-assemble and form rings to constrict the membrane and, finally, separate the nascent vesicle from the cell. In contrast, for inclusions having a larger radius ($a_0 = 1.1$), our MC simulations reveal that they collectively align in the longitudinal direction. Therefore, as shown in Fig. 2.4c, if the number of particles is less than that fits the length of the tube they aggregate into one line. The boundary for which the transition from rings to lines occurs is shown in Fig. 2.3b: if the radius of inclusions is such that it cannot fall in the attractive area, they self-assemble into lines. If we increase the particle density (Figs. 2.4d and 2.4e), such that they do not all fit on a single line anymore, they do not make other configurations, but distribute around two lines on the opposite poles. The reason for this is actually hidden in the assumptions of the theoretical model we use. First, inclusions are treated as point like constraints that impose a uniform curvature in all directions. Second, while as in our model, a fluid membrane cannot resist any stretch, it has recently been shown that in an elastic membrane the competition between bending and stretching rigidities gives rise to different configurations like helical structures [22]; in the limit of very small stretching rigidity, linear aggregations like rings and rods are the only configurations that one can get for an elastic tube.

2.5. Conclusion

We have investigated the curvature mediated interactions between identical inclusions. We have shown that while rings have strong short-range repulsion (and weak long-range attraction), identical rods can either attract or repel each other depending on the angular distances between them. For two point like inclusions embedded in a tubular membrane, our analytical solutions show that they attract and repel each other in the

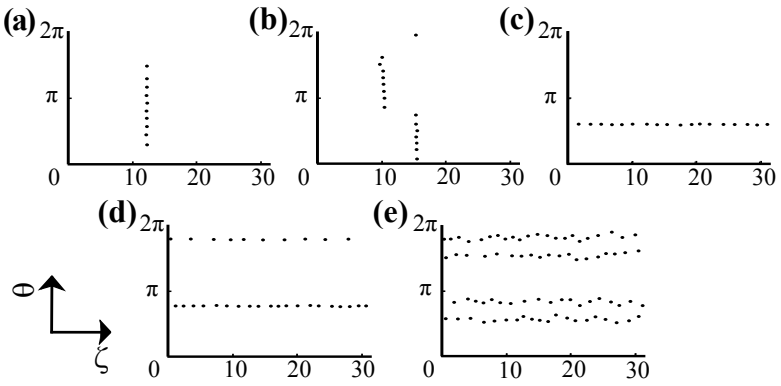

Figure 2.4: Equilibrium configurations obtained by Monte Carlo simulation for a system containing (a) 10 inclusions with hard-core radius of $a_0 = 0.2$ (b) 16 inclusions with hard-core radius of $a_0 = 0.2$ (c) 16 inclusions with hard-core radius of $a_0 = 1.1$ (d) 30 inclusions with hard-core radius of $a_0 = 1.1$ (e) 80 inclusions with hard-core radius of $a_0 = 1.1$.

transversal and longitudinal direction, respectively. Our study of a membrane tube containing many inclusions has highlighted the importance of many body interactions for the inclusions in order to collectively induce aggregations. Having done Monte Carlo simulations on such a system, we observed that depending on the defined hard core radius, inclusions self-assemble into line or ring like structures. The results may explain the mechanisms by which inclusions self-assemble during membrane constriction in the processes like exocytosis and cytokinesis.

acknowledgments

We would like to thank Dr. J. L. A. Dubbeldam for fruitful discussions. This work was supported by the Netherlands Organisation for Scientific Research (NWO/OCW), as part of the Frontiers of Nanoscience program.

2.6. Supplemental Material

S. 6.1. Model

We use the methodology developed by Dommersnes and Fournier [27, 28]. As stated in the main text, we apply this method to membranes with a cylindrical topology. The unperturbed system is a perfect cylinder, parametrized by angular (θ) and longitudinal ($\zeta = Z/R$, with R the radius of the cylinder) coordinates. We describe deviations from the perfect cylindrical shape using the Monge gauge:

$$\mathbf{r}(\theta,\zeta) = R\begin{pmatrix}(1+u(\theta,\zeta))\cos(\theta)\\(1+u(\theta,\zeta))\sin(\theta)\\\zeta\end{pmatrix}, \tag{S. 3}$$

where $u(\theta,\zeta) << 1$ and $R = \sqrt{\kappa/2\sigma}$. Assuming that $u(\theta,\zeta)$ is sufficiently differentiable, we calculate the mean curvature H and surface element $\mathrm{d}A$ as

$$H = \frac{-2u_\zeta u_\theta u_{\theta\zeta} - (1+u_\zeta^2)(-u_{\theta\theta}+u+1) + u_{\zeta\zeta}\left(u_\theta^2 + (u+1)^2\right) - \frac{2u_\theta^2}{(u+1)}}{2R\left((u+1)^2\left(u_\zeta^2+1\right)+u_\theta^2\right)^{3/2}}, \tag{S. 4}$$

$$\mathrm{d}A = R^2(u+1)\sqrt{\left(u_\zeta^2+1\right)+u_\theta^2}\,\mathrm{d}\theta\mathrm{d}\zeta, \tag{S. 5}$$

where $u_\zeta = \partial u/\partial\zeta$ etc. Assuming N inclusions in the membrane at the positions $(\mathbf{r}_1,\mathbf{r}_2,...,\mathbf{r}_N)$ imposing the curvature matrix $\mathbf{C} = \left(...,C^p_{\theta\theta},C^p_{\zeta\theta},C^p_{\zeta\zeta},...\right)$, where $C^p_{ij} = \partial_{ij}u(\theta,\zeta)\delta(\theta-\theta_p,\zeta-\zeta_p)$, $p = 1,...,N$, the curvature energy functional becomes:

$$E = \int_S \mathrm{d}A\left(2\kappa H^2 + \sigma - \Lambda_\alpha C_\alpha\right), \tag{S. 6}$$

where the Λ_α are $3N$ Lagrange multipliers and $\alpha = 1,...,3N$. Since we use a Monge gauge parameterization in which we assume that $u(\theta,\zeta)$ is very small, the topology of our system is invariant. We therefore disregard the Gaussian curvature contribution, because according to the Gauss-Bonnet theorem the integral over a surface of fixed topology is constant. We also assume that the spontaneous curvature, which describes the asymmetry of the membrane, is zero. Substituting H and $\mathrm{d}A$ into the energy functional and minimizing it up to first order in $u(\theta,\zeta)$, we obtain:

$$\left(\nabla^4 + 2\partial_{\theta\theta} + 1\right)u(\theta,\zeta) = \Lambda_\alpha D_\alpha(\theta,\zeta), \tag{S. 7}$$

where $\nabla^4 = \partial_{\theta\theta\theta\theta} + 2\partial_{\zeta\zeta\theta\theta} + \partial_{\zeta\zeta\zeta\zeta}$ is the biharmonic operator in cylindrical coordinates, and

$$\mathbf{D} = \left(\delta^1_{\theta\theta},\delta^2_{\zeta\theta},\delta^3_{\zeta\zeta},...,\delta^{3N-2}_{\theta\theta},\delta^{3N-1}_{\zeta\theta},\delta^{3N}_{\zeta\zeta}\right),$$

with $\delta^\alpha_{ij} = \partial_{ij}\delta(\theta-\theta_\alpha,\zeta-\zeta_\alpha)$. Because equation (S. 7) is linear, we can solve it using superposition once we know the Green's function, for which we obtain:

$$G(\theta,\zeta) = \sum_{n\neq\pm1} \frac{\left(\frac{e^{-\zeta\alpha_-(n)}}{\alpha_-(n)} - \frac{e^{-\zeta\alpha_+(n)}}{\alpha_+(n)}\right)}{4\pi\left(\alpha_+(n)^2 - \alpha_-(n)^2\right)}\cos(n\theta), \tag{S. 8}$$

where $\alpha_\pm(n) = \sqrt{n^2 \pm \sqrt{2n^2-1}}$. The solution of equation (S. 7) is then given by

$$u(\theta,\zeta) = \Lambda_\alpha G_\alpha(\theta,\zeta), \tag{S. 9}$$

where the elements of the vector $\mathbf{G}$ are given by $\mathbf{G} = \left(...,C^p_{\theta\theta},C^p_{\zeta\theta},C^p_{\zeta\zeta},...\right)$. To relate the Lagrange multipliers Λ_α to the actual constraints C_α, we rewrite equation (S. 7) as

$$\mathscr{L}_\alpha u = C_\alpha, \tag{S. 10}$$

which gives us $\mathscr{L}_\alpha(\Lambda_\beta G_\beta) = \mathscr{L}_\alpha(G_\beta)\Lambda_\beta = C_\alpha$. Defining $M_{\alpha\beta} = \mathscr{L}_\alpha(G_\beta)$, we get:

$$\Lambda_\alpha = M^{-1}_{\alpha\beta} C_\beta, \tag{S. 11}$$

$$u(\theta,\zeta) = M^{-1}_{\alpha\beta} G_\beta(\theta,\zeta) C_\beta, \tag{S. 12}$$

$$E = \frac{\kappa}{2} M^{-1}_{\alpha\beta} C_\alpha C_\beta. \tag{S. 13}$$

In the case of self-interactions, we calculate the derivatives of the Green's function in Fourier space,

$$G_{klrs}(0,0) = \frac{1}{2\pi^2} \sum_{n\neq\pm1}^{\Lambda_\theta} \int_0^{\Lambda_\zeta} \frac{\partial^4}{\partial k \partial l \partial r \partial s} \left(\frac{e^{i(q\zeta+n\theta)}}{(q^2+n^2)^2 - 2n^2 + 1} \right) |_{\zeta=0,\theta=0} \, \mathrm{d}q, \tag{S. 14}$$

where the indices k, l, r and s are either θ or ζ, and the cutoff wavevectors are related to the membrane thickness a through $\Lambda_\zeta = 1/a$ and $\Lambda_\theta = 2\pi R/a$, as given in the main text.

S. 6.2. Green's and energy functions

To evaluate the interaction between rings whose deformations depend only on the longitudinal coordinate (ζ), we obtained simplified relations for one dimension. By letting the position vector of the membrane depend only on the longitudinal coordinate, we obtain the Green's function and the excess energy of the membrane between two rings:

$$G(\zeta) = \frac{e^{-|\zeta|/\sqrt{2}}}{\sqrt{2}} \left[\sin\left(\frac{|\zeta|}{\sqrt{2}}\right) + \cos\left(\frac{\zeta}{\sqrt{2}}\right) \right], \tag{S. 15}$$

$$E(\Lambda_\zeta, L) = \frac{\sqrt{2}\arctan\left(\frac{2\sqrt{2}\Lambda_\zeta}{(\Lambda_\zeta^2+1)^2-2}\right) - 2\sqrt{2}\pi + 4\Lambda_\zeta + 4\sqrt{2}\pi e^{-\frac{L}{\sqrt{2}}}\left(\sin\left(\frac{L}{\sqrt{2}}\right) + \cos\left(\frac{L}{\sqrt{2}}\right)\right)}{\frac{1}{16\pi^2}\left(\sqrt{2}\arctan\left(\frac{2\sqrt{2}\Lambda_\zeta}{(\Lambda_\zeta^2+1)^2-2}\right) - 2\sqrt{2}\pi + 4\Lambda_\zeta\right)^2 - 2e^{-\sqrt{2}L}\left(\sin\left(\sqrt{2}L\right)+1\right)}, \tag{S. 16}$$

where Λ_ζ is the cutoff wave vector in the longitudinal direction. All the lengths are non-dimensionalized by expressing them in terms of the unperturbed tube radius R; by plugging back R into the equations we find that the equilibrium distance between the rings increases with R (Fig. S. 5).

For the interactions between two infinite rods, the Green's function becomes:

$$G(\Theta) = \frac{1}{32\pi}\Big[\cos(\Theta)\left(4\mathrm{Li}_2\left(e^{-i\Theta}\right) + 4\mathrm{Li}_2\left(e^{i\Theta}\right) - 11\right) + 12(\Theta-\pi)\sin(\Theta)\Big], \tag{S. 17}$$

where $\mathrm{Li}_n(z) = \sum_{m=1}^{\infty} \frac{z^m}{m^n}$ (with $z \in \mathbb{C}$) is the polylogarithm function. Like the interaction between two rings, the inclusions' attraction and repulsion strength depends on the radius of the tube (Fig. S. 6).

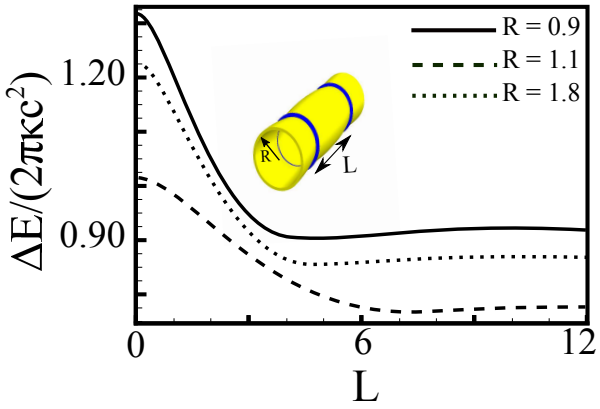

Figure S. 5: The competition between bending modulus and surface tension of the tube determines both the radius of the tube ($R = \sqrt{\kappa/2\sigma}$) and the equilibrium distance between two rings.

Evaluating the summation series in Eq. S. 8, we obtain the Green's function for point like inclusions:

$$
\begin{aligned}
G(\theta,\zeta) = {} & \frac{e^{-\frac{\zeta}{\sqrt{2}}}\left(\sin\left(\frac{\zeta}{\sqrt{2}}\right)+\cos\left(\frac{\zeta}{\sqrt{2}}\right)\right)}{4\sqrt{2}\pi} + \frac{e^{-\frac{1}{2}(2+\sqrt{2})\zeta - i\theta}}{512\pi} \\
& - \left(\left(115+64\sqrt{2}\right)e^{\sqrt{2}\zeta} - 64\sqrt{2} + 115\right)\left(1+e^{2i\theta}\right) + e^{\zeta+i\theta}\left(32\sqrt{2}\left(e^{\sqrt{2}\zeta}-1\right)\mathrm{Li}_2\left(e^{-\zeta-i\theta}\right)\right. \\
& + 32\sqrt{2}\left(e^{\sqrt{2}\zeta}-1\right)\mathrm{Li}_2\left(e^{i\theta-\zeta}\right) + 32\left(e^{\sqrt{2}\zeta}+1\right)\mathrm{Li}_3\left(e^{i\theta-\zeta}\right) + 32\left(e^{\sqrt{2}\zeta}+1\right)\mathrm{Li}_3\left(e^{-\zeta-i\theta}\right) \\
& + 32\sqrt{2}\left(e^{\sqrt{2}\zeta}-1\right)\mathrm{Li}_4\left(e^{-\zeta-i\theta}\right) + 32\sqrt{2}\left(e^{\sqrt{2}\zeta}-1\right)\mathrm{Li}_4\left(e^{i\theta-\zeta}\right) + 40\left(e^{\sqrt{2}\zeta}+1\right)\mathrm{Li}_5\left(e^{-\zeta-i\theta}\right) \\
& + \left.40\left(e^{\sqrt{2}\zeta}+1\right)\mathrm{Li}_5\left(e^{i\theta-\zeta}\right) + 43\left(e^{\sqrt{2}\zeta}+1\right)\mathrm{Li}_7\left(e^{i\theta-\zeta}\right) + 43\left(e^{\sqrt{2}\zeta}+1\right)\mathrm{Li}_7\left(e^{-\zeta-i\theta}\right)\right)\Big).
\end{aligned}
\tag{S. 18}
$$

S. 6.3. Effect of Casimir forces

Membrane mediated interactions between inclusions like proteins embedded in a biological membrane originate from both the average deformation of the membrane and the constraints imposed on the fluctuations of the membrane. One can investigate the thermal fluctuation effects by constructing the canonical partition function of the fluctuation field (which in our work is parametrized by $u(\theta,\zeta)$) and applying the boundary conditions that are imposed by the inclusions. Following early work done by Ref. 43 of the main text, we would get exactly the same relation for the thermal energy:

$$
\Delta E^{\mathrm{C}} = \frac{k_B T}{2} \ln\det(M), \tag{S. 19}
$$

where M is the matrix composed of derivatives of the Green's function that we derived for a membrane tube. Considering thermal Casimir effects, the total energy of the membrane becomes $\Delta E = \Delta E^{\mathrm{bend}} + \Delta E^{\mathrm{C}}$, where ΔE^{bend} is the bending energy of the mem-

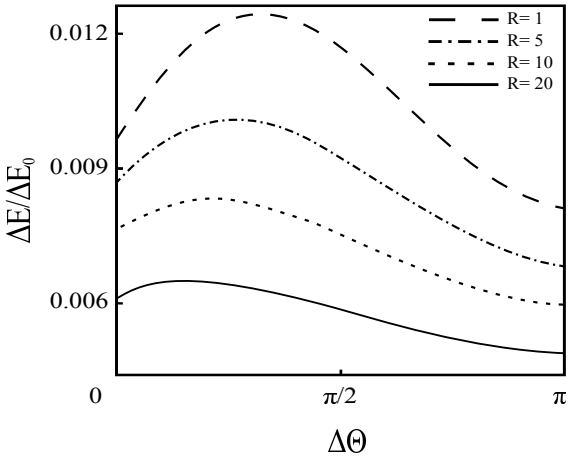

Figure S. 6: In the limit of large radii, the interaction between two rods becomes mostly repulsive, approaching the planar membrane case of pure repulsion.

brane, which is our primary interest in this work. As one can see, ΔE^{C} depends only on the distance between the inclusions, which is hidden in the matrix M, and not the amount of curvature that is imposed. As illustrated in Fig. S. 7, the thermal effect is about an order of magnitude weaker than the mean-field contribution in the total energy of the membrane.

S. 6.4. Monte Carlo simulations

During MC simulations, we simultaneously equilibrate two copies of our system in two different inverse temperatures ($\beta = \kappa / k_{\mathrm{B}} T$). For each copy of the system we use the Metropolis algorithm [41]: we accept any change in the configuration of our system with the probability $P[\Omega_n \rightarrow \Omega_{n+1}] = \min[1, \exp(-\beta \Delta E)]$. Global movements of inclusions are also allowed during simulations. The maximum step size of inclusions is adjusted such that acceptance rate of proposed moves is 50 %. In the end, in addition to (locally) minimizing the energy of the system in two different temperatures (β_1 and β_2) separately, we also (globally) exchange the whole configurations corresponding to the temperatures based on the Metropolis algorithm: $P_{\mathrm{Exch.}} = \min[1, \exp\big(-(\beta_2 - \beta_1)(E_2 - E_1)\big)]$. More details about the method can be found in Refs. 41 and 42 of the main text.

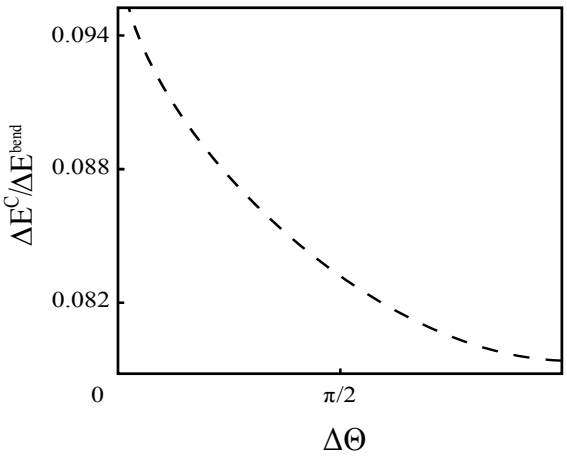

Figure S. 7: Ratio of fluctuation-induced energy to bending energy for an imposed curvature of $c = \frac{10}{R}$ and a bending modulus of $\kappa = 25 k_B T$.

References

[1] G. Koster, A. Cacciuto, I. Derényi, D. Frenkel, and M. Dogterom, *Force barriers for membrane tube formation,* Phys. Rev. Lett. **94**, 068101 (2005).

[2] E. Evans, H. Bowman, A. Leung, D. Needham, and D. Tirrell, *Biomembrane templates for nanoscale conduits and networks,* Science **273**, 933 (1996).

[3] A. Karlsson, R. Karlsson, M. Karlsson, A.-S. Cans, A. Strömberg, F. Ryttsén, and O. Orwar, *Molecular engineering: networks of nanotubes and containers,* Nature **409**, 150 (2001).

[4] T. R. Powers, G. Huber, and R. E. Goldstein, *Fluid-membrane tethers: minimal surfaces and elastic boundary layers,* Phys. Rev. E **65**, 041901 (2002).

[5] A. Roux, G. Cappello, J. Cartaud, J. Prost, B. Goud, and P. Bassereau, *A minimal system allowing tubulation with molecular motors pulling on giant liposomes,* Proc. Natl. Acad. Sci. U.S.A. **99**, 5394 (2002).

[6] Y. Shibata, J. Hu, M. M. Kozlov, and T. A. Rapoport, *Mechanisms shaping the membranes of cellular organelles,* Annual Review of Cell and Developmental **25**, 329 (2009).

[7] R. Bar-Ziv and E. Moses, *Instability and" pearling" states produced in tubular membranes by competition of curvature and tension,* Phys. Rev. Lett. **73**, 1392 (1994).

[8] I. Derényi, F. Jülicher, and J. Prost, *Formation and interaction of membrane tubes,* Phys. Rev. Lett. **88**, 238101 (2002).

[9] J.-B. Fournier and P. Galatola, *Critical fluctuations of tense fluid membrane tubules,* Phys. Rev. Lett. **98**, 018103 (2007).

[10] S. Monnier, S. B. Rochal, A. Parmeggiani, and V. L. Lorman, *Long-range protein coupling mediated by critical low-energy modes of tubular lipid membranes,* Phys. Rev. Lett. **105**, 028102 (2010).

[11] E. V. Polishchuk, A. Di Pentima, A. Luini, and R. S. Polishchuk, *Mechanism of constitutive export from the golgi: bulk flow via the formation, protrusion, and en bloc cleavage of large trans-golgi network tubular domains,* Mol. Biol. Cell **14**, 4470 (2003).

[12] M. Goulian, R. Bruinsma, and P. Pincus, *Long-range forces in heterogeneous fluid membranes,* Europhys. Lett. **22**, 145 (1993).

[13] T. R. Weikl, M. M. Kozlov, and W. Helfrich, *Interaction of conical membrane inclusions: Effect of lateral tension,* Phys. Rev. E **57**, 6988 (1998).

[14] K. S. Kim, J. C. Neu, and G. F. Oster, *Many-body forces between membrane inclusions: A new pattern-formation mechanism,* Europhys. Lett. **48**, 99 (1999).

[15] J.-B. Fournier, P. G. Dommersnes, and P. Galatola, *Dynamin recruitment by clathrin coats: a physical step?* C. R. Biologies **326**, 467 (2003).

[16] T. Auth and G. Gompper, *Budding and vesiculation induced by conical membrane inclusions,* Phys. Rev. E **80**, 031901 (2009).

[17] E. Atilgan and S. X. Sun, *Shape transitions in lipid membranes and protein mediated vesicle fusion and fission,* J. Chem. Phys **126**, 095102 (2007).

[18] B. J. Reynwar, G. Illya, V. A. Harmandaris, M. M. Müller, K. Kremer, and M. Deserno, *Aggregation and vesiculation of membrane proteins by curvature-mediated interactions,* Nature **447**, 461 (2007).

[19] S. Morlot and A. Roux, *Mechanics of dynamin-mediated membrane fission,* Annu. Rev. Biophys. **42**, 629 (2013).

[20] T. Idema, S. Semrau, C. Storm, and T. Schmidt, *Membrane mediated sorting,* Phys. Rev. Lett. **104**, 198102 (2010).

[21] B. J. Reynwar and M. Deserno, *Membrane-mediated interactions between circular particles in the strongly curved regime,* Soft Matter **7**, 8567 (2011).

[22] J. C. Pàmies and A. Cacciuto, *Reshaping elastic nanotubes via self-assembly of surface-adhesive nanoparticles,* Phys. Rev. Lett. **106**, 045702 (2011).

[23] A. Šarić and A. Cacciuto, *particle self-assembly on soft elastic shells,* Soft Matter **7**, 1874 (2011).

[24] D. Zhang, A. Chai, X. Wen, L. He, L. Zhang, and H. Liang, *Ordered regular pentagons for semiflexible polymers on soft elastic shells,* Soft Matter **8**, 2152 (2012).

[25] A. Šarić and A. Cacciuto, *Self-assembly of nanoparticles adsorbed on fluid and elastic membranes,* Soft Matter **9**, 6677 (2013).

[26] N. Ramakrishnan, P. B. S. Kumar, and R. Radhakrishnan, *Mesoscale computational studies of membrane bilayer remodeling by curvature-inducing proteins,* Phys. Rep. **543**, 1 (2014).

[27] P. G. Dommersnes and J.-B. Fournier, *N-body study of anisotropic membrane inclusions: Membrane mediated interactions and ordered aggregation,* Eur. Phys. J. E **12**, 9 (1999).

[28] P. G. Dommersnes and J.-B. Fournier, *The many-body problem for anisotropic membrane inclusions and the self-assembly of "saddle" defects into an "egg carton",* Biophys. J. **83**, 2898 (2002).

[29] J.-B. Fournier, *Dynamics of the force exchanged between membrane inclusions,* Phys. Rev. Lett. **112**, 128101 (2014).

[30] R. Shlomovitz and N. Gov, *Membrane-mediated interactions drive the condensation and coalescence of ftsz rings,* Phys. Biol. **6**, 046017 (2009).

[31] P. B. Canham, *An earlier derivation of the curvature free energy appeared in j. theor,* Biol **26**, 61 (1970).

[32] W. Helfrich, *Elastic properties of lipid bilayers: theory and possible experiments,* Zeitschrift für Naturforschung C **28**, 693 (1973).

[33] C. Barbetta, A. Imparato, and J.-B. Fournier, *On the surface tension of fluctuating quasi-spherical vesicles,* Eur. Phys. J. E **31**, 333 (2010).

[34] V. G. Almendro-Vedia, F. Monroy, and F. J. Cao, *Mechanics of constriction during cell division: a variational approach,* PLoS ONE **8**, e69750 (2013).

[35] V. G. Almendro-Vedia, F. Monroy, and F. J. Cao, *Analytical results for cell constriction dominated by bending energy,* Phys. Rev. E **91**, 012713 (2015).

[36] J. Z. Y. Chen and S. Mkrtchyan, *Adhesion between a rigid cylindrical particle and a soft fluid membrane tube,* Phys. Rev. E **81**, 041906 (2010).

[37] M. M. Müller, M. Deserno, and J. Guven, *Balancing torques in membrane-mediated interactions: Exact results and numerical illustrations,* Phys. Rev. E **76**, 011921 (2007).

[38] N. Metropolis, A. W. Rosenbluth, M. N. Rosenbluth, A. H. Teller, and E. Teller, *Equation of state calculations by fast computing machines,* J. Chem. Phys **21**, 1087 (1953).

[39] U. H. E. Hansmann, *Parallel tempering algorithm for conformational studies of biological molecules,* Chem. Phys. Lett. **281**, 140 (1997).

[40] H. Li and M. Kardar, *Fluctuation-induced forces between manifolds immersed in correlated fluids,* Phys. Rev. A **46**, 6490 (1992).

[41] H.-K. Lin, R. Zandi, U. Mohideen, and L. P. Pryadko, *Fluctuation-induced forces between inclusions in a fluid membrane under tension,* Phys. Rev. Lett. **107**, 228104 (2011).

3

Curvature sensing inclusions

Eukaryotic cells are densely packed with macromolecular complexes and intertwining organelles, which are continually transported and reshaped. Intriguingly, organelles avoid clashing and entangling with each other in such limited space. Mitochondria, for example, form extensive networks that are constantly remodeled by fission and fusion. In this chapter we study how such fission and fusion events can be triggered, facilitated and even driven by mechanical forces generated by the shape of proteins. Collective membrane induced interactions particulaly occur in highly curved and closed organelle membranes. Using Monte Carlo simulations, we investigate the effect of protein shape on their interactions in a tubular membrane. We particularly reveal that spherical proteins collectively self-assemble into ringlike structures. We further demostrate that depending on the curvature of crescent-shaped proteins, they form different patterns. Finally, we use our simulations to explain some recently obtained experimental results showing that the mitochondrial fission machinery utilizes a similar mechanism to discern mechanically stressed (highly curved) regions of tubular membranes. Consequently, they are recruited by such regions and in sufficiently high densities proteins drive subsequent division in order to prevent entanglement with tubes of the ER network.

A version of this chapter has been published as: S. C. J. Helle *et al.*, *Mechanical force induces mitochondrial fission*, eLife **6** (2017)

3.1. Introduction

Constant shape transformations are a hallmark of cellular and subcellular lipid membranes. Despite the constant fission and fusion of membranes, a cell can maintain its integrity and compartmentalization to a fascinately high degree. The extrinsic shape of membranous organelles are controlled by various mechanisms, most of which are comprehensively discussed in chapter 1. Dynamic feature of membranes leads to spanning the whole volume of the cell and of the organelles inside the cell with interconnected and intertwining membranous structures. Flattened sacs of membranes connected with tubular networks and enclosed vesicles in organelles like the Golgi apparatus, the endoplasmic reticulum (ER) and mitochondria are the prime examples (see [1, 2] and the references therein). In all of these organelles, such diversity in shape and size can exist without entanglement or encroachment of the confined structures. In the particular case of mitochondria, a complicated network of tubular membranes are enclosed in a limited volume. The occurence of drastic entanglements could lead to the release of cytochrome c from mitochondria into the cytosol which is a key step in the induction of apoptosis [3] – the process of cell self-destruction. Recent studies have identified some specific proteins called mitochondrial fission factors (MFF) that are responsible for recruiting the necessary machineries like Drp1 proteins involved in mitochondrial constrictions [4]. It has also been uncovered that in the ER, specific types of membrane-shaping proteins contribute in the generation of highly curved tubules [5].

Having unraveled the protein-dependent shape of membranes, it is intriguing to investigate how proteins can collectively discern and respond to membrane curvature. An enormous amount of experimental[6–10] and numerical[11–17] research has therefore been dedicated to understand how proteins induce curvature and subsequently how they interact via the deformation they impose on the shape of membrane. Proteins not only can induce the curvature, but also sense the geometrical shape of membranes. These two features are closely connected to each other, acting as two sides of the same coin. In high concentrations, curvature sensing inclusions can aggregate into a cluster and as a whole stabilize the shape and even deform the membrane (see chapter 1). In contrast to previous studies, in most of which membranes usually follows the preferential shape of proteins, we investigate how curved proteins on the surface of a tubular membrane can dictate the curvature.

Through a numerical approach, using a triangulated network, we explain how these two seemingly paradoxical features are connected to each other. We first explain the model in detail as it will be used in the later chapters as well. We then show that the curvature of membranes results in completely different emergent patterns of proteins: Spherical colloids self-assemble into ringlike structures and crescent-shaped proteins form either lines or clusters of many inclusions. We further demonstrate that mechanically stressed regions of a membrane tube drive proteins to accumulate there. In the end, we use our results to explain some recently obtained experimental findings on the constriction of mitochondria. The results show that mitochondrial fission factors (MFF) in high concentration, attract each other and constrict the membrane. They also exhibit an affinity for mechanically pre-constricted regions, consistent with the result of our simulations.

3.2. Model

It is not always possible to analytically solve the shape equation of a membrane for any given arbitrary geometry. Hence, as a remedy, many models has been developed to numerically analyze the curvature energy. Depending on the scale of the problem, one may choose between the proposed models. For example, models like molecular dynamics simulations have extensively been used to study the atomistic structure of BAR domains [18]. Since it is computationally too costly to use full atomistic models to investigate the phenomena like membrane mediated interactions occurring on larger length scales [1], various course-grained methods have been suggested. Such modelings can be done either using numerical tools or in continuum regimes. Continuum models are already explained in chapter 1 and applied to tubular membranes in chapter 2. In contrast to fully atomistic models which are explicit, numerical coarse-grained methods treat the membrane implicitly. They describe the membrane as a thin layer composed of many segments, where each unit represents a collection of atoms in the actual membrane [19]. One of the popular coarse grained models is the dynamically triangulated network (see Ref. [16] and references therein) which we use as our approach throughout this thesis.

As shown in Fig. 3.1A and B, we assume our hollow membrane tube is composed of many vertices (shown in the figure and henceforth referred to as beads) which are connected by proper bonds to form a triangulated mesh. The model assumes that the lipid bilayer consists of many patches (of size ~ 10 nm), with each patch representing a collection of molecules. We use the classical Canham-Helfrich model (in the form of a dihedral angle potential) to define the curvature energy of the membrane:

$$\Delta E_{\mathrm{CH}} = \kappa \sum_{<ij>} 1 - \mathbf{n}_i \cdot \mathbf{n}_j, \tag{3.1}$$

where $\mathbf{n}_i$ and $\mathbf{n}_j$ are the normal vectors of each pair of triangles (as shown in Fig. 3.1B) and κ is the bending modulus. The summation runs over all pairs of neighboring triangles i and j. To simulate the fluidity of the membrane, we allow the common edge between any pair of neighboring triangles to flip, provided that it is energetically beneficial for the system (Fig. 3.1D). We have ignored the spontaneous and Gaussian curvatures in this approach. Including the latter, based on Gauss-Bonnet theorem, would not change the final results as our topology is conserved during the simulation. The change in the membrane area due to the movement of beads is not for free and associated with an energy penalty as:

$$\Delta E_{\mathrm{s}} = \gamma \mathrm{dA}. \tag{3.2}$$

We impose no conditions on the total area and volume of the tube. To enable the proteins to adhere to the membrane, we introduce a ligand-receptor like attraction potential between the colloids and membrane beads, given by:

$$\Delta E_{\mathrm{Ad}} = \begin{cases} -\varepsilon \left(\frac{D_{\min}}{r} \right)^6, & \theta < \theta_{\mathrm{wr}} \\ 0, & \text{otherwise} \end{cases} \tag{3.3}$$

[1] For the lengths that are several order of magnitude greater than the thickness of the membrane which is about 5 nm.

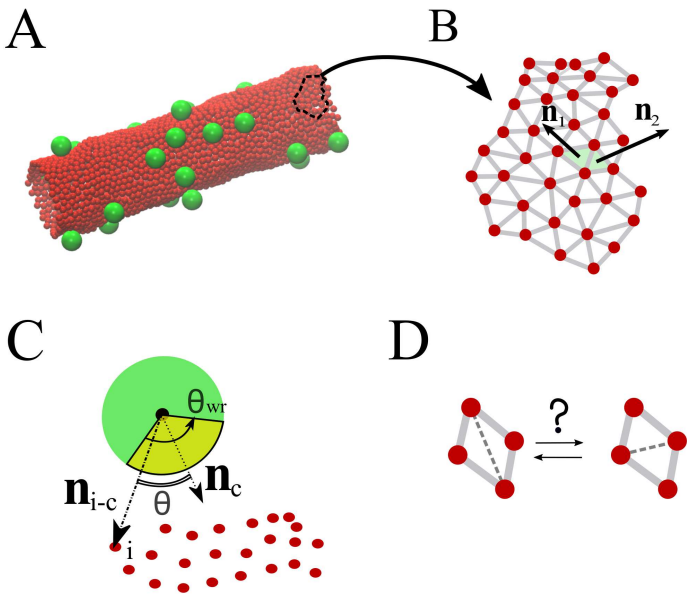

Figure 3.1: We model the membrane tube as composed of many vertices (red beads in (A)) which form a triangulated network (B). Fluidity of membrane is simulated by changing the connection in any two neghboring pairs of triangles (D). In order to study the membrane mediated interactions, we introduce an adhesion force between the colloids (colored in green in (A)) and beads to deform the tube (C). The surface area of every colloid is paratitioned into two passive and active (controlled by angle θ_{wr}) parts. We found the membrane beads that are exposed to the active part via introducing an angle between the director vector of the active patch ($\mathbf{n}_{\text{c}}$) and the vector connecting the center of the colloid to any arbitrary neighboring bead i ($\mathbf{n}_{\text{i}-\text{c}}$).

where ε is the adhesive strength, and D_{min} and r are, respectively, the minimum allowed distance and the center to center distance between colloids and membrane beads. Using the Kern and Frenkel patchy model [20], we introduce a wrapping angle θ_{wr} as shown in Fig. 3.1C, so proteins attract the membrane only by the active part of their structure.

Having defined all the terms contributing to the total energy of the tube ($\Delta E = \Delta E_{\text{Ad}} + \Delta E_{\text{s}} + \Delta E_{\text{CH}}$), we use Monte Carlo simulations to minimize the total energy of the membrane and find the most energetically favorable configuration. We use the common Metropolis algorithm for this purpose [21]. This algorithm perturbs the system by random moves and then checks for the energy change to examine whether it is beneficial for the system or not. It correspondingly accepts the move with a certain probability (see supplemental material in chapter 2). The configuration of the system is distorted by various moves: First, we randomly move the proteins and membrane beads. Second, we slightly rotate the colloids' normal vector ($\mathbf{n}_c$ in Fig. 3.1C).

We also want to examine the interaction between crescent-like proteins, for which we first need to model such shapes. In order to do so, we construct the proteins with a linear chain of five spheres positioned on a circular arc with a radius of R_{pr} (Fig. 3.2A). Having introduced such proteins into the system, in addition to the previous MC moves, we also include rotating the two wings of a protein around its central colloid (keeping

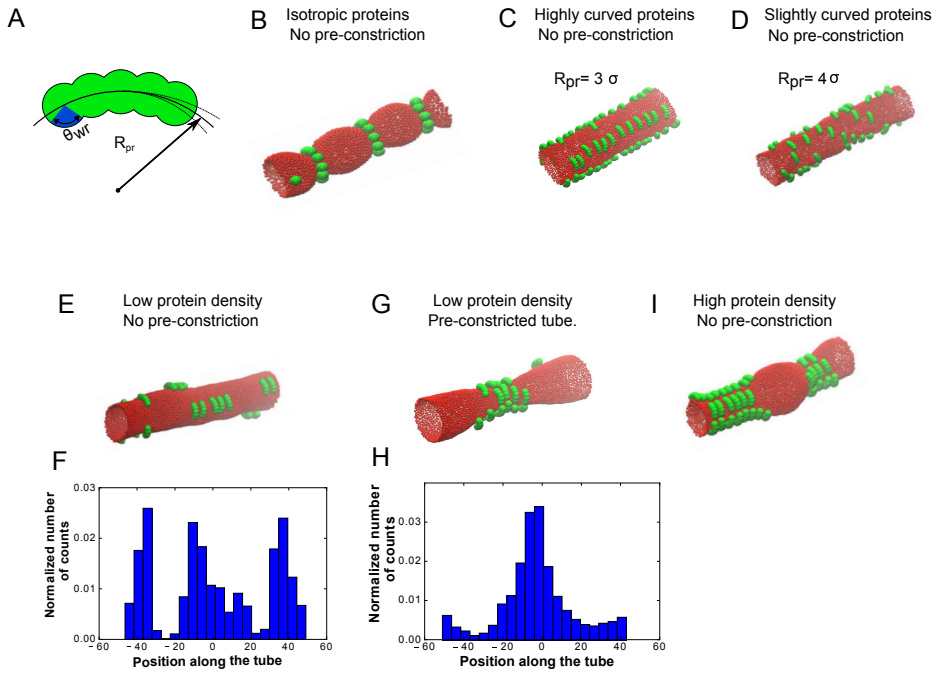

Figure 3.2: Monte Carlo simulation of protein-membrane interactions for different conditions. (A) Proteins were modelled as a linear chain built out of five spheres positioned on a circular arc. Each sphere has a diameter of $4\,\sigma$. (B) Spherical proteins form ring-like structures. (C) Highly curved proteins attracted each other, but only in the longitudinal, and not angular, direction. (D) Slightly curved proteins do not self-assemble at all. In contrast to D and C there is an optimum curvature of proteins for which they attract each other in both angular and longitudinal directions. This requires high density of proteins. (E and F) Proteins with optimum curvature do not exhibit significant collective interaction in low densities. (G and H) In contrast, when the tube is pre-constricted, they sense the region that is under stress and accumulate there. (I) In sufficiently high number, proteins attract each other and constrict the tube (without having pre-constriction).

the angle between them fixed), rotating the whole protein around a random axis, and changing the angle between the wings of any randomly chosen protein.

All the lengths are measured in the units of the diameter of membrane beads (σ). Correspondingly, we choose the following biologically relevant values for the parameters in our model during the simulations: $D_{col} = 4\sigma$, $\kappa = 20$ kT, $\varepsilon = 3.8$ kT, $\gamma = 1\,\mathrm{kT}/\sigma^2$. For the coarse-grained length scale of $\sigma = 20$ nm (large enough to neglect any kinds of intermolecular interactions), we have proteins of diameter 80 nm and a surface tension of $\gamma = 0.01$ pN/nm.

3.3. Results

First we simulate a system with a tube of diameter $\mathrm{D_t} = 13\sigma$ and length $\mathrm{L_t} = 55\sigma$, containing $N_{pr} = 30$ spherical proteins and $\mathrm{N_b} = 2000$ beads. MC simulations were performed in the npT ensemble with periodic boundary conditions, with $p = 0$, to generate the most energetically favorable configuration. We choose the initial configuration of pro-

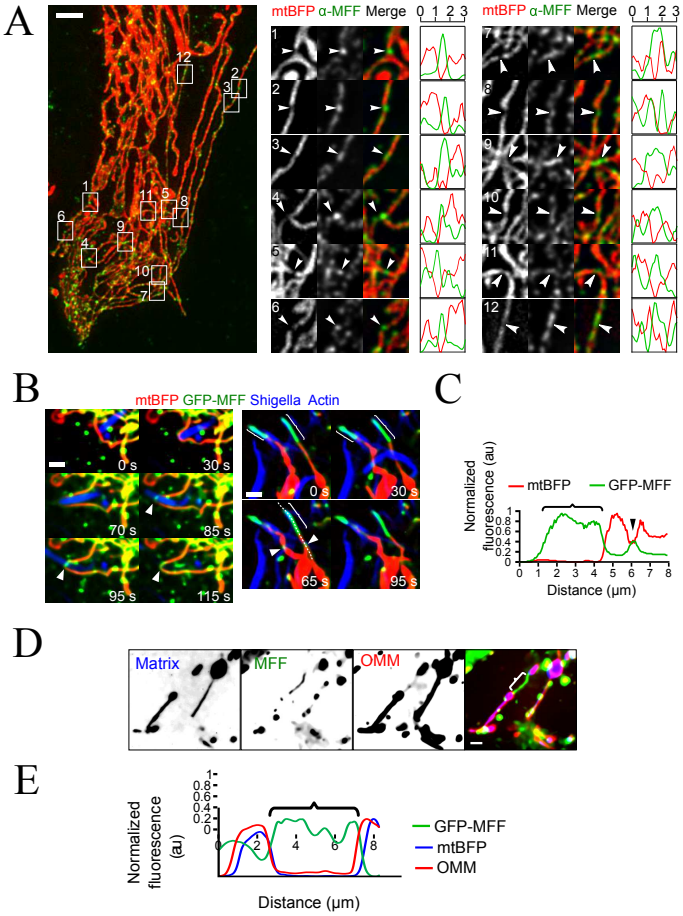

Figure 3.3: Membrane fission machinery recruitment by mechanical cues in mitochondria. (A) Immunofluorescence of KERMIT cells transduced with shDRP1, using an anti-MFF antibody (green). Mitochondrial matrix (mtBFP) is shown in red. Insets on the right correspond to the framed areas on the left. Arrowheads point at naturally occuring constrictions on the mitochondria. Plots are linescans of the mitochondria (red) and MFF (green) signals around the constriction. X-axis is in µm. Y-axis is normalized fluorescence in arbitrary units. (B) MFF is recruited to sites of encounter with *S. flexneri* (white arrowheads). Right panels also show two examples of MFF enrichment at sites of mitochondria thinning (curly brackets), as indicated by reduction of matrix mtBFP signal, independent of *Shigella* encounter. (C) Line scan of mtBFP and MFF signal of the white dotted line in (B). Arrowhead and curly bracket correspond to same zones in (B). Normalized background-subtracted pixel values are plotted as arbitrary units. (D) MFF spontaneously stabilizes thin mitochondrial section (curly brackets) that are devoid of matrix staining but retain continuous OMM signal. (F) Line scan of mtBFP, GFP-MFF and OMM signal of the curly bracket in (D).
Scale bars, A: 5 μm, B,D: 2 μm. Reprinted from [8].

teins randomly (Fig. 3.1A). As depicted in Fig. 3.2B, spherical proteins attract each other only in the transversal, and not in the longitudinal direction. When there are many of them, they form ring like structures. This result is consistent with the analytical calculations we did in chapter 2. One might expect helical like structures for the final shape of self-assembled colloids, but we found that these do not occur on fluid membranes. Having done similar simulations on elastic tubes, Pàmies and Cacciuto [17] showed that spherical nanoparticles adhering to the outer surface of an elastic nanotube form diverse aggregates including helical, linelike and ringlike structures. They also showed that in the regime where the membranes are stretch-free (like fluid membranes), particles form rings.

Next, we examine the interaction between banana-shaped proteins (Fig. 3.2A). The center-to-center distance between the spheres within a protein was adjusted to 2/3 of the diameter of the individual spheres. The two "wings" of the protein (constituted by the two spheres on each side of the central one) were rigid and allowed to rotate around the middle sphere. We also incorporated flexibility between the two wings by imposing an angular potential between them as: $E_{flex} = \frac{1}{2} k_{flex}(\theta - \theta_{eq})^2$, where k_{flex} and θ_{eq} are the strength of the potential and the equilibrium angle between the two wings, respectively. We set these parameters as $k_{flex} = 20kT$ and $\theta_{eq} = 2\pi/3$. As one can imagine, we can get different patterns depending on how curved the proteins are. Our proteins have two features: First they can discern the curvature of the tube via their inner surface area. Second, they imposed their shape on the tube. The equilibrium shape of the tube therefore depends on which of these two effects dominates. For low protein curvature the proteins act as rigid rods and show no significant patterns, as they repel each other in all directions (Fig. 3.2D). In contrast, when proteins are highly curved, they favor accumulating in longitudinal direction (Fig. 3.2C). The reason that the resultant lines of proteins do not merge originates from the sharp tails of the deformation following the shape of proteins in the transversal direction.

After finding the optimal ratio of the protein and tube diameters that lead to protein assembly, we perform another simulation, where we use an arbitrarily low protein density (Fig. 3.2E). Under such conditions, the proteins diffuse freely on the membrane tube and remain homogenously distributed (Fig. 3.2F). We then run the simulation again, but this time, we pre-impose a constriction in the membrane tube, to mimic mechanical stimulation, and observe that the proteins accumulate at the pre-constricted site (Figs. 3.2 G and H). Next, we simulate a system with a high density of protein. Interestingly, under these conditions the proteins spontaneously constrict the membrane tube even without a pre-imposed constriction (Fig. 3.2I). The results of our generic model suggest that in high protein densities, curvature sensing proteins can act as curvature inducing objects. Proteins can respond to mechanical forces on the membrane through the induced deformations. They sense the shape, accumulate at the region of deformation and stabilize the pre-curved regions, leading to membrane fission. In a high density, proteins can also constrict membrane tubes.

The results of our simulations strongly resemble the MFF-stabilized, matrix-free thin mitochondria sections observed in recently published experiments by Helle et al. [8]. They have investigated the molecular mechanisms in mitochondria underlying not only their response to biochemical, but also to mechanical cues. Such forces drive the recruit-

ment and activation of the fission effector DRP1, and raised the question of how such mechanical stimulus was sensed at the molecular level. DRP1 is a cytosolic protein, and is recruited to mitochondria by integral mitochondrial membrane adaptor molecules such as MFF. Helle et al. have done the experiments in two ways: First, they have investigated to see how mitochondria cope with being hit by an intracellular fast-moving object, namely, *Shigella flexneri*. Upon entry into the cytoplasm of infected cells, a subpopulation of the bacteria hijacks the actin cytoskeleton and stimulates its polymerization on the bacterial surface, forming so-called actin comet tails [22] allowing them to propel rapidly through the cytoplasm reaching speeds of up to 0.5μm/s. Second, they have over-expressed MFF to see if it can constrict mitochondria.

As depicted in Fig. 3.3A (arrowheads in right panels), MFF has a tendency to accumulate at constrictions that happen sporadically on a non-perturbed mitochondrial tubule. Also, upon *Shigella*-triggered mechanical stimulations, MFF exhibits an affinity towards those spots (Figs. 3.3B and C). Finally, in sufficiently high density of MFF, they accumulate and constrict mitochondria even without any externally mechanical triggers(Figs. 3.3D and E).

3.4. In a nutshell

Because it seemed contradicting that some proteins behave as both a sensor and inducer of membrane curvature, we wondered whether these two properties may be coupled. To test this hypothesis, we turned to computer-assisted Monte Carlo (MC) simulations and modelled a generic protein with an affinity for constricted tubes like those in mitochondria. We showed that proteins in a high density and with an optimum curvature self-assemble, in consistence with aggregation of mitochodrial fission factor proteins in recently reported experiments. Similar collective curvature mediated interactions can also occur in other sub-cellular organelles.

References

[1] H. T. McMahon and J. L. Gallop, *Membrane curvature and mechanisms of dynamic cell membrane remodelling,* Nature **438**, 590 (2005).

[2] H. T. McMahon and E. Boucrot, *Membrane curvature at a glance,* J Cell Sci **128**, 1065 (2015).

[3] V. Gogvadze, S. Orrenius, and B. Zhivotovsky, *Multiple pathways of cytochrome c release from mitochondria in apoptosis,* Biochimica et Biophysica Acta (BBA)-Bioenergetics **1757**, 639 (2006).

[4] H. Otera, C. Wang, M. M. Cleland, K. Setoguchi, S. Yokota, R. J. Youle, and K. Mihara, *Mff is an essential factor for mitochondrial recruitment of drp1 during mitochondrial fission in mammalian cells,* The Journal of cell biology **191**, 1141 (2010).

[5] J. Hu, Y. Shibata, C. Voss, T. Shemesh, Z. Li, M. Coughlin, M. M. Kozlov, T. A. Rapoport, and W. A. Prinz, *Membrane proteins of the endoplasmic reticulum induce high-curvature tubules,* Science **319**, 1247 (2008).

[6] M. Perry and A. B. Gilbert, *Yolk transport in the ovarian follicle of the hen (gallus domesticus): lipoprotein-like particles at the periphery of the oocyte in the rapid growth phase,* Journal of cell science **39**, 257 (1979).

[7] H. Ewers, W. Römer, A. E. Smith, K. Bacia, S. Dmitrieff, W. Chai, R. Mancini, J. Kartenbeck, V. Chambon, L. Berland, *et al.*, *Gm1 structure determines sv40-induced membrane invagination and infection,* Nature cell biology **12**, 11 (2010).

[8] S. C. J. Helle, Q. Feng, M. J. Aebersold, L. Hirt, R. R. Grüter, A. Vahid, A. Sirianni, S. Mostowy, J. G. Snedeker, A. Šarić, *et al.*, *Mechanical force induces mitochondrial fission,* eLife **6** (2017).

[9] B. J. Peter, H. M. Kent, I. G. Mills, Y. Vallis, P. J. G. Butler, P. R. Evans, and H. T. McMahon, *Bar domains as sensors of membrane curvature: the amphiphysin bar structure,* Science **303**, 495 (2004).

[10] I. Koltover, J. O. Radler, and C. R. Safinya, *Membrane mediated attraction and ordered aggregation of colloidal particles bound to giant phospholipid vesicles,* Phys. Rev. Lett. **82**, 1991 (1999).

[11] P. G. Dommersnes and J.-B. Fournier, *The many-body problem for anisotropic membrane inclusions and the self-assembly of "saddle" defects into an "egg carton",* Biophys. J. **83**, 2898 (2002).

[12] T. Auth and G. Gompper, *Budding and vesiculation induced by conical membrane inclusions,* Phys. Rev. E **80**, 031901 (2009).

[13] B. J. Reynwar, G. Illya, V. A. Harmandaris, M. M. Müller, K. Kremer, and M. Deserno, *Aggregation and vesiculation of membrane proteins by curvature-mediated interactions,* Nature **447**, 461 (2007).

[14] M. Simunovic, G. A. Voth, A. Callan-Jones, and P. Bassereau, *When physics takes over: Bar proteins and membrane curvature,* Trends in cell biology **25**, 780 (2015).

[15] D. Nelson, T. Piran, and S. Weinberg, *Statistical mechanics of membranes and surfaces* (World Scientific, 2004).

[16] H. Noguchi, *Membrane simulation models from nanometer to micrometer scale,* Journal of the Physical Society of Japan **78**, 041007 (2009).

[17] J. C. Pàmies and A. Cacciuto, *Reshaping elastic nanotubes via self-assembly of surface-adhesive nanoparticles,* Phys. Rev. Lett. **106**, 045702 (2011).

[18] A. Arkhipov, Y. Yin, and K. Schulten, *Four-scale description of membrane sculpting by bar domains,* Biophysical journal **95**, 2806 (2008).

[19] B. J. Reynwar and M. Deserno, *Membrane-mediated interactions between circular particles in the strongly curved regime,* Soft Matter **7**, 8567 (2011).

[20] N. Kern and D. Frenkel, *Fluid–fluid coexistence in colloidal systems with short-ranged strongly directional attraction,* The Journal of chemical physics **118**, 9882 (2003).

[21] N. Metropolis, A. W. Rosenbluth, M. N. Rosenbluth, A. H. Teller, and E. Teller, *Equation of state calculations by fast computing machines,* J. Chem. Phys **21**, 1087 (1953).

[22] K. Ray, B. Marteyn, P. J. Sansonetti, and C. M. Tang, *Life on the inside: the intracellular lifestyle of cytosolic bacteria,* Nature Reviews Microbiology **7**, 333 (2009).

4

Towards stability conditions of membranous tubules covered with intercalated molecules

Cellular membranes define the physical boundaries of a cell and intracellular organelles, in addition to serving as a platform for the function of many inclusions like proteins. The recruitment and spatial organization of macromolecules on the surface of membranes is crucial for driving dynamic cellular phenomena such as cell division or endo-/exo-cytosis. In this chapter, we study how the presence of intercalated molecules in a tubular lipid bilayer influences their characteristic properties, including bending modulus and effective surface tension. We further show that the lipid bilayer in turn induces an inhomogeneous distribution of the embedded molecules. In particular, a uniform density of proteins on a tubular membrane exhibits unstable behavior and segregates into different domains. Understanding such an interplay between the membrane shape and the organization of embedded proteins is of fundamental interest and necessary for the ongoing attempts to artificially mimic membrane associated processes – as a crucial step in the creation of synthetic cells.

This chapter is based on: A. Vahid and T. Idema, *Pattern formation of intercalated molecules in tubular membranes* (in preparation)

4.1. Introduction

Cellular membranes such as the plasma membrane are soft thin layers that encapsulate the internal content of a cell and intracellular organelles, separating their inside from the outside environment. Such biological membranes posses a range of characteristic shapes. Lipid membranes also host a diverse collection of inclusions, from integral and peripheral proteins to small impurities like cholesterol molecules. The spatial organization of membranes plays a substantial role in the interactions between embedded proteins, underlying diverse dynamic cellular phenomena like intracellular transport, cell division, and signal transduction [1]. The stability of membranous structures in turn depends on the shape and density of the molecules they contain [2, 3]. Such a coupling mechanism between membrane and proteins stems from the physical properties that biological membranes are endowed with. A membrane behaves like an elastic material when it undergoes any out-of-plane deformations. The deformations can be imposed by inclusions that are either embedded in or adhered to the membrane. The in-plane fluidity of the membrane, on the other hand, allows for the diffusion of the concomitant inclusions. Changing the membrane composition also affects this diffusion process. For example, it has recently been shown that protein crowding induces membrane deformations such as buds and tubules [4, 5] (see also **chapter 3**). Recruitment of dynamin proteins during the scission of endocytic/exocytic buds from the plasma membrane of a cell is another example of the extraordinary coordination between the membrane and proteins [1, 6].

Studying the physical principals governing the shape and dynamics of cellular membranes during the above-mentioned processes has been the subject of many theoretical [7–11] and experimental works [12, 13] (see also [1] and the references therein). On the theory side, it's been well understood that individual inclusions that are much larger than the size of lipids, communicate through non-pairwise interactions [11, 14, 15]. As a result, the membrane adopts a conformation that corresponds to the least deformation energy cost. We have used such a framework in previous chapters. We have particularly revealed various patterns that are spontaneously formed depending on interaction between the imposed curvature and the shape of the membrane. We can however have a different regime where the size (and number) of the proteins are comparable to that of the lipids. The compositional inhomogeneity of the lipid bilayer also belongs to such a scenario which is common both in a biological context and in artificial systems. Therefore, it is of great interest to understand how the cooperation between membrane shapes and the distribution of proteins is orchestrated. Here, we model a continuous density of proteins (or other types of inclusions) that can laterally diffuse on the plane of a membrane tube. We assume that the proteins act as a source of non-zero spontaneous curvature on the tube (and are, resultantly, coupled to the shape), otherwise a random distribution of the proteins would naturally ensue. Consequently, the proteins undergo segregation, both of which are strongly controlled by the elastic behavior of the membrane and the size of induced curvature.

We first describe the modified version of the Canham-Helfrich energy functional explained in **chapter 1**, coupled to the density of proteins. The modifications account for the curvature inducing feature of the proteins. We then obtain the new stability conditions for a tube in the presence of such molecules. Next, we derive two sets of evolution

equations for the distribution of proteins and the membrane shape. We apply linear stability analysis to the dynamic equations to characterize the unstable regime as a function of the relevant phenomenological parameters. Finally, we present some preliminary results that illustrate the spontaneous pattern formation of the proteins.

4.2. Results and discussion

We model the proteins as a continuous density that varies from one point to the other on the surface of the tube, in addition to its dependence on time. We assume that they induce weak deformations on the shape of the membrane. Using the phenomenological Landau-Ginsburg energy functional, we describe the density of molecules [1] on the membrane as:

$$E_\phi = \int \left[-\frac{\alpha}{2}\phi^2 + \frac{\beta}{4}\phi^4 + \frac{\gamma}{2}\left|\nabla\phi\right|^2 \right] dS, \tag{4.1}$$

where ϕ is the density difference, dS is the surface element, and α, β and γ are phenomenological coefficients determining the properties of molecules. The competition between β and α controls the equilibrium density difference in the system, $\left|\phi_{eq}\right| = \sqrt{\frac{\alpha}{\beta}}$, and the interface thickness between the final phase is in the order of $\delta^* = \sqrt{\frac{\gamma}{\alpha}}$ [16]. We define the curvature energy of the membrane using the common Canham-Helfrich energy functional as:

$$E_{el} = \int \left[\frac{\kappa}{2}(2H - \phi H_0)^2 + \sigma \right] dS, \tag{4.2}$$

where H, H_0 and σ are the mean curvature, the spontaneous curvature imposed by molecules and the surface tension of the membrane tube, respectively. The spontaneous curvature is defined as the amount of curvature (h_0) imposed by a patch of membrane of area s: $H_0 = h_0 \times s$ [3]. For a uniform density of molecules (ϕ_0) with a similar induced spontaneous curvature on the tube, the total energy density (E_{tot}) reads:

$$E_{\text{tot}} = 2\pi RL\left[-\frac{\alpha}{2}\phi_0^2 + \frac{\beta}{4}\phi_0^4 + \frac{\kappa}{2}(\frac{1}{R} - \phi_0 H_0)^2 + \sigma \right] - fL \tag{4.3}$$

with f the applied force required to pull a tube with length L and radius R from a "giant" unilamellar vesicle (GUV). Such tubes can be extracted experimentally from GUVs by various techniques like optical tweezers [12]. Having minimized Eq. 4.3 with respect to R and L, we obtain the following important relations for the equilibrium radius of a stable tube and corresponding required force:

$$\begin{aligned} R &= \sqrt{\frac{2\kappa}{\phi_0^2\left(-2\alpha + \beta\phi_0^2 + 2H_0^2\kappa\right) + 4\sigma}} \\ f &= -2\pi\kappa\phi_0 H_0 + \pi\sqrt{2\kappa\phi_0^2\left(-2\alpha + \beta\phi_0^2 + 2H_0^2\kappa\right) + 8\kappa\sigma} \end{aligned} \tag{4.4}$$

[1] We use the words proteins and molecules interchangeably throughout the whole chapter!

Setting the density of molecules to $\phi_0 = 0$ yields the same relations as in Ref. [12]. These predictions may experimentally be examined by pulling a tube out of a GUV composed of lipids of different types. In the presence of weak deformations, we use the Monge parametrization to describe the deformed surface of the tube as a function of the orthonormal coordinates (θ, z) in the plane: $\vec{\mathbf{r}}(\theta,z) = [(R+u(\theta,z))\cos(\theta), (R+u(\theta,z))\sin(\theta), z]$, where $0 \le \theta \le 2\pi$, $0 \le z \le L$ and $u(\theta,z)$ is the deformation field. From differential geometry, up to second order, we obtain:

$$\begin{aligned} dS &= R + u + \frac{u_\theta^2}{2R} + \frac{R u_z^2}{2}, \\ H &= -\frac{1}{2R} + \frac{u}{2R^2} - \frac{u^2}{2R^3} - \frac{u_\theta^2}{4R^3} + \frac{u_{\theta\theta}}{2R^2} - \frac{u u_{\theta\theta}}{R^3} + \frac{3u_z^2}{4R} + \frac{u_{zz}}{2}, \end{aligned} \tag{4.5}$$

where the subscripts "θ" or "z" in these expressions denote partial differential with respect to them. Substituting Eq. 4.5 into Eqs. 4.2 and 4.1, the total energy of the membrane ($E = E_{\mathrm{el}} + E_\phi$) reads:

$$\begin{aligned} \frac{E}{\kappa/R^2} = \int \Bigg(& \frac{1}{2} + \frac{R^2\sigma}{\kappa} + \left[\frac{R\sigma}{\kappa} - \frac{1}{2R}\right] u + \frac{u^2}{2R^2} + \left[\frac{R^2\sigma}{2\kappa} - \frac{5}{4}\right] |\nabla u|^2 + \frac{2u u_{\theta\theta}}{R^2} \\ & + \frac{2u\theta^2}{R^2} + \frac{R^2}{2}\left[\nabla^2 u\right]^2 - \left[R + \frac{H_0 \phi R^2}{2}\right] \nabla^2 u - \frac{(\alpha + \kappa H_0^2) R^2}{2\kappa} \phi^2 + \frac{H_0 R \phi}{2} \\ & + \frac{\beta R^2}{4\kappa}\phi^4 + \frac{\gamma R^2}{2\kappa} |\nabla \phi|^2 \Bigg) d(R\theta) dz. \end{aligned} \tag{4.6}$$

To function correctly, cells have to reshape constantly forming an out-of-equilibrium system. Therefore, it is important to understand how the density function and deformation field of the membrane tube evolve in time. For the dynamical analysis of the membrane there exist various approaches [17]. For example, one can couple these equations to the Navier-Stocks hydrodynamic equations standing for the fluid underneath the membrane, as S. Leibler has proposed in Ref. [18]. Here we use the following kinetic equations:

$$\begin{aligned} \frac{\partial u}{\partial t} &= -L_u \frac{\delta E}{\delta u}, \\ \frac{\partial \phi}{\partial t} &= L_\phi \nabla^2 \frac{\delta E}{\delta \phi}. \end{aligned} \tag{4.7}$$

In these equations L_u and L_ϕ are the transport coefficients related to the mobility of the membrane. We set both of these parameters to 1, meaning that we measure time and length in units of τ_h and $\sqrt{L_\phi \tau_h}$, with τ_h the typical relaxation time in the system [19]. Inserting the energy functional (Eq. 6) into Eq. 4.7, the time evolution for our quantities of interest $\phi(\theta,z)$ and $u(\theta,z)$ is given by:

$$\begin{aligned} \frac{\partial u(\theta,z)}{\partial t} = & -\kappa \nabla^4 u(\theta,z) - \left(\frac{\kappa}{2R^2} - \sigma\right) \nabla^2 u(\theta,z) + \kappa H_0 \nabla^2 \phi(\theta,z) \\ & - \frac{2\kappa}{R^4} u_{\theta\theta}(\theta,z) - \frac{\kappa u(\theta,z)}{R^4} + \frac{\kappa}{2R^3} - \frac{\sigma}{R}, \end{aligned} \tag{4.8}$$

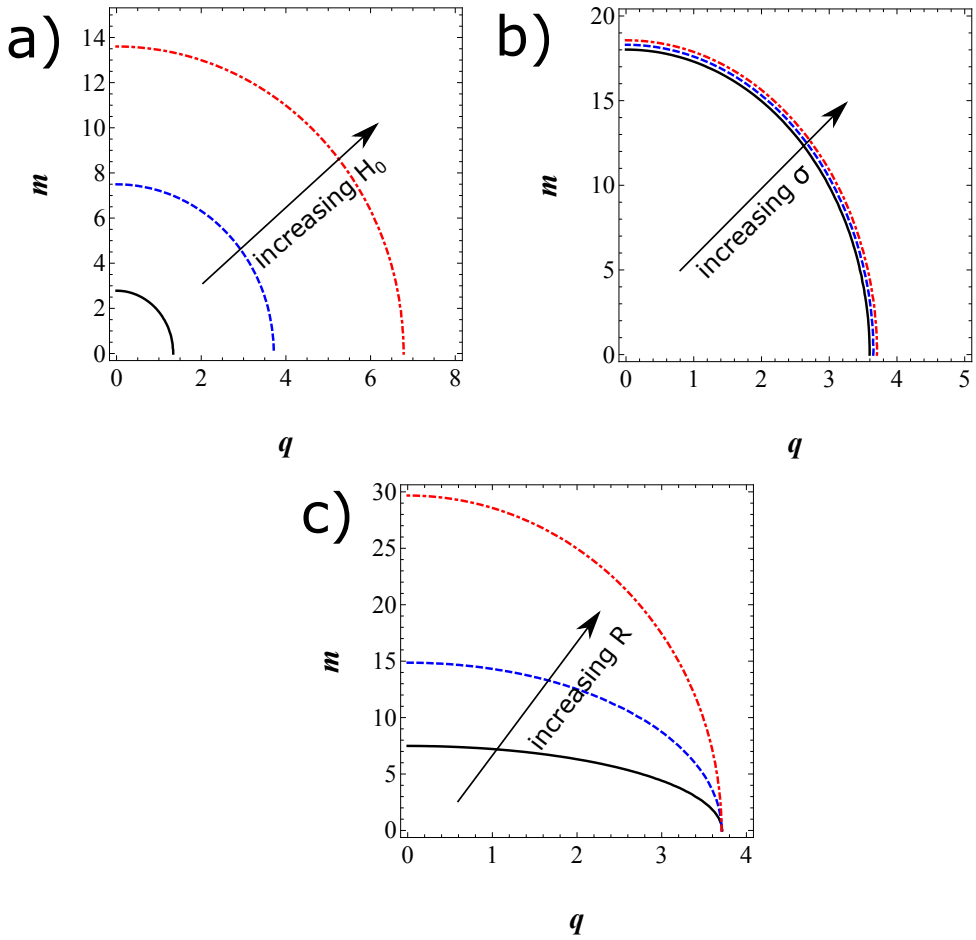

Figure 4.1: Contour plots of the largest eigenvalue ω_+ of the evolution matrix of our system, as a function of angular and longitudinal modes. For the modes below the plotted contour lines, ω_+ is positive and the membrane tube becomes unstable. a) Increasing the spontaneous curvature makes the tube more unstable. The black solid, blue dashed and red dashed-dotted lines correspond to $H_0 = 0.2$, $H_0 = 0.4$ and $H_0 = 1.2$, respectively. b) Decreasing the surface tension increases (although very slightly) the unstable area. The black solid, blue dashed and red dashed-dotted lines correspond to $\sigma = 20$, $\sigma = 10$ and $\sigma = 10/8$, respectively. c) The larger the radius of the tube is, the more unstable the tube becomes in the angular direction. The black solid, blue dashed and red dashed-dotted lines correspond to $R = 2$, $R = 4$ and $R = 8$, respectively. In all the cases, $\gamma = 1$ and $\alpha = 1$.

$$\frac{\partial\phi(\theta,z)}{\partial t} = -\gamma\nabla^4\phi(\theta,z) - \kappa H_0\nabla^4 u - (\alpha+\kappa H_0^2)\nabla^2\phi(\theta,z) + \beta\nabla^2(\phi(\theta,z)^3). \tag{4.9}$$

Next, we evaluate the stability of both the membrane tube and the absorbed proteins. We test the stability of Eqs. 4.8 and 4.9 by adding small perturbations to the uniform stationary states of the density and deformation fields. In the limit of an infinite tube, Fourier transform of these equations yields:

$$\begin{aligned}
&\begin{pmatrix}\dot{u}_{q,m}\\ \dot{\phi}_{q,m}\end{pmatrix} = \begin{pmatrix}M_{11} & M_{12}\\ M_{21} & M_{22}\end{pmatrix}\begin{pmatrix}u_{q,m}\\ \phi_{q,m}\end{pmatrix}, \text{ where}\\
&M_{11} = -\kappa\left(q^2+\frac{m^2}{R^2}\right)^2 + \left(\frac{\kappa}{2R^2}-\sigma\right)\left(q^2+\frac{m^2}{R^2}\right) + \frac{\kappa}{R^4}(2m^2-1),\\
&M_{12} = -\kappa H_0\left(q^2+\frac{m^2}{R^2}\right),\\
&M_{21} = -\kappa H_0\left(q^2+\frac{m^2}{R^2}\right)^2 \text{ and}\\
&M_{22} = -\gamma\left(q^2+\frac{m^2}{R^2}\right)^2 + \left(\alpha+\kappa H_0^2\right)\left(q^2+\frac{m^2}{R^2}\right)
\end{aligned} \tag{4.10}$$

where $m = 0,\pm1,...,\pm M$ and $q = 0,\pm1,...,\pm Q$. The upper limits M and Q are related to the smallest wave vector that exists in the membrane (which relates to the number and size of lipids), and hence are in the order of membrane thickness [20]. We examine the eigenvalues of Eq. 4.10 to extract the possible unstable regions. In this regime, any small fluctuations in either the shape of the membrane tube or the density of molecules grow in time. The eigenvalues read:

$$\omega_\pm = \frac{1}{2}\left(\mathrm{Tr}(M) \pm \sqrt{\mathrm{Tr}(M)^2 - 4\mathrm{Det}(M)}\right), \tag{4.11}$$

which can clearly cause instabilities only for the positive value (ω_+). Fig. 4.1 depicts the unstable region for the biologically relevant values of physical parameters in Eq. 4.10. As shown, increasing the amount of spontaneous curvature and the radius of the tube dramatically increases the instability region. Although choosing a surface tension of $\sigma = \sqrt{\frac{\kappa}{2R^2}}$ would stabilize a bare tube, introducing any types of inclusions in the system causes the membrane to suffer from instability – as the new stability conditions obey Eq. 4.4. Thus, a uniform density of molecules on the surface of a membrane tube is not stable. The natural question that arises is: What are then the stable solutions? To answer this question and elucidate the final equilibrium density and shape of the membrane, we numerically solve their corresponding evolution equations (Eqs. 4.8 and 4.9). We start the simulation from a small random perturbation around the $u = 0$ and $\phi = 0$ state. For short (but still large, compared to the radius) lengths of the tube, we get either line-like or helical structures. A typical snapshot (for helical structures) of the equilibrium shape of the system is shown in Fig. 7.2. The depicted result illustrates the fact that phase separation and aggregation of similar proteins is a signature of having a membrane with impurities. This is biologically relevant. For example, in cell division, endo-/exco-cytosis

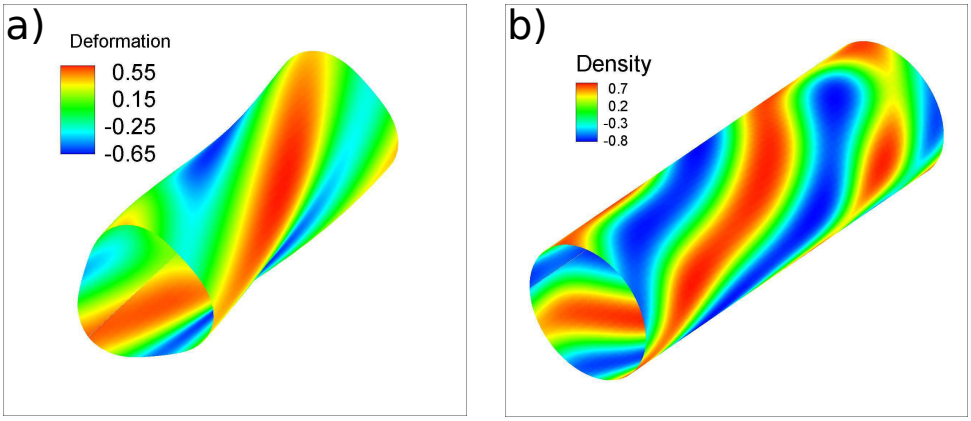

Figure 4.2: The final deformation field (a) and the density of molecules (b) for a membrane started from a state with small random perturbations around $u = 0$ and $\phi = 0$. The relevant parameters are set to $H_0 = 0.2$, $R = 5$, $L = 35$, $\gamma = 1$ and $\alpha = 1$.

and membrane fissions in intracellular organelles like in the ER, inclusions of the same type show preference for the regions of the same shape (curvature), and as a cluster they start bending the membrane.

Solving equations 4.8 and 4.9 numerically is not straightforward, because of the nonlinear terms. This is the reason why we have chosen a very large radius for the tube. Future research is necessary in order to enhance the convergence rate [2], accuracy and stability of the numerical method, from which we can obtain more conclusive simulation results on how the pattern formation of proteins depends on the physical parameters we have in the model.

4.3. In a nutshell

Starting from a simple model of a tubular fluid membrane covered with intercalated curvature-inducing proteins, we have shown how introducing a density of proteins alters the stability conditions of the tube. We further revealed how the unstable regions depend on the physical parameters like the amount of induced curvature, surface tension and radius of the tube. Finally, we have elucidated that segregation and integration of proteins is a natural result of the interplay between the shape of membrane and the density of proteins. Such a mechanism may underlie the biological dynamic processes where the spontaneous spatial organization of proteins (or other types of embedded inclusions) is required.

[2] With the current semi-implicit method we have a time step of $\Delta t = 10^{-9}$ for the convergence rate.

References

[1] H. T. McMahon and J. L. Gallop, *Membrane curvature and mechanisms of dynamic cell membrane remodelling,* Nature **438**, 590 (2005).

[2] M. Simunovic, E. Evergren, I. Golushko, C. Prévost, H.-F. Renard, L. Johannes, H. T. McMahon, V. Lorman, G. A. Voth, and P. Bassereau, *How curvature-generating proteins build scaffolds on membrane nanotubes,* Proceedings of the National Academy of Sciences , 201606943 (2016).

[3] J. Agudo-Canalejo and R. Golestanian, *Pattern formation by curvature-inducing proteins on spherical membranes,* arXiv preprint arXiv:1705.08425 (2017).

[4] J. C. Stachowiak, C. C. Hayden, and D. Y. Sasaki, *Steric confinement of proteins on lipid membranes can drive curvature and tubulation,* Proceedings of the National Academy of Sciences **107**, 7781 (2010).

[5] G. Guigas and M. Weiss, *Effects of protein crowding on membrane systems,* Biochimica et Biophysica Acta (BBA)-Biomembranes **1858**, 2441 (2016).

[6] M. Perry and A. B. Gilbert, *Yolk transport in the ovarian follicle of the hen (gallus domesticus): lipoprotein-like particles at the periphery of the oocyte in the rapid growth phase,* Journal of cell science **39**, 257 (1979).

[7] W. Helfrich, *Elastic properties of lipid bilayers: theory and possible experiments,* Zeitschrift für Naturforschung C **28**, 693 (1973).

[8] A. H. Bahrami, R. Lipowsky, and T. R. Weikl, *Tubulation and aggregation of spherical nanoparticles adsorbed on vesicles,* Physical review letters **109**, 188102 (2012).

[9] J. C. Pàmies and A. Cacciuto, *Reshaping elastic nanotubes via self-assembly of surface-adhesive nanoparticles,* Phys. Rev. Lett. **106**, 045702 (2011).

[10] B. J. Reynwar, G. Illya, V. A. Harmandaris, M. M. Müller, K. Kremer, and M. Deserno, *Aggregation and vesiculation of membrane proteins by curvature-mediated interactions,* Nature **447**, 461 (2007).

[11] B. J. Reynwar and M. Deserno, *Membrane-mediated interactions between circular particles in the strongly curved regime,* Soft Matter **7**, 8567 (2011).

[12] G. Koster, A. Cacciuto, I. Derényi, D. Frenkel, and M. Dogterom, *Force barriers for membrane tube formation,* Phys. Rev. Lett. **94**, 068101 (2005).

[13] B. J. Peter, H. M. Kent, I. G. Mills, Y. Vallis, P. J. G. Butler, P. R. Evans, and H. T. McMahon, *Bar domains as sensors of membrane curvature: the amphiphysin bar structure,* Science **303**, 495 (2004).

[14] P. G. Dommersnes and J.-B. Fournier, *The many-body problem for anisotropic membrane inclusions and the self-assembly of "saddle" defects into an "egg carton",* Biophys. J. **83**, 2898 (2002).

[15] C. van der Wel, A. Vahid, A. Šarić, T. Idema, D. Heinrich, and D. J. Kraft, *Lipid membrane-mediated attraction between curvature inducing objects,* Scientific Reports **6** (2016).

[16] F. L. Brown, *Continuum simulations of biomembrane dynamics and the importance of hydrodynamic effects,* Quarterly reviews of biophysics **44**, 391 (2011).

[17] P. M. Chaikin and T. C. Lubensky, *Principles of condensed matter physics* (Cambridge university press, 2000).

[18] S. Leibler, *Curvature instability in membranes,* Journal de Physique **47**, 507 (1986).

[19] R. Reigada, J. Buceta, and K. Lindenberg, *Nonequilibrium patterns and shape fluctuations in reactive membranes,* Physical Review E **71**, 051906 (2005).

[20] J.-B. Fournier and P. Galatola, *Critical fluctuations of tense fluid membrane tubules,* Phys. Rev. Lett. **98**, 018103 (2007).

II

Enclosed vesicles

5

Membrane mediated interactions between partially wrapped colloids

The interplay of membrane proteins is vital for many biological processes, such as cellular transport, cell division, and signal transduction between nerve cells. Theoretical considerations have led to the idea that the membrane itself mediates protein self-organization through minimization of membrane curvature energy. In this section, we present a combined experimental and numerical study of the interaction between fully wrapped colloids. We use coarse-grained Monte-Carlo simulations to study such interactions. Our results illustrate that colloids that are (almost) fully wrapped by the lipids of a spherical membrane attract each other. Having many of such fully wrapped colloids on a spherical vesicle results in the formation of linear patterns. Our theoretical predictions are in agreement with recently performed experiments, in which such interactions are directly quantified for the first time. The numerical results of this chapter in combination with the experimental evidence point to membrane curvature as a common physical origin for interactions between any membrane-deforming objects, from nanometre-sized proteins to micrometre-sized particles.

Parts of this chapter are based on:
C. M. van der Wel, A. Vahid *et al.*, *Lipid membrane-mediated attraction between curvature inducing objects*, Scientific reports **6**, 32825 (2016)
A. Vahid *et al.*, *Collective interaction between Janus-like objects on fluid vesicles*, in preparation

5.1. Introduction

Interactions between membrane proteins are of key importance for the survival of cells as they are involved in many dynamical processes. The organization of membrane proteins into complexes and their effect on membrane shape enables for instance intracellular transport, cell division, cell migration, and signal transduction [1]. Understanding the underlying principles of protein organization is therefore crucial to unravel processes such as cell-cell signalling in the brain [2] or disease mechanisms like membrane-associated protein aggregation in Parkinson's disease [3].

As comprehensively discussed in Chapter 1 and Part I, besides specific protein–protein interactions and interactions with the cytoskeleton, protein organization in membranes is also driven by a universal interaction force arising from membrane deformations. Theoretical models [4–7] and simulations [8–11] predict that by deforming the membrane locally, membrane proteins can self-assemble into complex structures such as lines, rings, and ordered packings like the patterns we have reported in chapters 2-5 on tubular membranes. Observations in living cells [3, 12] support the existence of such membrane-mediated interactions, but have yet to provide conclusive experimental proof of their common physical origin: separation of contributions arising from specific protein-protein interactions and interactions with the cytoskeleton is extremely challenging.

Previous studies [13, 14] have investigated the interaction between membrane – wrapped colloids. The interaction between colloids may depend on the wrapping fraction of the colloids and various constraints. For example, depending on how we treat the constraints associated with the surface area and volume of the vesicle, completely different interactions can be reached. In the particular case of the wrapping fraction, for example, while previous studies have reported a repulsion between partially wrapped particles [13], recent experiments characterized for the first time the effect of a single adhesive colloidal particle on the local membrane shape using confocal microscopy [15]. The experiments show that a colloidal particle adhered to a vesicle is either fully wrapped by the membrane or not wrapped at all, depending on the adhesion strength. Therefore, it is warranted to investigate the interaction between such fully wrapped objects as they are experimentally relevant.

In this chapter we first briefly explain the model and an experimental setup corresponding to the method we take. Using Monte Carlo simulations, we then reveal that two particles, fully wrapped by the membrane, attract each other. Having multiple of such partially wrapped particles on a vesicle results in either linear patterns or vesiculation of the membrane. Since these simulations do not contain any absolute length scale, we conclude that the measured attraction caused by lipid membrane deformations is scale-independent. Therefore, we can compare our numerical results to experiments in which our colleagues have measured the interaction between two fully wrapped particles on Giant Unilamellar Vesicles (GUVs). They found that only fully wrapped particles show a reversible attraction, which implies that the attraction is purely caused by the membrane deformation. Our combined simulations and experimental results quantitatively describe the interactions of any membrane deforming object, ranging from nanometre-sized proteins to micrometre-sized colloidal particles.

5.2. Model

We utilize the model that is explained in detail in Chapter 3. There are however some differences. We therefore briefly explain the model again in this chapter.

We describe the vesicle by a network of vertices that are connected in a triangular network with a minimum edge length σ. The curvature energy of our discretized membrane is given by:

$$\Delta E_{\mathrm{Curv}} = \sqrt{3}\kappa \sum_{<ij>} 1 - \mathbf{n}_i \cdot \mathbf{n}_j, \tag{5.1}$$

where $\mathbf{n}_i$ and $\mathbf{n}_j$ are the normal vectors to any pair of adjacent triangles i and j, respectively. The summation runs over all pairs of such triangles. To simulate the fluidity of the membrane, we change the connectivity of the network: we cut and reattach connections between the four vertices of any two neighbouring triangles. The surface area A and volume V of the vesicle are maintained by constraints $\Delta E_A = K_A(A-A_t)^2/A_t$ and $\Delta E_V = K_V(V-V_t)^2/V_t$ with $K_A = 10^3 k_B T/\sigma^2$ and $K_V = 4\times 10^3 k_B T/D_p\sigma^2$, where $k_B T$, D_p, A_t and V_t are the thermal energy, the diameter of the particles, the target surface area and the target volume of the vesicle, respectively. In each simulation we set the target values of surface area and volume of the vesicle with diameter $D_v = 50\sigma$ as $A_t = 1.05A_0$ and $V_t = V_0$, respectively. A_0 and V_0 are the initial surface area and volume of the vesicle. These parameters cause the final volume and surface area to deviate less than 0.01% from the target values. To let the vertices of the membrane wrap around the particles, we introduce an attraction potential between them:

$$\Delta E_{\mathrm{Ad}} = \begin{cases} -\varepsilon(l_m/r)^6 & \text{if } \theta \le \theta_{\mathrm{Wr}}, \\ 0 & \text{otherwise}, \end{cases} \tag{5.2}$$

where ε is the particles' adhesion energy and r is the centre to centre distance between particles and vertices. θ is the angle between the vector normal to the active area of the particles and the vectors that connect the particles to vertices (see Fig. 5.1a). The maximum angle θ_{Wr} is defined to control the area that is forced to be wrapped by the membrane, preventing very sharp membrane bends (see Fig. 3.1C in Chapter 3 for more details). $l_m = (\sigma + D_p)/2$ is the shortest distance between particles and vertices, where the diameter of the particles is set to $D_p = 8\sigma$. We set a cut-off radius for the attraction potential at 1.2σ to make sure that other than forming a layer of membrane on the surface of the particles, it has no extra effects. The total energy ΔE_{T} of the system is the sum of the curvature energy (Eq. 5.1), the energy associated with geometrical constraints (ΔE_{A} and ΔE_{V}), and the adhesion energy (Eq. 5.2).

To analyse the equilibrium shape of the membrane, we implement the Monte Carlo simulated annealing algorithm in order to minimize the total energy of the system. For our Monte Carlo simulations, we use the Metropolis algorithm to move vertices and particles, and flip the edges of the membrane triangulation, in order to change the configuration of the system (shape of the membrane). The temperature of the system is also slowly decreased so that we suppress the fluctuation of the membrane and identify the minimum-energy configuration.

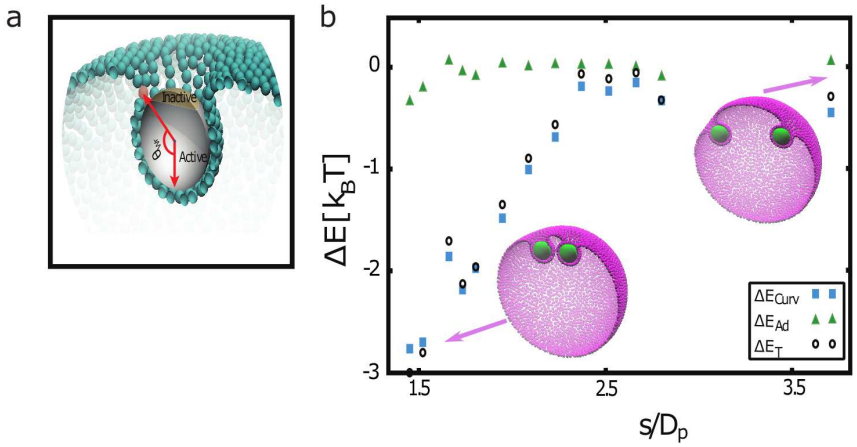

Figure 5.1: Wrapping of particles by the membrane and the resulting total membrane energy in our numerical model. (a) Wrapping happens through adhesion of membrane vertices to colloid particles, due to a strong adhesion potential (Eq. 5.2). We can specify an inactive region at the top of the colloid, preventing the membrane from making very sharp turns (with very high bending energies); in the given example, $\theta_{Wr} = 11\pi/12$. (b) Curvature, adhesion, and total energy of the system, with zero set at the value of two wrapped particles located at opposite poles of the vesicle. After the wrapping process, the adhesion energy (ΔE_{Ad}) does not change significantly and therefore the curvature energy (ΔE_{Curv}) determines the behaviour of the particles.

5

5.3. Results

We set the volume and surface area of the vesicle to the target values such that about 90% of the particles' total area is wrapped by the membrane beads. Note that there is no absolute length scale involved in these simulations.

We first examine the interaction between two fully-wrapped particles. We let the membrane wrap around the active part of the colloids at different separations, equilibrate the shape of the vesicle and record the value of the relevant terms in the total energy including the adhesion, curvature and total energies. As depicted in Fig. 5.1b, after reaching the equilibrium shape, the adhesion energy remains constant. In contrast, the curvature energy of the membrane decreases by decreasing the geodesic distance between the two colloids. This implies that the attraction of the colloids is purely due to the shape distortion of the vesicle – because of not only the imposed curved membrane between the colloids but also the closed nature of the vesicle. For larger distances the energy of the vesicle is barely affected by a change of the separation between the particles. The minimum distance is set by the resolution of our coarse grained description of the membrane: at $1.5D_p$ we can be sure to always have two layers of vertices between the particles. Because of this limitation our simulations cannot capture the short-range effects observed in the higher resolution simulations of Reynwar *et al.* [8, 16].

The attraction of particles is strong enough (about ~ 4 times stronger than thermal fluctuations) to be measured using experimental tools. Our collaborators [1] in Leiden university have measured such membrane induced interactions for the first time. They

[1] Dr. Casper van der Wel and Dr. Daniela Kraft

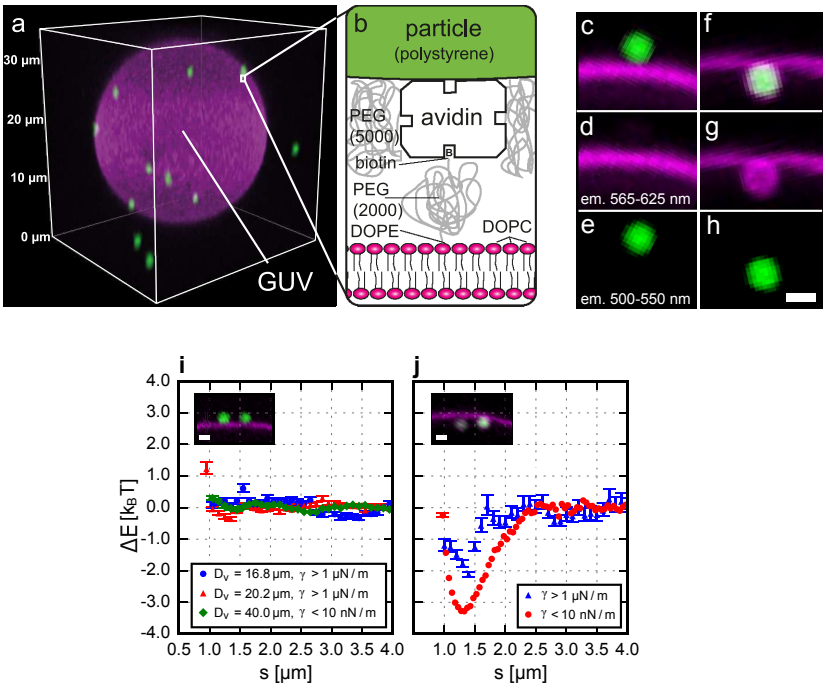

Figure 5.2: Experimental data (a) Three-dimensional confocal image of a typical Giant Unilamellar Vesicle (GUV, in magenta) with attached colloidal particles (in green). (b) Schematic of the avidin-biotin linkage between membrane and particle. By varying the avidin concentration on the particles we control the adhesion strength. Polyethylene glycol (PEG) suppresses electrostatic interactions between membrane and particles, as well as non-specific adhesion between particles. (c) Fluorescence signal of a non-wrapped particle (green) and a membrane (magenta). The separate fluorescence signals of the membrane and particle are displayed in (d,e), respectively. In (f–h) the wrapped state is displayed analogously. (i, j) Interaction energy ΔE as a function of geodesic particle separation distance s for (i) two non-wrapped particles and (j) two wrapped particles. For non-wrapped particles (i) there is no significant interaction on both tense and floppy membranes. For wrapped particles (j) the interaction potential shows a long-ranged attraction. The scale bars are $1\mu m$.

have constructed a system very similar to our numerical set-up: Micrometre-sized colloidal particles (polystyrene, $0.98 \pm 0.03\ \mu m$ in diameter) adhered to single-component Giant Unilamellar Vesicles (GUVs, diameters ranging from $5 - 100\ \mu m$), which allowed them to study membrane-mediated interactions with confocal microscopy (see Fig. 5.2a). Such an adhering mechanism is very similar to the one we have implemented in the simulations. The GUV membrane consists of DOPC lipids, which are above their melting point at room temperature, ensuring a single-phase liquid membrane. The connection between membrane and particle is realized by coating the particles with varying amounts of avidin, a protein that binds strongly and specifically to biotin, which we attach to the membrane through a functionalised lipid. By choosing different fluorescent markers for the particles and lipid membranes, the effect of a single particle on a lipid membrane is visualized (see Figs. 5.2c-h). Particles exist in either a completely wrapped state or a completely non-wrapped state: partial wrapping is only observed as a tran-

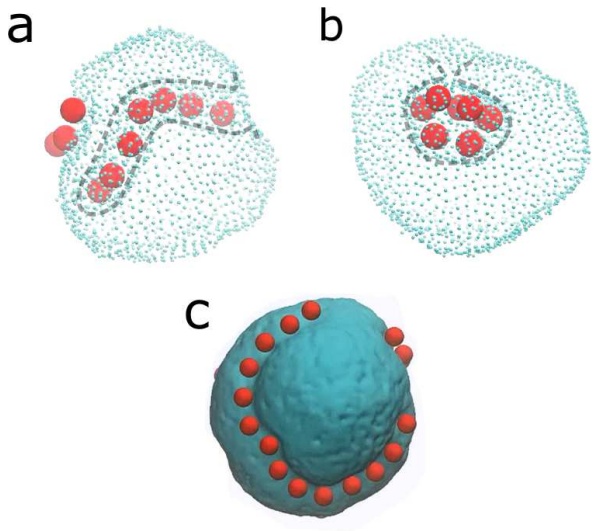

Figure 5.3: Altering the determining constraints relating to the wrapping angle (θ_{wr}), total surface area and enclosed volume leads to completely different collective behaviors. (a and b) There is no conditions on the total surface area and volume of the vesicle, but we only penalize any changes in the surface area. Having fully active particles drives the tubulation of the membrane (a) and partially active particles ($\theta_{wr} = \pi/2$) collectively induce membrane vesiculation. The adhesion strength and surface tension are set to $\varepsilon = 2.8 k_B T$ and $\gamma = 1 k_B T/\sigma^2$, respectively. (c) Imposing a constant-volume condition drives the formation of linear patterns on the surface of the vesicle.

sient situation. Non-wrapped particles are located on the outside of the vesicle without deforming the membrane (Figs. 5.2c-e), while wrapped particles are protruding into the interior of the vesicle (Figs. 5.2f-h). As depicted in Figs. 5.2i-j, only for fully wrapped particles a significant interaction between colloids is detected. When the particles approach within a distance of several particle diameters, there exists a reversible, long-ranged attraction between them. The interaction strength for floppy membranes is $-3.3 k_B T$ and the attraction extends over a range of $2.5 \mu m$, which is equivalent to 2.5 particle diameters. These measurements are in agreement with the results of our simulations.

Next we investigate the many-body interaction between colloids, with a focus on the effect of the determinant factors including the wrapping angle of colloids (θ_{wr}), total surface area and enclosed volume of the vesicle. The initial size of the vesicle and colloids are adjusted to $D_v = 28\sigma$ and $D_p = 4\sigma$, respectively. We also set the adhesion strength and surface tension of the membrane to $\varepsilon = 2.8 k_B T$ and $\gamma = 1 k_B T/\sigma^2$. Typical results of these simulations are shown in Fig. 5.3. In the absence of a constant-volume condition, particles either formed tubules or generated vesiculation of the membrane, depending on the wrapping angle of the colloids. Fully wrapped particles form tubes in order to minimize both the adhesion energy and curvature energy of the membrane (Fig. 5.3a). Similar patterns have previously been reported both theoretically [17] and experimentally [18]. Partially wrapped particles, on the other hand, induce vesiculation of the membrane. Such pattern formation has also been observed in living system [19]. Having no constraint on the total volume and surface area of the vesicle corresponds to a

situation in which our system is supported by a reservoir of lipids. As shown in Fig. 5.3c, constant-volume constraints leads to linear patterns of the colloids. Such aggregation of particles, as we will discuss in the next chapter, can be controlled via introducing a curvature variation on the shape the vesicle.

5.4. In a nutshell

We have discussed the interaction between colloidal particles that are adhered to spherical membranes. We revealed that two fully wrapped colloids on the surface of a vesicle with constant surface area and enclosed volume attract each other, in order to minimize the curvature energy of the membrane. Our numerical prediction of such an attraction force agrees with recently performed experimental results on the interaction of particles adhering to Giant Unilamellar Vesicles. The simulation results combined with the experimental evidence quantitatively describe the interactions of membrane-deforming objects, ranging from nanometre-sized proteins to micrometre-sized colloidal particles, as there is no length scale in the theoretical model. In this chapter we further provided some results to clarify the effect of various parameters on the pattern formation of colloids and macromolecules adhered to a vesicle. These results indicate that the wrapping angle of colloids, the total surface area of the vesicle and its enclosed volume have significant influence on the emerging patterns of the colloids.

References

[1] H. T. McMahon and J. L. Gallop, *Membrane curvature and mechanisms of dynamic cell membrane remodelling,* Nature **438**, 590 (2005).

[2] D. Freche, U. Pannasch, N. Rouach, and D. Holcman, *Synapse geometry and receptor dynamics modulate synaptic strength,* PloS one **6**, e25122 (2011).

[3] C. M. Pfefferkorn, Z. Jiang, and J. C. Lee, *Biophysics of α-synuclein membrane interactions,* Biochimica et Biophysica Acta (BBA)-Biomembranes **1818**, 162 (2012).

[4] M. Goulian, R. Bruinsma, and P. Pincus, *Long-range forces in heterogeneous fluid membranes,* Europhys. Lett. **22**, 145 (1993).

[5] K. Kim, J. Neu, and G. Oster, *Curvature-mediated interactions between membrane proteins,* Biophys. J. **75**, 2274 (1998).

[6] P. G. Dommersnes and J.-B. Fournier, *N-body study of anisotropic membrane inclusions: Membrane mediated interactions and ordered aggregation,* Eur. Phys. J. E **12**, 9 (1999).

[7] M. M. Müller, M. Deserno, and J. Guven, *Interface-mediated interactions between particles: a geometrical approach,* Physical Review E **72**, 061407 (2005).

[8] B. J. Reynwar, G. Illya, V. A. Harmandaris, M. M. Müller, K. Kremer, and M. Deserno, *Aggregation and vesiculation of membrane proteins by curvature-mediated interactions,* Nature **447**, 461 (2007).

[9] J. C. Pàmies and A. Cacciuto, *Reshaping elastic nanotubes via self-assembly of surface-adhesive nanoparticles,* Phys. Rev. Lett. **106**, 045702 (2011).

[10] M. Simunovic, A. Srivastava, and G. A. Voth, *Linear aggregation of proteins on the membrane as a prelude to membrane remodeling,* Proc. Natl. Acad. Sci. U.S.A. **110**, 20396 (2013).

[11] A. Šarić and A. Cacciuto, *Self-assembly of nanoparticles adsorbed on fluid and elastic membranes,* Soft Matter **9**, 6677 (2013).

[12] B. J. Peter, H. M. Kent, I. G. Mills, Y. Vallis, P. J. G. Butler, P. R. Evans, and H. T. McMahon, *Bar domains as sensors of membrane curvature: the amphiphysin bar structure,* Science **303**, 495 (2004).

[13] A. H. Bahrami, R. Lipowsky, and T. R. Weikl, *Tubulation and aggregation of spherical nanoparticles adsorbed on vesicles,* Physical review letters **109**, 188102 (2012).

[14] A. Šarić and A. Cacciuto, *Fluid membranes can drive linear aggregation of adsorbed spherical nanoparticles,* Phys. Rev. Lett. **108**, 118101 (2012).

[15] C. van der Wel, A. Vahid, A. Šarić, T. Idema, D. Heinrich, and D. J. Kraft, *Lipid membrane-mediated attraction between curvature inducing objects,* Scientific Reports **6** (2016).

[16] B. J. Reynwar and M. Deserno, *Membrane-mediated interactions between circular particles in the strongly curved regime,* Soft Matter **7**, 8567 (2011).

[17] A. Šarić and A. Cacciuto, *Mechanism of membrane tube formation induced by adhesive nanocomponents,* Physical review letters **109**, 188101 (2012).

[18] H. Ewers, W. Römer, A. E. Smith, K. Bacia, S. Dmitrieff, W. Chai, R. Mancini, J. Kartenbeck, V. Chambon, L. Berland, *et al.*, *Gm1 structure determines sv40-induced membrane invagination and infection,* Nature cell biology **12**, 11 (2010).

[19] M. Perry and A. B. Gilbert, *Yolk transport in the ovarian follicle of the hen (gallus domesticus): lipoprotein-like particles at the periphery of the oocyte in the rapid growth phase,* Journal of cell science **39**, 257 (1979).

6

Curvature variation controls particle aggregation on fluid vesicles

Cellular membranes exhibit a large variety of shapes, strongly coupled to their function. Many biological processes involve dynamic reshaping of membranes, usually mediated by proteins. This interaction works both ways: while proteins influence the membrane shape, the membrane shape affects the interactions between the proteins. To study these membrane-mediated interactions on closed and anisotropically curved membranes, we use colloids adhered to ellipsoidal membrane vesicles as a model system. We find that two particles on a closed system always attract each other, and tend to align with the direction of largest curvature. Multiple particles form arcs, or, at large enough numbers, a complete ring surrounding the vesicle in its equatorial plane. The resulting vesicle shape resembles a snowman. Our results indicate that these physical interactions on membranes with anisotropic shapes can be exploited by cells to drive macromolecules to preferred regions of cellular or intracellular membranes, and utilized to initiate dynamic processes such as cell division. The same principle could be used to find the midplane of an artificial vesicle, as a first step towards dividing it into two equal parts.

Parts of this chapter have been published as: A. Vahid *et al.*, *Curvature variation controls particle aggregation on fluid vesicles*, Soft Matter **13**, 4924-4930 (2017)

6.1. Introduction

Cellular membranes are two-dimensional fluid interfaces that consist of a large variety of components. They form the boundary between the cell and the outside world, and, for eukaryotic cells, separate the inside of the cell into numerous compartments known as organelles. In order for biological processes like cell division, vesicular trafficking and endo/exocytosis to occur, cellular membranes have to reshape constantly. Consequently, membranes exhibit a variety of morphologies, from a simple spherical liposome to bewildering complex structures like interconnected tubular networks as found in Mitochondria and the Endoplasmic Reticulum (ER), or connected stacks of perforated membrane sheets in the Golgi apparatus[1–4]. There are different mechanisms by which membranes achieve these structures, the most important of which is through the interplay between membrane lipids and various proteins[5–7]. A biological membrane is home to different types of proteins that are adhered to or embedded in it. These proteins deform the membrane and, consequently, they can either repel or attract each other [8–13]. Spatial organization of such proteins in biological membranes is essential for stabilizing the membrane and for the dynamic behaviour of cellular organelles [14–17].

Recently, it has been experimentally [18–20] and theoretically [8, 9, 11, 21–26] revealed that membrane-curving particles, like colloids or identical proteins, adhered to a membrane self-assemble into striking patterns. For instance it has been shown that colloids adhered to a spherical membrane form linear aggregations [18, 24]. In all of the studies to date, the global shape of the membrane is selected from one of three options: planar, spherical, or tubular. These global membrane shapes impose a homogeneous background curvature, which is considered to be conserved throughout the process under investigation. Outside factors changing the membrane have not yet been included in the study of membrane-mediated interactions. Membranes in cellular compartments such as in ER and the Golgi complex are however dynamic entities and possess peculiar shapes forming regions with high local curvature and regions with less curvature [3]. Forming and stabilizing such shape inhomogeneities is necessary for cellular functions like sensing and trafficking [27]. It is therefore warranted to investigate how the interactions between membrane inclusions are affected by anisotropies in the membrane curvature.

Recently, studies have been performed to understand the role of non-uniform curvature in the interaction of single particles with a fluid membrane, both in the tension-dominated [28] and bending-dominated [29, 30] regimes. In this study, through a numerical experiment, we investigate many body interactions between colloids adhered to a quasi-ellipsoidal membrane with a varying curvature. We also include all other factors from earlier studies such as surface tension, adhesion energy (required for colloids to adhere to the membrane) and constant volume effects. We use a dynamic triangulation network to model the membrane, and computationally minimize the total energy of the membrane via a Monte Carlo algorithm. Firstly, we show that the interaction between two colloids adhered to spherical vesicles is significantly affected by the vesicle curvature. Secondly, we demonstrate that linear aggregates of colloids exploit the curvature anisotropy and adjust their orientation to minimize the total energy on a quasi-ellipsoidal membrane. Using umbrella sampling, we further show that the total energy

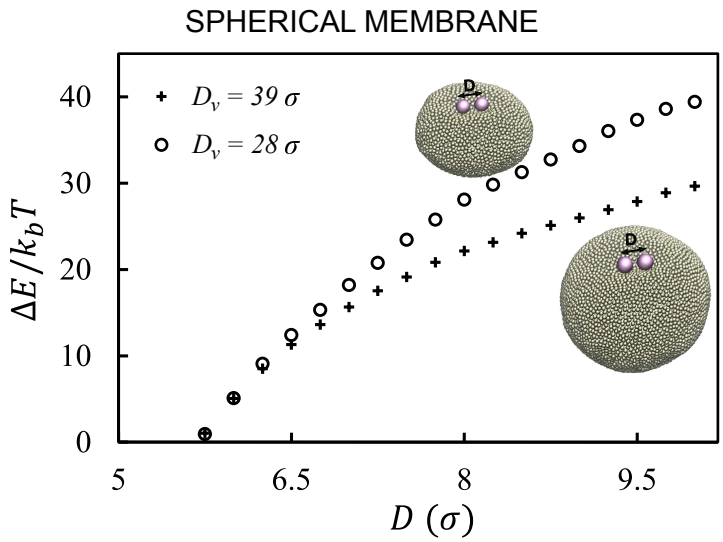

Figure 6.1: Curvature energy of the membrane for spherical vesicles of diameters $D_v = 28\sigma$ (circles) and $D_v = 39\sigma$ (pluses) containing two colloids. The force between colloids in the smaller vesicle is stronger and has a larger interaction range.

of the membrane favors two colloids to attract each other at the mid-plane of a prolate ellipsoid that is perpendicular to its major axis. Finally, we investigate how the various terms in the total energy of the membrane affect the strength of the interactions. Our results show that the variation in the membrane shape can play a crucial role in a variety of cellular functions that require macromolecular assembly or membrane remodeling.

6.2. Model

The conformation of a fluid membrane can be described as the shape minimizing the classical Helfrich energy functional (see chapter 1). Here, we use a computational scheme that discretizes the membrane by a triangulated network, whose triangles represent course-grained patches of the membrane [32, 33]. As explained in chapter 3, using a discretized form of the Helfrich energy, we define the curvature energy as: $\Delta E_{\mathrm{Curv}} = \kappa \sum_{<ij>} 1 - \mathbf{n}_i \cdot \mathbf{n}_j$, In order to guarantee the fluidity of the membrane, we cut and reattach the connection between the four vertices (which we label with and refer to as beads) of any two neighboring triangles. The membrane in our system does not undergo any topological changes and we can thus ignore the Gaussian curvature contribution in the bending energy. We impose the conservation of membrane surface area (A) and enclosed volume (V) by adding the terms $\Delta E_{\mathrm{A}} = K_{\mathrm{A}}(A - A_t)^2/A_t$ and $\Delta E_{\mathrm{V}} = K_{\mathrm{V}}(V - V_t)^2/V_t$ to the energy during the minimization process, with A_t and V_t the target values of the membrane's area and enclosed volume. In the following these target values are set as: $V_t = V_0$ and $A_t = 1.1A_0$, where A_0 and V_0 are, respectively, the initial surface area and volume of a perfect spherical vesicle with diameter D_v. We provide an excess area of $dA = 0.1A_0$ to vesicles in order to enable the adhered particles to interact with each other. The cor-

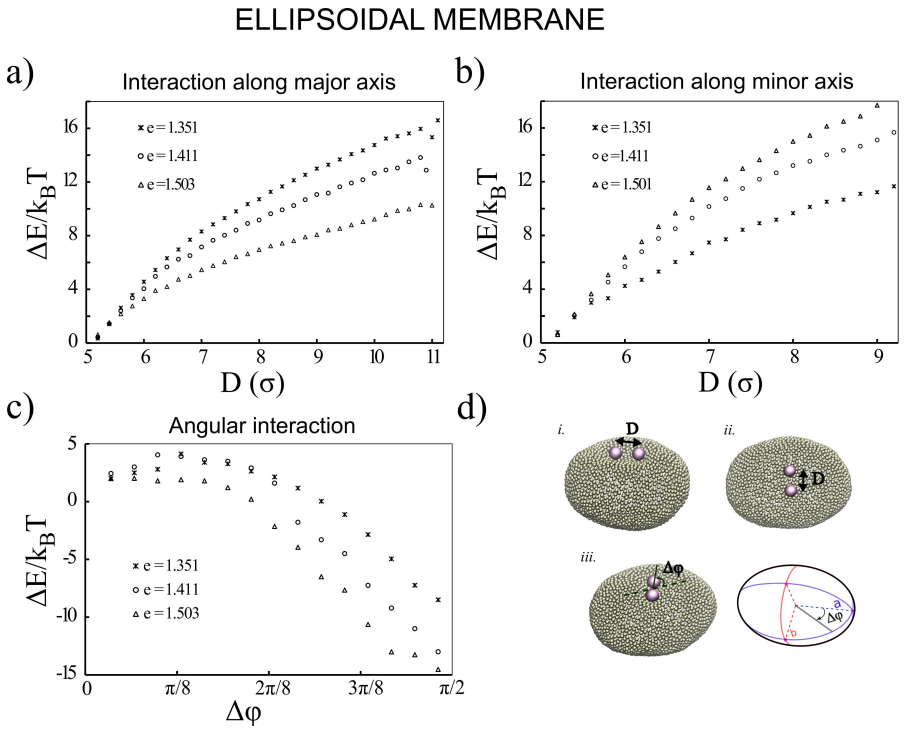

Figure 6.2: Colloids adhered to a quasi-ellipsoidal membrane behave differently in different directions. Decreasing the ellipticity of the vesicle, which is defined as $e = a/b$, (a) strengthens the attractions between the colloids along the major axis and (b) weakens the interaction between the colloids along the minor axis. Figure (c) illustrates that the energy of a membrane containing a pair of colloids decreases when the angle between the pair and the semi-major axis increases.

responding constants are chosen such that both the area and volume deviate less than 0.05% from their target values. To enable colloids to adhere to the membrane, we introduce an adhesion potential, $\Delta E_{\text{Ad}} = -\varepsilon(l_m/r)^6$, between colloids and the membrane, where ε is the strength of the adhesion energy and, r and l_m are, respectively, the center to center distance and the minimum allowed separation between colloids and membrane beads. Finally, we need to give the membrane an anisotropic shape for which we deform our spherical membrane into a prolate ellipsoid. In order to do so, we introduce two weak (compared to the strength of the adhesion energy) spring-like potentials between two small areas of the vesicle (the two poles of the ellipsoid) and the center of the vesicle, $\Delta E_{\text{Ell}} = K_{\text{Ell}}(L-a)^2$; K_{Ell}, a and L are the potential strength, the major axis of the ellipsoid and the length of any line connecting the beads situated at the poles of the ellipsoid to the center, respectively. Since the adhesion energy is stronger than the applied harmonic potential, colloids effectively do not feel any difference between the energy cost for bending the membrane at these two areas and at the regions belonging to the rest of the ellipsoid. We verified this claim by considering a spherical membrane, and find that there is no significant difference between the case of including u_{Ell} with a

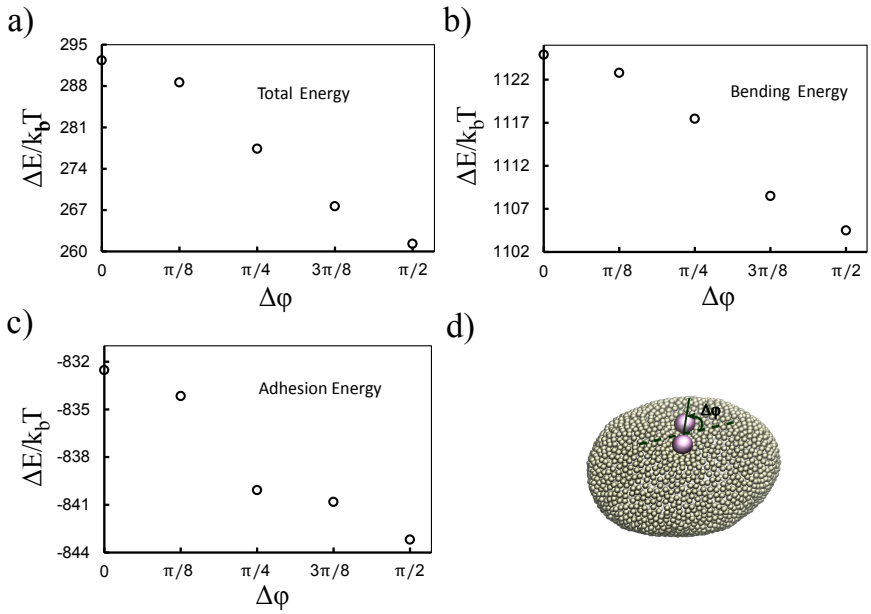

Figure 6.3: Bending is the dominant term in the attraction of colloids. As shown in (b) and (c), both the adhesion energy and the curvature energy are decreasing when the pair of colloids gets aligned with semi-minor axis of the ellipsoid. The latter has a larger contribution in the total energy.

being the radius of the vesicle, and the case we do not include such a potential.
Having defined all the contributions to the total energy of the membrane ($\Delta E_{\text{Total}} = \Delta E_{\text{Curv}} + \Delta E_{\text{A}} + \Delta E_{\text{V}} + \Delta E_{\text{Ad}} + \Delta E_{\text{Ell}}$), we perform Monte Carlo simulations to reach the equilibrium shape of an ellipsoid containing an arbitrary number of colloids. To do so, we implement the Metropolis algorithm, in which we have three types of moves: we can modify the position of a random bead of the membrane, impose a rearrangement in the connections of beads, or move the colloids around. The first two moves are energetically evaluated based on the total energy, while any changes in the position of colloids are only based on the adhesion energy. Our computer model is coarse-grained and cannot capture the fine corrugations of biological membranes that take place at small length-scales. The relative size of such corrugations is very small in comparison to that of colloids in this study [34]. Therefore their effects will be much smaller than the elastic interactions caused by colloids [35].
During the simulations, we keep the number of particles constant and set all the relevant parameters as: $\kappa = 36 k_{\text{B}}T$, $\varepsilon = 8.5 k_{\text{B}}T$, $K_{\text{A}} = 2 \times 10^3 k_{\text{B}}T/\sigma^2$, $K_{\text{V}} = 250 k_{\text{B}}T/\sigma^3$ and $K_{\text{Ell}} = 0.1 k_{\text{B}}T/\sigma^2$, where $k_{\text{B}}T$ is the thermal energy and σ is the diameter of the beads constructing the membrane. The values of κ and ε are chosen such that the colloids are partially wrapped and form linear patterns [24]. For very low values of ϵ colloids would not bind to the membrane and for very high values they aggregate into tubes. The diameter of the colloids is set to $\sigma_{\text{Coll}} = 5\sigma$.

6.3. Results and discussion

First, we analyze the interaction between two colloids adhered to the surface of two vesicles of different diameters. We keep the size of colloids and beads the same in both cases. We use umbrella sampling [36] to calculate the excess energy of the membrane as a function of the distance between the colloids. In effect, we apply a harmonic potential $u = \frac{1}{2}k(D-D_0)^2$, as our biased potential, between the two colloids directed along the coordinate of interest in order to restrain the system to sample around each distance D_0. Having performed the sampling process, we use the weighted histogram analysis method (WHAM) for obtaining the optimal estimate of the unbiased probability distribution, from which we can calculate the free energy of the system. The free energy is calculated with respect to the initial position of the colloids $\Delta E = E$(at the coordinate of interest) − E(initial coordinate). As expected from earlier experimental and computational work [37], colloids in both vesicles attract each other. In contrast to the case studied in Ref. [37], here the attraction is not solely because of the bending energy and closed nature of vesicles, but also due to maximizing the adhesion energy of the system. As illustrated in Fig. 6.1, the depth of the excess energy of the membrane with a smaller radius is significantly larger. In contrast, for the larger vesicle after a short distance colloids do not feel each other and the energy becomes flat. As the only difference between two test cases is the curvature, we conclude that this effect is due to vesicles being of different radii.

Next, we examine the interaction between two colloids on the surface of a quasi-ellipsoidal membrane. Following the recipe given in Section 2, we form an ellipsoidal membrane from spherical vesicles of size $D_v = 28\sigma$. We position the colloids symmetrically along the major axis of the ellipsoid (see Fig. 7.2d(*i*)). We repeat the sampling procedure for different aspect ratios, $e = a/b$, of the ellipsoid. Since the volume is conserved during the shape evolution, one can easily calculate the semi-minor axis, b, as: $b = \sqrt{3V/4\pi a}$. As depicted in Fig. 7.2a, along the major axis colloids attract each other in order to minimize both the adhesion and curvature energies. Decreasing the asphericity of the ellipsoid ($e \to 1.0^+$) in this direction enhances the amount of *available* excess area, hence the strength of the attraction energy increases. Suppose that we have two ellipsoids with major axes $a_1 > a_2$ with the same excess area (dA). The ellipsoid with the larger major axis (a_1) is more elongated and has smaller cross section, hence the amount of initially given excess area (dA) available at the mid-plane between the colloids is less than for the case we have the smaller axis a_2. Therefore, the more elongated the vesicle is (meaning that the more asphericity we have), the less available initially-given excess area we have at the mid-plane.

Similarly, particles that are situated along the semi-minor axis (as depicted in Fig. 7.2d(*ii*)) attract each other. There is, however, an important difference between the two directions. In contrast to the previous case, decreasing the asphericity of the ellipsoid makes the attraction force between colloids weaker. Since the number of membrane beads adhered to each colloid remains the same, this behavior cannot be explained by the adhesion energy of the membrane. To illuminate the reason that colloids select the direction along the minor axis to attract each other, we investigate the energy of a pair of colloids along a different coordinate. As shown in Fig. 7.2d(*iii*), we rotate a pair of colloids, that are constrained at the fixed distance of 3σ to their center, along the angle spanning the space between the semi-major and -minor axes. As Fig. 7.2c depicts, the

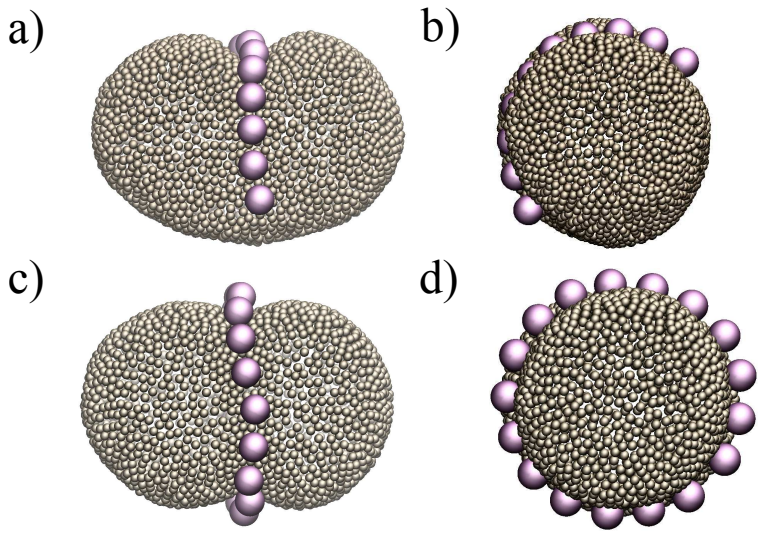

Figure 6.4: Colloids attract each other on ellipsoids, and in order to minimize the curvature energy, they form an arc (a & b) and a ring (c & d) at the mid-plane of the ellipsoid.

most energetically favorable configuration is when the colloids are aligned with the direction perpendicular to the major axis. This itself introduces a mechanism by which, without involving any other factors, two colloids find the mid-plane perpendicular to the symmetry axes of the ellipsoid, as it minimizes the total energy of the membrane. In contrast, in the case of having a perfect spherical membrane, it is not possible to predict the localization of colloidal aggregates as it will be randomly chosen. Increasing the major axis of the membrane (making e larger), drives the colloid reorientation stronger. One should be careful about the values for the bending moduli and adhesion coefficients during the simulations, as it can cause an effect where colloids are arrested and prevented from diffusing on the surface of the membrane [24]. In addition, a very high value of K_{Ell}, in addition to influencing the adhesion energy between the colloids and the membrane, would also pull two tubes out of the vesicle.

Although the above results quantitatively show different behavior in two directions, the dominant contribution in the total energy of the membrane causing this effect is not yet clarified. In order to approximately determine it, we proceed as follows: we pick a vesicle with $e = 1.351$ and constrain the position of the colloids with a strong potential at distance of 6σ from each other. Here, in contrast to earlier, we do not use the sampling method. Instead we let the system explore possible configurations of the membrane after reaching equilibrium, and then take the average of the energies for all those configurations. As depicted in Fig. 7.3, both the adhesion energy and the curvature of the membrane decrease when the angle between the line connecting two colloids and the semi-major axis of the ellipsoid (Fig. 7.3d) approaches $\pi/2$. The bending energy, as quantified in Fig. 7.3b, has a larger contribution to the total energy than the adhesion energy (Fig. 7.3c).

Putting all the results together, we expect that when we have more than two colloids they

will initially attract each other to form linear aggregates (to minimize the adhesion energy), and afterwards these aggregations change their orientation to align with the minor axes of the ellipsoid. This is indeed what we observe in our simulations. Fig. 7.4 depicts the equilibrium shape of the membrane for different numbers of colloids. In all the test cases colloids tend to form a ring-like structure in the mid-plane of the ellipsoid. With a sufficiently large number of colloids (Figs. 7.4c and 7.4d), they form a full ring in this plane (see also the supplemental movie SM1). It is important to mention that these patterns are quite stable during the whole simulation. In contrast, in spherical vesicles there is no preferred direction for the aggregation of particles. Although colloids attract each other on a spherical membrane (Fig. 6.1), there is no preference for the direction of the attraction. This means that even in case of forming a perfect ring on a vesicle, particles self-assemble in an arbitrary direction on the membrane. It has also recently been predicted that particles adhered to a prolate vesicle can feel the curvature gradient and localize at the equatorial line of a vesicle[30].

As the final experiment, we look at the movement of particles on a vesicle containing

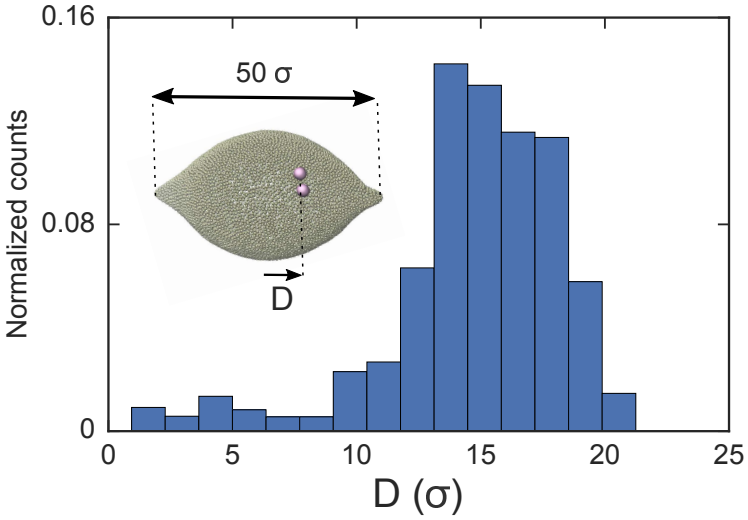

Figure 6.5: Histogram of the geometric center of a colloid dimer on a vesicle (of size $D_v = 40\sigma$) with negatively curved regions (inset). The dimer spends most of the time in the negatively curved part of the vesicle.

regions with negative mean curvature. To create these vesicles, we first overstretch the springs and form two small negatively curved regions in a big vesicle ($D_v = 40\sigma$). Overstretching the spring increases the tension in the membrane, making the role of tension more significant compared to the previous test cases. Having inserted a dimer in the system, we then look at the migration of the dimer. As shown in Fig. 7.5 in this case the dimer does not stay at the mid-plane of the vesicle. It instead spends much of its time during MC simulation at the areas that are closer to the negatively curved regions. Since the springs are overstretched, in the regions close to poles there is no excess area for the dimer to adhere to and therefore the dimer cannot explore that area (see also supplemental movies SM2-4). This prediction is consistent with Ref. [28] where the mi-

gration of a dimer in the tension dominant regime has experimentally been investigated.

The type of pattern formation we observe in our simulations is reminiscent of recruiting proteins by the membrane during different biological processes. It has been shown that, for example, dynamin proteins form a ring like structure during exocytosis to facilitate membrane scission [38] and that FtsZ proteins self-assemble into rings during the last step of bacterial cell division, namely cytokinesis [39]. Because most of the proteins in biological cells are either anchored to or embedded in the membrane, their interaction is a response to the deformation of the membrane they themselves impose. As in our simulation the varying curvature is a determining factor that drives the pattern formation, we can relate our results to those membrane trafficking machinery functions. Although in this study we adjusted the included harmonic potential strength K_{Ell} such that it would not affect the interaction of the colloids with the membrane, it has been proven that during the cell division we have the same situation. Cytoplasmic dynein, as a multi-subunit molecular motor, generates the force that is exploited by the cell to direct the orientation of the division axis by mitotic spindles [40]. Our results show that curvature inhomogeneity and anisotropy can at least facilitate the process of protein self-assembly in the mid-plane of the cell.
Although we have only investigated the interaction between identical isotropic inclusions, our results can explain the behavior of a system containing anisotropically shaped inclusions as well. Based on the local deformation of an ellipsoid, we expect that anisotropic inclusions adhered to a spherical membrane attract each other in the direction of negative curvature (with respect to the curvature of the membrane). This situation corresponds to having an isotropic inclusion embedded in a membrane with an anisotropic shape, which is the case we have studied here.

6.4. Conclusion

We studied the role of curvature heterogeneity and anisotropy on the interaction between colloids adhered to a membrane. First, we showed that the strength of the interaction between two colloids on the surface of a spherical vesicle is altered by changing the size of the vesicle. Next, we focused on such interactions on a membrane with an ellipsoidal shape. We revealed that the interaction on such an inhomogeneously shaped membrane depends on direction. For example, decreasing the asphericity of an ellipsoidal membrane makes the attraction between the colloids stronger along the semi-major axis and weaker in the semi-minor direction. Similarly, it has been previously shown in simulations that, on an elastic cylindrical membrane, colloids assemble perpendicularly to its major axis in the regime dominated by the bending energy [26, 33]. In case of fluid membranes, through an analytical framework, it has also been shown that inclusions *"embedded"* in a tubular membrane can attract each other in a transversal direction[21]. Simulating a vesicle containing many colloids, we showed how they form a ringlike structure around the mid-plane of the ellipsoid. While the cluster of colloids freely explores all the surface of a spherical membrane, less curved area energetically is more favorable for colloids on an ellipsoid. Our results suggest that forming regions of different curvatures on membrane vesicles can control pattern formation of inclusions, and this can be important from both nanotechnological application and bi-

ological points of view.

References

[1] H. T. McMahon and E. Boucrot, *Membrane curvature at a glance,* J Cell Sci **128**, 1065 (2015).

[2] M. Schmick and P. I. Bastiaens, *The interdependence of membrane shape and cellular signal processing,* Cell **156**, 1132 (2014).

[3] Y. Shibata, J. Hu, M. M. Kozlov, and T. A. Rapoport, *Mechanisms shaping the membranes of cellular organelles,* Annual Review of Cell and Developmental **25**, 329 (2009).

[4] H. T. McMahon and J. L. Gallop, *Membrane curvature and mechanisms of dynamic cell membrane remodelling,* Nature **438**, 590 (2005).

[5] S. Wang, H. Tukachinsky, F. B. Romano, and T. A. Rapoport, *Cooperation of the er-shaping proteins atlastin, lunapark, and reticulons to generate a tubular membrane network,* eLife **5**, e18605 (2016).

[6] L. Johannes, C. Wunder, and P. Bassereau, *Bending "on the rocks"—a cocktail of biophysical modules to build endocytic pathways,* Cold Spring Harb. Perspect. Biol. **6**, a016741 (2014).

[7] G. Drin and B. Antonny, *Amphipathic helices and membrane curvature,* FEBS Lett. **584**, 1840 (2010).

[8] B. J. Reynwar, G. Illya, V. A. Harmandaris, M. M. Müller, K. Kremer, and M. Deserno, *Aggregation and vesiculation of membrane proteins by curvature-mediated interactions,* Nature **447**, 461 (2007).

[9] P. G. Dommersnes and J.-B. Fournier, *The many-body problem for anisotropic membrane inclusions and the self-assembly of "saddle" defects into an "egg carton",* Biophys. J. **83**, 2898 (2002).

[10] Y. Schweitzer and M. M. Kozlov, *Membrane-mediated interaction between strongly anisotropic protein scaffolds,* PLoS Comput. Biol. **11**, e1004054 (2015).

[11] K. S. Kim, J. C. Neu, and G. F. Oster, *Many-body forces between membrane inclusions: A new pattern-formation mechanism,* Europhys. Lett. **48**, 99 (1999).

[12] T. R. Weikl, M. M. Kozlov, and W. Helfrich, *Interaction of conical membrane inclusions: Effect of lateral tension,* Phys. Rev. E **57**, 6988 (1998).

[13] M. Goulian, R. Bruinsma, and P. Pincus, *Long-range forces in heterogeneous fluid membranes,* Europhys. Lett. **22**, 145 (1993).

[14] D. Thalmeier, J. Halatek, and E. Frey, *Geometry-induced protein pattern formation,* Proc. Natl. Acad. Sci. U.S.A. **113**, 548 (2016).

[15] A. R. English and G. K. Voeltz, *Endoplasmic reticulum structure and interconnections with other organelles,* Cold Spring Harb. Perspect. Biol. **5**, a013227 (2013).

[16] M. Pannuzzo, A. Raudino, D. Milardi, C. La Rosa, and M. Karttunen, *α-helical structures drive early stages of self-assembly of amyloidogenic amyloid polypeptide aggregate formation in membranes,* Sci. Rep. **3**, 2781 (2013).

[17] M. Ehrlich, W. Boll, A. van Oijen, R. Hariharan, K. Chandran, M. L. Nibert, and T. Kirchhausen, *Endocytosis by random initiation and stabilization of clathrin-coated pits,* Cell **118**, 591 (2004).

[18] I. Koltover, J. O. Radler, and C. R. Safinya, *Membrane mediated attraction and ordered aggregation of colloidal particles bound to giant phospholipid vesicles,* Phys. Rev. Lett. **82**, 1991 (1999).

[19] R. Sarfati and E. R. Dufresne, *Long-range attraction of particles adhered to lipid vesicles,* Phys. Rev. E **94**, 012604 (2016).

[20] B. J. Peter, H. M. Kent, I. G. Mills, Y. Vallis, P. J. G. Butler, P. R. Evans, and H. T. McMahon, *Bar domains as sensors of membrane curvature: the amphiphysin bar structure,* Science **303**, 495 (2004).

[21] A. Vahid and T. Idema, *Pointlike inclusion interactions in tubular membranes,* Phys. Rev. Lett. **117**, 138102 (2016).

[22] A. H. Bahrami, R. Lipowsky, and T. R. Weikl, *Tubulation and aggregation of spherical nanoparticles adsorbed on vesicles,* Phys. Rev. Lett. **109**, 188102 (2012).

[23] M. Simunovic, A. Srivastava, and G. A. Voth, *Linear aggregation of proteins on the membrane as a prelude to membrane remodeling,* Proc. Natl. Acad. Sci. U.S.A. **110**, 20396 (2013).

[24] A. Šarić and A. Cacciuto, *Fluid membranes can drive linear aggregation of adsorbed spherical nanoparticles,* Phys. Rev. Lett. **108**, 118101 (2012).

[25] A. Šarić and A. Cacciuto, *particle self-assembly on soft elastic shells,* Soft Matter **7**, 1874 (2011).

[26] J. C. Pàmies and A. Cacciuto, *Reshaping elastic nanotubes via self-assembly of surface-adhesive nanoparticles,* Phys. Rev. Lett. **106**, 045702 (2011).

[27] S. Aimon, A. Callan-Jones, A. Berthaud, M. Pinot, G. E. Toombes, and P. Bassereau, *Membrane shape modulates transmembrane protein distribution,* Dev. Cell **28**, 212 (2014).

[28] N. Li, N. Sharifi-Mood, F. Tu, D. Lee, R. Radhakrishnan, T. Baumgart, and K. J. Stebe, *Curvature-driven migration of colloids on tense lipid bilayers,* Langmuir (2016).

[29] J. Agudo-Canalejo and R. Lipowsky, *Adhesive nanoparticles as local probes of membrane curvature,* Nano letters **15**, 7168 (2015).

[30] J. Agudo-Canalejo and R. Lipowsky, *Uniform and janus-like nanoparticles in contact with vesicles: energy landscapes and curvature-induced forces,* Soft Matter **13**, 2155 (2017).

[31] W. Helfrich, *Elastic properties of lipid bilayers: theory and possible experiments,* Zeitschrift für Naturforschung C **28**, 693 (1973).

[32] D. Nelson, T. Piran, and S. Weinberg, *Statistical mechanics of membranes and surfaces* (World Scientific, 2004).

[33] A. Šarić, J. C. Pàmies, and A. Cacciuto, *Effective elasticity of a flexible filament bound to a deformable cylindrical surface,* Phys. Rev. Lett. **104**, 226101 (2010).

[34] S. Semrau, T. Idema, L. Holtzer, T. Schmidt, and C. Storm, *Accurate determination of elastic parameters for multicomponent membranes,* Physical review letters **100**, 088101 (2008).

[35] H.-K. Lin, R. Zandi, U. Mohideen, and L. P. Pryadko, *Fluctuation-induced forces between inclusions in a fluid membrane under tension,* Phys. Rev. Lett. **107**, 228104 (2011).

[36] G. M. Torrie and J. P. Valleau, *Nonphysical sampling distributions in monte carlo free-energy estimation: Umbrella sampling,* J. Comput. Phys. **23**, 187 (1977).

[37] C. van der Wel, A. Vahid, A. Šarić, T. Idema, D. Heinrich, and D. J. Kraft, *Lipid membrane-mediated attraction between curvature inducing objects,* Scientific Reports **6** (2016).

[38] T. J. Pucadyil and S. L. Schmid, *Real-time visualization of dynamin-catalyzed membrane fission and vesicle release,* Cell **135**, 1263 (2008).

[39] R. Shlomovitz and N. Gov, *Membrane-mediated interactions drive the condensation and coalescence of ftsz rings,* Phys. Biol. **6**, 046017 (2009).

[40] A. Lesman, J. Notbohm, D. A. Tirrell, and G. Ravichandran, *Contractile forces regulate cell division in three-dimensional environments,* J. Cell Biol. **205**, 155 (2014).

7

Interaction between microtubule-driven protrusions in a vesicle

The plasma membrane and cytoskeleton of living cells are closely coupled dynamical systems. Internal cytoskeletal elements such as actin filaments and microtubules continually exert forces on the membrane, resulting in the formation of membrane protrusions. In this paper we investigate the interplay between the shape of a cell distorted by pushing and pulling forces generated by microtubules and the resulting rearrangement of the microtubule network. From analytical calculations, we find that two microtubules that deform the vesicle can both attract or repel each other, depending on their angular separations, the size, and the direction of imposed perturbations. We likewise find the necessary conditions for attractive interactions between multiple microtubules. Our results suggest that the commonly reported parallel structures of microtubules in both biological and artificial systems can be a natural consequence of membrane mediated interactions.

This chapter is based on: A. Vahid and T. Idema, *Interactions between microtubule-driven membrane protrusions induce filament bundling* (submitted)

7.1. Introduction

Cells are enveloped by a plasma membrane which serves as a selective soft physical barrier as well as being home to many functional proteins. The stability and shape of cellular membranes are determined not only by inherent properties of the membrane, but also by interactions with the cell's cytoskeleton [1]. The highly dynamic cytoskeletal network is vital for numerous biological processes, including cell motility, cell migration, and cell signaling [2, 3]. A typical feature occurring in such processes is the formation of membrane protrusions. Protrusions commonly emerge in the form of microvilli, filopodia or lamellipodia [4, 5]. These leading-edge protrusions, the existence of which is vital for responding to external cues, can be driven, controlled and elongated by a complicated crosstalk between the membrane and underlying filaments.

The spatial arrangement of cytoskeletal filaments, force generation mechanisms, and cytoskeletal networks coupling to the shape of cells have been investigated extensively, both theoretically and experimentally [6–10]. For example, when growing encapsulated microtubules inside an artificial spherical membrane, it has been shown that the vesicle exhibits a diverse range of morphologies, from a simple elongated shape to dumbbell-like geometries [7]. The diversity in the shape of such vesicles results from both the elongation dynamics of the filaments inside them and the material properties of the membrane. Such spatial rearrangement of filaments does not occur spontaneously but stems from the conditions imposed on them from various elements, one of which is the cell shape.

In this chapter, we investigate the interplay between the shape of vesicles, that are deformed by internal force generating filaments like microtubules, and the rearrangement of those filaments. In a biological cell, microtubules undergo treadmilling and dynamic instabilities (catastrophes) which are controlled by associated proteins [11]. Only a few of the microtubules that grow inside a cell can reach the cell membrane [12]. The pushing and pulling forces generated by those few microtubules can be harnessed for creating protrusions of the membrane [13]. Membrane mediated interactions between microtubule-induced protrusions may influence the arrangement of other functional filaments in addition to microtubules themselves [14, 15]. Therefore, it is warranted to study how the presence of a biological membrane, which has both elastic and fluid properties, alters the interaction between microtubules. This interaction could both drive processes like the formation of filament bundles or inhibit microtubule aggregation.

We use a modified version of the theoretical framework that has been developed for investigating membrane mediated interactions between proteins embedded in or bounded to a fluid membrane [16, 17]. We first explain the model in detail. We then study the effects of all the possible elements on the interaction between microtubules. In particular, we demonstrate that changing the in-plane tension in the membrane qualitatively affects the equilibrium shape that a vesicle can adopt. We further reveal that the size and relative orientation of the imposed deformations determines the nature of their interactions. Our results thus elucidate the effective role of the membrane in determining the equilibrium arrangement of protrusions imposed by the cytoskeleton.

7.2. Model

We assume that microtubules (including their tip) are rigid and impose sharp deformations on the membrane. To analyze the effect of such perturbations on the shape of an undeformed spherical membrane, we use the conventional Canham-Helfrich bending free energy including fixed surface area (S) and volume (V) constraints, given by:

$$E_{\mathrm{CH}} = \int \mathrm{d}S \left[2\kappa H^2 + \sigma\right] + \Delta P \int \mathrm{d}V \tag{7.1}$$

with H, σ and ΔP the sum of the two principal curvatures, surface tension and pressure difference, respectively. Due to the conservation of topology we can ignore the Gaussian curvature contribution in the energy functional. Using the spherical analog of the Monge parametrization, we describe the shape of a deformed vesicle as:

$$r(\theta,\phi) = R\left(1 + u(\theta,\phi)\right) \tag{7.2}$$

where R is the radius of an undisturbed vesicle and $u(\theta,\phi)$ is the deformation field. As the only constraints present are those imposed by the microtubules, we fix the amount of induced deformation at their tip (Fig. 7.1), $\bar{\mathbf{u}}_0 = (u(\theta_1,\phi_1),\ldots,u(\theta_N,\phi_N))$ with N the number of microtubules. Mathematically, we apply this condition via Lagrange multipliers,

$$E_{\mathrm{MTs}} = \int \mathrm{d}S \left[\mathbf{L}\cdot\left(\bar{\boldsymbol{\delta}}(\Omega-\Omega_0)\,u(\theta,\phi)\right)\right], \text{where } \bar{\boldsymbol{\delta}}(\Omega-\Omega_0) = \begin{bmatrix} \delta(\Omega-\Omega_1) \\ . \\ . \\ . \\ \delta(\Omega-\Omega_N) \end{bmatrix} \tag{7.3}$$

where $\mathbf{L}$ is a vector of Lagrange multipliers and $\delta(\Omega-\Omega_i) = \delta\left(\cos(\theta-\theta_i)\right)\delta(\phi-\phi_i)$ is the Dirac delta function for spherical coordinates. In terms of the deformation field and the applied constrains, the total energy of the membrane is given by:

$$\begin{aligned} \frac{E_{\mathrm{Total}}}{\kappa} = \int \mathrm{d}\Omega \Bigg[& 2\left(1 - \nabla^2 u + \frac{1}{4}(\nabla^2 u)^2 + u\nabla^2 u + \frac{1}{2}|\nabla u|^2\right) \\ & + \bar{\sigma}\left((1+u)^2 + \frac{1}{2}|\nabla u|^2\right) - \frac{\overline{\Delta P}}{3}(1+u)^3 - \mathbf{L}\cdot(\bar{\boldsymbol{\delta}}u)\Bigg], \end{aligned} \tag{7.4}$$

where the nondimensionalized surface tension and pressure difference are defined as $\bar{\sigma} = \frac{R^2\sigma}{\kappa}$ and $\overline{\Delta P} = \frac{R^3\Delta P}{\kappa}$, respectively. In the small deformation regime, we can approximate the relative behavior of the pressure difference and surface tension as that of the Laplace pressure for a sphere: $\overline{\Delta P} = 2\bar{\sigma}$. We then obtain the linearized form of the shape equation by minimizing Eq. 7.4, which gives:

$$\nabla^2\nabla^2 u + (2-\bar{\sigma})\nabla^2 - 2\bar{\sigma}u = \mathbf{L}.\bar{\boldsymbol{\delta}} \tag{7.5}$$

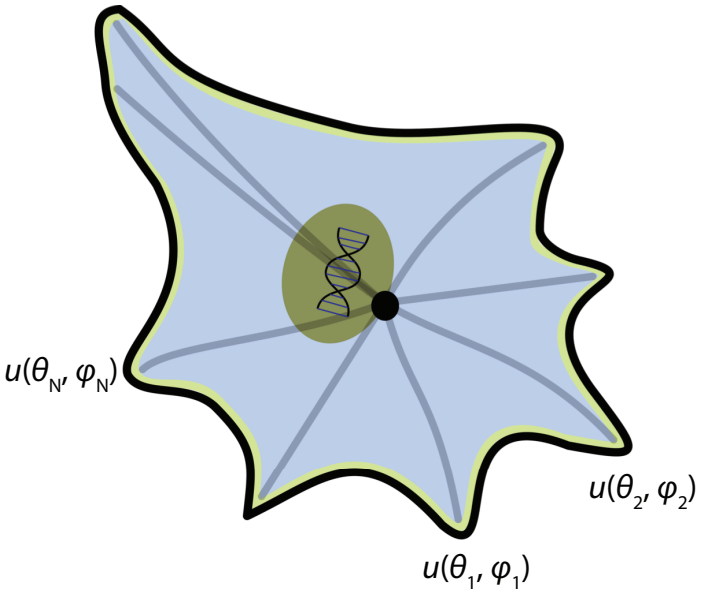

Figure 7.1: Schematic shape of a cell containing some microtubules. We model the microtubules by the imposed deformation ($\tilde{\mathbf{u}}_0 = (u(\theta_1,\phi_1),\ldots,u(\theta_N,\phi_N))$) at their tips.

Because the resultant equation is linear, the final solution for the deformation field of the membrane can be constructed as:

$$u(\theta,\phi) = \mathbf{L}\cdot\tilde{\mathbf{g}}(\Omega-\Omega_0), \text{where } \tilde{\mathbf{g}}(\Omega-\Omega_0) = \begin{bmatrix} G(\Omega-\Omega_1) \\ . \\ . \\ . \\ G(\Omega-\Omega_N) \end{bmatrix}. \tag{7.6}$$

In these equations $G(\Omega-\Omega_i)$ is the Green's function of the left hand side of Eq. 7.5. We expand the Dirac delta function in terms of spherical harmonics[1], and solve for the Green's function, which gives:

$$G(\theta-\theta',\phi-\phi') = \sum_{l=2}^{\infty}\sum_{m=-l}^{l} \frac{Y_l^m(\theta,\phi)\,Y_l^{m*}(\theta',\phi')}{l^2(l+1)^2-(2-\bar{\sigma})\,l(l+1)-2\bar{\sigma}}. \tag{7.7}$$

In Eq. 7.7 we have excluded the first two modes. The zeroth mode corresponds to motion of the center of mass. Excluding the first mode is necessary to prevent inflation of the vesicle, as we have already penalized any changes in the volume in Eq. 7.4. Excluding these modes implies correcting the Dirac delta in Eq. 7.5, which is reasonable for small deformations. Finally, taking into account the constraints associated with the

[1] $\delta(\phi-\phi')\delta\left(\cos\left(\theta-\theta'\right)\right) = \sum_{l=0}^{\infty}\sum_{m=-l}^{l} Y_l^m(\theta,\phi)\,Y_l^{m*}(\theta',\phi')$, where the symbol '*' denotes complex conjugate.

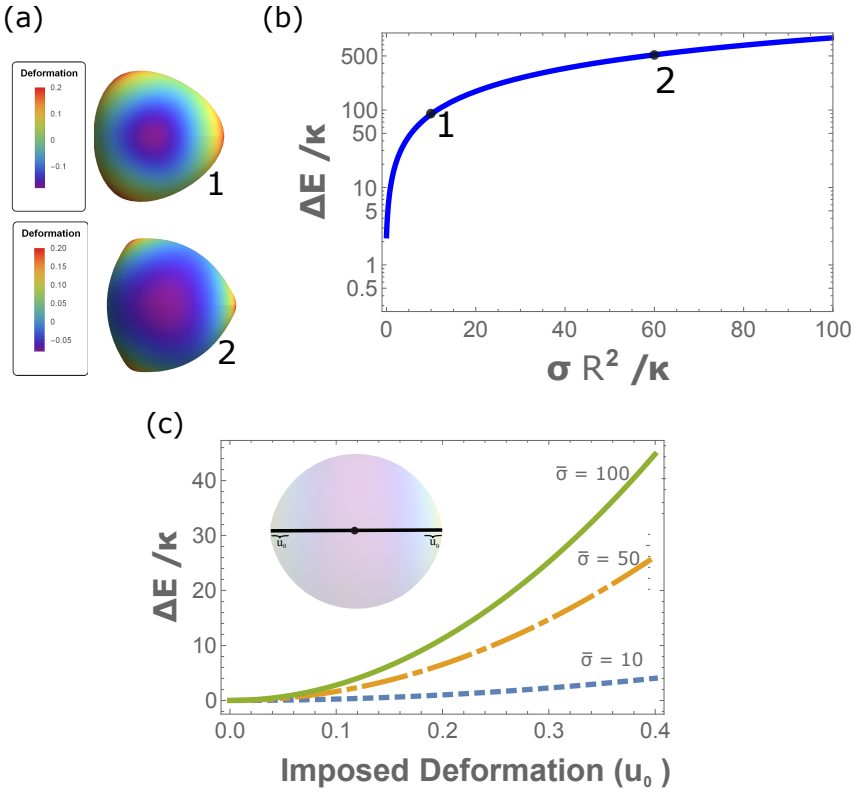

Figure 7.2: Membrane deformation due to the presence of microtubules. (a) Snapshots of a deformed vesicle for low (1) and high (2) values of the surface tension. The imposed deformation vector reads $\bar{\mathbf{u}}_0 = (0.1, 0.1, 0.1)$. (b) Increasing the in-plane tension makes the membrane deformation more spiky, in contrast to low surface tension regimes where we have rounded deformations. Numbers correspond to the images in (a). (c) The deformation energy of a spherical membrane containing two growing microtubules for different values of the surface tension.

microtubules (the vector $\bar{\mathbf{u}}_0$), we obtain the Lagrange multipliers and the induced deformation field as:

$$\mathbf{L} = \bar{\mathbf{u}}_0^T \cdot \mathbf{M}^{-1}, \text{ and } u(\theta,\phi) = \bar{\mathbf{u}}_0^T \cdot \mathbf{M}^{-1} \cdot \tilde{\mathbf{g}}(\Omega - \Omega_0), \tag{7.8}$$

where $\mathbf{M}$ is an $N \times N$ matrix whose components are constructed as $m_{ij} = G(\theta_i - \theta_j, \phi_i - \phi_j)$, with $i = 1,\ldots,N$ and $j = 1,\ldots,N$. For the diagonal components of the matrix $\mathbf{M}$ (when $i = j$, corresponding to self-interactions), because we have a constant number of lipids and the vesicle is closed, we consider a maximum mode $l = L_{\max}$ in Eq. 7.7. Substituting the derived deformation field $u(\theta,\phi)$ in Eq. 7.4, one can get the total energy of the membrane as:

$$\frac{E_{\text{Total}}}{\kappa} = \frac{1}{2}\bar{\mathbf{u}}_0^T \cdot \mathbf{M}^{-1} \cdot \bar{\mathbf{u}}_0 + 8\pi\left(1 + \frac{\bar{\sigma}}{3}\right). \tag{7.9}$$

Given an arbitrary number of microtubules, all we need is the amount of deformation they impose to investigate their interactions. The only relevant length scale of our sys-

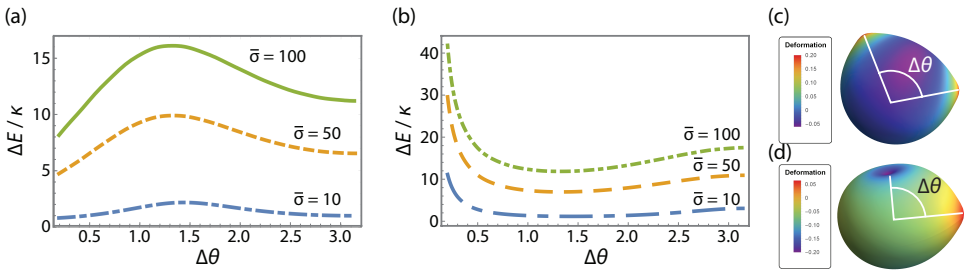

Figure 7.3: The interaction between microtubule-driven protrusions. (a) Microtubules that deform the membrane identically, attract each other and bundle for separations smaller than a critical angle $\Delta\theta_c \simeq 5\pi/12$. The elastic nature of the membrane hinders microtubule coalescence for larger separations. (b) Protrusions of opposite orientation repel each other for small distances and attract for large angular separations. Right panel: Snapshots of two protrusions that are imposed either identically (c) or oppositely (d).

tem relates surface tension to the bending modulus, given by $\lambda = \sqrt{\kappa/\sigma}$. In a biological context, the pertinent values of λ are in the range of $60-100$ nm [18, 19]. Given this length scale, one can obtain the nondimesionalized physiologically relevant values of surface tension as: $\bar{\sigma} = (R/\lambda)^2$. For a value of $\lambda = 100$ nm, for example, we get $\bar{\sigma} = 100$ for a vesicle size of $R = 1$ μm.

To examine the effect of surface tension on the equilibrium shape of the membrane, we position three microtubules inside a vesicle such that they form an equilateral triangle, and all impose the same amount of deformation on the membrane ($u_0 = 0.1$). For small values of $\bar{\sigma}$, we are in a bending dominated regime. The membrane, therefore, minimizes the total mean curvature, as illustrated in Fig. 7.2a. Increasing $\bar{\sigma}$ alters the local shape of membrane at the tip of microtubules from being smoothly curved into sharp spikes with higher total energy (Fig. 7.2b). Next, we analyze the total energy of a vesicle encapsulating two growing microtubules that push the membrane in opposite directions (Fig. 7.2c). We assume that the two microtubules distort the membrane similarly. As expected, the more a vesicle elongates, the larger the stored energy becomes. Also, membrane vesicles with a high in-plane tension require more energy to initiate a protrusion process. Microtubules are dynamic entities and constantly switch between growing and shrinking phases that are characterized by rescue and catastrophe events [**?**]. Not only are they able to generate a pushing force during growing into obstacles like membrane, microtubules can also release a force in the course of shrinking, which can be harnessed for pulling purposes (in case of deformable obstacles). The pushing forces are in the range of $2-3$ pN [20], leading to an energy of $40-60\,\kappa$ for a deformation[2] of $u_0 = 0.1$. Therefore, having membrane protrusions that cost a total energy (E_{Total}) of not more than $60-100\,\kappa$ would still allow tubulin dimers to aggregate at the end of the microtubules. The depolymerization-dependent forces are about one order of magnitude stronger ($\sim 30-65$ pN [21]) than those generated during the growth state. Therefore, the force numbers in the biological context are high enough to impose distortions of a similar size as we suppose in our calculations – although depending on the length of the microtubules, some processes like buckling may decrease the maximum force they exert

[2] We assume a bending modulus of $\kappa = 25 k_B T$ for the membrane and a vesicle size of 1 μm.

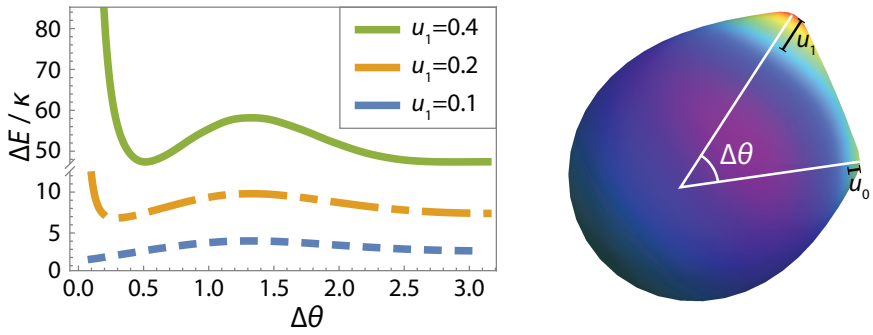

Figure 7.4: Interaction between microtubule-driven protrusions of different strength. As shown in the graph, introducing a difference in the magnitude of the protrusions results in a very strong short range repulsion between them ($u_0 = 0.1$; $\bar{\sigma} = 10$).

on the membrane.

The arrangement of filaments plays a key role in the emergent shape of protrusions and consequently in sensing the extracellular environment. To unravel the nature of elastic interaction between protrusions, we investigate a vesicle containing two protrusions with a varying angular separation between them. For identical deformations, as illustrated in Fig. 7.3, we have both short-range attraction and long-range repulsion regimes, that are connected at a critical angle $\theta_c = 5\pi/12$. The plot suggests that cellular membranes facilitate the aggregation of microtubules for short separations and hinder their assembly for longer distances. Although the global minimum of the energy is when two protrusions are merged, there is an energy barrier, the value of which increases with the surface tension. Inversely, two oppositely oriented protrusions repel each other for short and attract for larger distances. When analyzing the interaction between protrusions of different sizes, we realize that altering the magnitude of deformation for one of the microtubules strikingly changes the nature of interactions in their small separations. For example, as illustrated in Fig. 7.4, making one of the constraints stronger/weaker than the other turns short range attraction into repulsion. This suggests that having such distortions on a vesicle is costly, and that cells will therefore try to minimize the amount of deformed material between them by adjusting their protrusions. Putting the results of the two previous experiments together, we find that when interacting with membranes, microtubules rearrange themselves in such a way to form parallel filaments. Such rearrangements are ubiquitous in cells, for instance in the early stages of filopodia. Our results therefore suggest that these phenomena can be a natural result of membrane mediated interactions between microtubules.

Our system easily extends to vesicles that contain more than two microtubules, with similar results. To illustrate this point, we plot the whole configuration space for the case of three microtubules (Fig. 7.5) to look for the possible (semi) stable configurations. It turns out that the global minimum of the resultant energy landscape is when all the microtubules are attached to each other. There are, however, some local minima, all of which correspond to the situation where two microtubules are bundled together and the other points to the opposite pole of the vesicle.

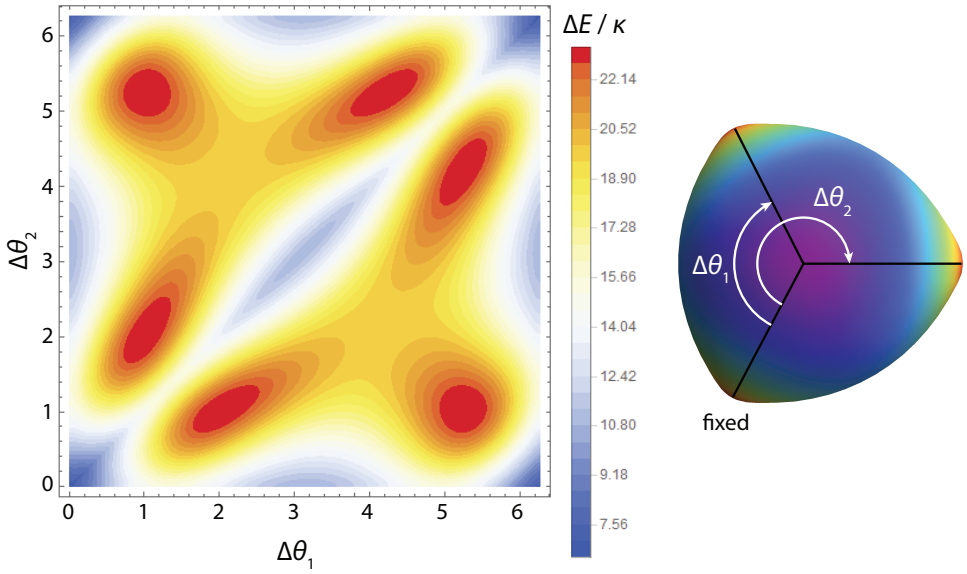

Figure 7.5: Plot of the configuration space of a vesicle with three enclosed microtubules, with the energy of each configuration shown in color. The closed shape of the vesicle favors the formation of parallel structures of microtubules. The global minimum of the energy corresponds to the situation where all the filaments are bundled, with local minima for the case of having two tubules together and one pointing in the opposite direction. Because filaments polymerize from the centrosome in opposite directions, the local minima may be biologically relevant.

7

7.3. Conclusion

Together with actin and intermediate filaments, microtubules form an architecture that governs the shape of a cell, and therefore that of the plasma membrane surrounding it. The membrane, in turn, mediates the interaction between attached microtubules. Using analytical tools, we studied the effect of membrane mediated interactions on the rearrangement of microtubules. Our results suggest that the elastic properties of cellular membranes facilitate the bundling of microtubules. In particular, we showed that two vesicle-encapsulated microtubules attract each other for small angular separations and repel for large angles. As we explicitly demonstrated for three microtubules, the outcome of collective interactions between multiple filaments is microtubule coalescence, which may be harnessed for protrusion formation [22]. Our results reveal that force generating microtubules, when colliding with a deformable obstacle like a fluid membrane, can coordinate their growing state through the shape of distorted membrane between them. Putting all the results together, our study suggests a possible mechanism underlying the preference of filaments for organizing in parallel configurations [23].

References

[1] D. A. Fletcher and R. D. Mullins, *Cell mechanics and the cytoskeleton,* Nature **463**, 485 (2010).

[2] C. Revenu, R. Athman, S. Robine, and D. Louvard, *The co-workers of actin filaments: from cell structures to signals,* Nature reviews. Molecular cell biology **5**, 635 (2004).

[3] H. Lodish, A. Berk, S. L. Zipursky, P. Matsudaira, D. Baltimore, and J. Darnell, *The actin cytoskeleton,* (2000).

[4] A. J. Ridley, *Rho gtpases and actin dynamics in membrane protrusions and vesicle trafficking,* Trends in cell biology **16**, 522 (2006).

[5] C. Le Clainche and M.-F. Carlier, *Regulation of actin assembly associated with protrusion and adhesion in cell migration,* Physiological reviews **88**, 489 (2008).

[6] D. K. Fygenson, J. F. Marko, and A. Libchaber, *Mechanics of microtubule-based membrane extension,* Physical review letters **79**, 4497 (1997).

[7] V. Emsellem, O. Cardoso, and P. Tabeling, *Vesicle deformation by microtubules: a phase diagram,* Physical Review E **58**, 4807 (1998).

[8] L. Mesarec, W. Góźdź, S. Kralj, M. Fošnarič, S. Penič, V. Kralj-Iglič, and A. Iglič, *On the role of external force of actin filaments in the formation of tubular protrusions of closed membrane shapes with anisotropic membrane components,* European Biophysics Journal , 1 (2017).

[9] M. S. e Silva, J. Alvarado, J. Nguyen, N. Georgoulia, B. M. Mulder, and G. H. Koenderink, *Self-organized patterns of actin filaments in cell-sized confinement,* Soft Matter **7**, 10631 (2011).

[10] E. Atilgan, D. Wirtz, and S. X. Sun, *Mechanics and dynamics of actin-driven thin membrane protrusions,* Biophysical journal **90**, 65 (2006).

[11] J. W. Kerssemakers, E. L. Munteanu, L. Laan, T. L. Noetzel, M. E. Janson, and M. Dogterom, *Assembly dynamics of microtubules at molecular resolution,* Nature **442**, 709 (2006).

[12] J. Howard and A. A. Hyman, *Dynamics and mechanics of the microtubule plus end,* Nature **422**, 753 (2003).

[13] M. Liu, V. C. Nadar, F. Kozielski, M. Kozlowska, W. Yu, and P. W. Baas, *Kinesin-12, a mitotic microtubule-associated motor protein, impacts axonal growth, navigation, and branching,* Journal of Neuroscience **30**, 14896 (2010).

[14] T. M. Svitkina, E. A. Bulanova, O. Y. Chaga, D. M. Vignjevic, S.-i. Kojima, J. M. Vasiliev, and G. G. Borisy, *Mechanism of filopodia initiation by reorganization of a dendritic network,* J Cell Biol **160**, 409 (2003).

[15] C. Conde and A. Cáceres, *Microtubule assembly, organization and dynamics in axons and dendrites,* Nature reviews. Neuroscience **10**, 319 (2009).

[16] P. G. Dommersnes and J.-B. Fournier, *The many-body problem for anisotropic membrane inclusions and the self-assembly of "saddle" defects into an "egg carton",* Biophys. J. **83**, 2898 (2002).

[17] A. Vahid and T. Idema, *Pointlike inclusion interactions in tubular membranes,* Physical review letters **117**, 138102 (2016).

[18] A. Evans, M. Turner, and P. Sens, *Interactions between proteins bound to biomembranes,* Physical Review E **67**, 041907 (2003).

[19] J. Dai and M. P. Sheetz, *Membrane tether formation from blebbing cells,* Biophysical journal **77**, 3363 (1999).

[20] M. Dogterom and B. Yurke, *Measurement of the force-velocity relation for growing microtubules,* Science **278**, 856 (1997).

[21] E. L. Grishchuk, M. I. Molodtsov, F. I. Ataullakhanov, and J. R. McIntosh, *Force production by disassembling microtubules,* Nature **438**, 384 (2005).

[22] J. Weichsel and P. L. Geissler, *The more the tubular: Dynamic bundling of actin filaments for membrane tube formation,* PLoS computational biology **12**, e1004982 (2016).

[23] A. P. Liu, D. L. Richmond, L. Maibaum, S. Pronk, P. L. Geissler, and D. A. Fletcher, *Membrane-induced bundling of actin filaments,* Nature physics **4**, 789 (2008).

8

Final remarks & Outlook

Lipid membranes are crucial to cell function. Their combination of fluid and elastic properties allows cells to cope with an out of equilibrium environment. Consequently, biological membranes possess various characteristic shapes and surface structures such as spheres and cylinders with extremely high curvatures. The shape of membranes is regulated by various factors, the most important of which are proteins and cytoskeletal filaments. In the beginning of this thesis, we have also seen that such a selective and soft barrier is necessary for regulating various biological functions ranging from cell division to vesicle trafficking.

Throughout this research, we have used mathematical tools and numerical simulations to investigate how the lipid bilayer mediates the interaction between either inclusions or microtubules attached to membranes of different geometries. One of the geometries that is commonly observed in intracellular organelles such as mitochondria is cylinder. Tubes can also be extracted from GUVs in artificial systems by optical tweezers [1]. **Part I** has thus been assigned to membrane mediated interactions between inclusions of different shapes embedded in or bounded to tubular membranes. We have first analyzed the interaction between point-like inclusions in **Chapter2**. In contrast to their planar counterpart where the interaction between two identical proteins is always repulsive [2], we have predicted that tubular membranes impose attraction between two identical inclusions. This type of interaction originates from both the curved and closed nature of tubes. With the help of simulated annealing Monte Carlo simulations, we have further revealed that inclusions spontaneously self-assemble into line- and ring-like structures, in consistent with previous numerical findings in elastic tubes [3]. We have modeled proteins as point-like perturbations which means taking a far-field approach. It's worthwhile to study the interaction between finite-sized objects embedded in a tubular membrane by solving its shape equation and applying appropriate conditions at the boundaries of inclusions.

In biological context proteins adopt different molecular conformations, hence they can either dictate their shape on the surface of the membrane or discern the curvature of different regions. To simulate such a scenario, we have again turned to computer simulations. We have particularly examined the emergent assembly of spherical and crescent-like proteins adhered to the membrane. As expected from our previous analytical calculations, spherical proteins form ring-like structures. In contrast, crescent-like proteins self-assemble into cluster of different shapes, depending on their curvature. Highly curved proteins aggregate in the longitudinal direction, forming line-like structures. For low protein curvature, we have observed no specific pattern formation as all the proteins repel each other. Strikingly, we have found an optimal curvature between two previous regimes, for which proteins attract each other in both longitudinal and transversal directions and subsequently constrict the tube. We have then used our results to explain some recently observed phenomena regarding to the fission and fusion events occurring in mitochondria. We have concluded that the curvature inducing and curvature sensing features are two parts of the same thing, depending on the density of proteins. In a high density, curvature sensing proteins (curvature sensors) accumulate in mechanically stressed regions, and then the resultant cluster act as a source of inducing deformation (curvature inducer). Indeed, as has been supported by providing recently obtained experimental evidences in **Chapter 3**, such properties of proteins are

harnessed by cellular organelles to avoid entangling with each other. For future directions, there are several questions that have remained untouched. For example, it would be interesting to investigate for what values of curvature, crescent-like proteins can stabilize an otherwise constricted region. It will also be worthwhile to explore the whole values of protein curvatures and, correspondingly, construct a phase diagram based on the emergent patterns.

As the final chapter of this part, we have focused on a completely different regime where some molecules, whose size is comparable to that of lipids, that are intercalated in the membrane can undergo fission and fusion (previously it was not allowed). To model such a system, we have taken a continuum theory approach. We have particularly predicted how introducing a density of molecules in a tubular lipid bilayer alters its stability conditions. For example, having a uniform density of molecules on the surface of a tube is not stable and will therefore segregate into different spatial domains (which is often referred as cell polarity). Understanding the interplay between membrane shape and its concomitant molecules may play an important role in the dynamic cellular phenomena. Due to time constraints, the simulation results have been remained far from complete. Therefore, as the next step, it would be interesting to see how the spatial organization of the molecules are dependent on the relevant parameters including the radius of tube, density of molecules and the amount of imposed curvature. Investigating the obtained stability conditions for a tube containing intercalated molecules experimentally can also advance our understanding of this phenomenon.

We have mostly elucidated the role of curvature in membrane mediated interactions between colloids adhered to spherical vesicles. Our results highlight two key points: First, depending on the wrapping angle, we can get different behaviors for the collective interaction of colloids. For example, we have shown that the formation tubulation, vesiculation and linear patterns can be achieved only by changing the wrapping angle of the colloids. Deriving a thorough phase diagram of the most energetically favorable patterns of the colloids as a function of their wrapping angle can better demystify their cooperative interaction mechanisms. Second, we have elucidated the role of background curvature on the collective interaction between colloids. Our results suggest that partially wrapped colloids have a preference for accumulation on the shallow-curved regions on the surface of membranes. An important question which has not been addressed yet is clarifying the exact effects of various geometrical parameters like the enclosed volume and surface area associated constraints on the interaction of colloids on a vesicle. In addition to these parameters, it would be also interesting to see how the presence of (crosslinked) cytoskeletal filaments will alter the interaction between membrane deforming objects. R. Okamoto *et al.* [4] have recently unraveled the effects of an elastic cytoskeletal network on the dynamics of a floating lipid bilayer membrane. It could be a reasonable follow-up to development the numerical approach we have taken throughout this work to include this effect in the system.

The cytoskeleton architecture plays a crucial role in the membrane remodeling processes. **Chapter 7** has investigated the link between the rearrangement of microtubule and their induced deformation to the shape of a cell. Such protrusions can also be driven by other types of filaments like actin and intermediate filaments. We have revealed the subtle effect of various parameters such as the surface tension of the membrane, size

of protrusions and the number of protrusions on the global shape of membrane. We have also unraveled that the commonly observed parallel configuration and bundling of microtubules (especially in artificial liposomes) can be a natural result of membrane mediated interactions. Here, we have only examined the interaction between weak protrusions, but we can also go beyond that and have drastic protrusions in flopodia-like structures. It will be worthwhile to study how such extreme protrusions interact with each other. Although the mathematics of such a problem will be very difficult, numerical approaches as the triangulated-network models can be of help in this regard. Such models have recently been used to simulate the bundling of growing microtubules attached to a planar membrane[5]. Employing a crosslinked actin network or coupling the treadmilling dynamics of microtubules to the membrane shape can be considered as other future directions, in order to enhance our understanding of the physical mechanisms underlying actin driven protrusions and, on the larger scales, cell migration.

References

[1] G. Koster, A. Cacciuto, I. Derényi, D. Frenkel, and M. Dogterom, *Force barriers for membrane tube formation,* Phys. Rev. Lett. **94**, 068101 (2005).

[2] T. R. Weikl, M. M. Kozlov, and W. Helfrich, *Interaction of conical membrane inclusions: Effect of lateral tension,* Phys. Rev. E **57**, 6988 (1998).

[3] J. C. Pàmies and A. Cacciuto, *Reshaping elastic nanotubes via self-assembly of surface-adhesive nanoparticles,* Phys. Rev. Lett. **106**, 045702 (2011).

[4] R. Okamoto, S. Komura, and J.-B. Fournier, *Dynamics of a bilayer membrane coupled to a two-dimensional cytoskeleton: Scale transfers of membrane deformations,* Physical Review E **96**, 012416 (2017).

[5] J. Weichsel and P. L. Geissler, *The more the tubular: Dynamic bundling of actin filaments for membrane tube formation,* PLoS computational biology **12**, e1004982 (2016).

Summary

Biological membranes are selective soft barriers that compartmentalize internal structure of a cell into organelles and separate them as a whole from the external environment. Due to their innate feature of being able to undergo constant reshaping, cellular membranes spatially attain diverse shapes ranging from simple spherical vesicles to more peculiar structures like the interconnected network of tubes found in the endoplasmic reticulum. Membranes are not only composed of lipids, but also host an enormous number of inclusions like proteins. Recent studies of biological membranes have revealed that such inclusions play a key role in diverse biological processes through either sensing or inducing perturbations to the membrane shape. In this dissertation, we studied the interplay between the shape of membrane and the spatial organization of attached curvature inducing objects using mathematical tools and numerical simulations in highly curved spherical and cylindrical geometries.

First, we investigated the interaction between inclusions of different shapes embedded in/adhered to tubular membranes. Our combined theoretical analysis and numerical simulation results evinced that tubular membranes, in contrast to their planar counterpart, transmit an attractive force between inclusions, stemming from their closed and curved geometry. We then elucidated that collective interaction between proteins results in the formation of line-like and ring-like clusters, depending on the their intrinsic shape **(Chapters 2–4)**. We further showed how curvature sensing crescent-like proteins in high densities can constrict tubular membranes and facilitate their splitting, demonstrating that both the curvature-sensing and curvature-inducing property of proteins are two sides of the same coin. Moreover, we used our simulation results to explain how mitochondorial machinery triggers, facilitates and drives membrane fission in its tubular network to avoid entanglements **(Chapter 3)**.

Next, we examined the interaction of spherical proteins adhered to closed vesicles. Our simulation results – supported by recent experimental evidence – revealed membrane curvature as a common physical origin for interactions between any membrane-deforming objects, from nanometre-sized proteins to micrometre-sized particles **(Chapter 5)**. Our further simulations unraveled how introducing curvature variation on the surface of a closed vesicle can be exploited by inanimate particles to regulate their pattern formation **(Chapter 6)**.

Finally, through theoretical calculations, we analyzed the interplay between the shape of a cell and the rearrangement of attached microtubules **(Chapter 7)**. Our results particularly suggested that the commonly reported parallel structure and bundling of microtubules can be induced by membrane mediated interactions.

Samenvatting

Biologische membranen zijn selectief, soepel en scheiden zowel interne onderdelen binnen de cel van elkaar, waardoor zich organellen vormen, als de cel zelf van zijn externe omgeving. Aangezien membranen soepel zijn kunnen deze constant van vorm veranderen. Cellulaire membranen nemen dan ook diverse vormen aan, van relatief simpele sferische blaasjes tot de meer complexe structuur van het endoplasmatisch reticulum bestaande uit een netwerk van buizen die met elkaar zijn verbonden. Behalve lipiden, omvat het membraan andere moleculen zoals proteïnen. Recente studies hebben laten zien deze "insluitsels" sleutelrollen vervullen in verscheidende Biologische processen door te regeren op, of door het mede bepalen van, de vorm van het membraan. In dit proefschrift hebben wij de wisselwerking tussen de vorm van sterk gekromde sferische en cilindrische membranen en de ruimtelijke organisatie van de daarin aanwezige objecten die op hun beurt het membraan kunnen deformeren bestudeerd met behulp van wiskundige technieken en numerieke simulaties. Als eerste hebben wij cilindrische membranen met daarin ingesloten moleculen bestudeerd. Onze theoretische analyse en numerieke simulaties tonen aan dat buisvormige membranen door hun gesloten en sterk gekromde geometrie, in tegenstelling tot vlakke membranen, een aantrekkende kracht tussen proteïnen induceren. Vervolgens hebben wij uitgelegd hoe een collectief van ingesloten proteïnen, aanvankelijk van hun intrinsieke vorm, samen ophopen in lijn-achtige of ring-achtige formaties **(Hoofdstuk 2-4)**. Verder hebben wij laten zien dat hoge concentraties van proteïnen die de form van een halvemaan hebben niet alleen de vorm van het membraan kunnen voelen, maar ook het membraan kunnen laten samentrekken tot het zich in tweeën opdeelt. Hiermee hebben wij laten zien dat het reageren op de vorm en het bepalen van de vorm van de membraan twee zijden van dezelfde medaille zijn. Met behulp van simulaties hebben wij uitgelegd hoe de machinerie van het mitochondriën het splijten van het membraan in gang zet en drijft te midden van een netwerk van buizen zonder dat deze in elkaar verstrengeld raken **(Hoofdstuk 3)**. Vervolgens hebben we de interactie tussen bolvormige proteïnen en gesloten membranen bestudeerd. Onze simulaties, en recent experimenteel onderzoek, laten zien dat de intrinsieke kromming van membranen een overeenkomende fysische oorzaak is van interacties tussen ingesloten objecten die het membraan kunnen deformeren. Dit geldt voor zowel proteïnen op de nanoschaal als grotere deeltjes op de microschaal **(Hoofdstuk 5)**. Verder lieten onze simulaties zien dat aspecifieke proteïnen patronen op een gesloten membraan vormen door gebruik te maken van variaties in de kromming van het membraanoppervlak **(Hoofdstuk 6)**. Tot slot, hebben wij de wisselwerking tussen de vorm van een cel en de reorganisatie van de daaraan vastzittende microtubili bestudeerd **(Hoofdstuk 7)**. Onze resultaten toonden aan dat microtubili –bundels, zoals veelvuldig gerapporteerd in de literatuur, zich mede kunnen vormen door interacties met het membraan aan te gaan.

Acknowledgements

While nearing the end of my PhD story, I cannot emphasis more that the work presented here could not have been possible if not for the constant support of many amazing people around me.
First and foremost, I am indebted to Timon for his invaluable support, great advices (as well as disagreements) and having so much faith in me throughout my time in his lab. I greatly appreciate him for allowing me to explore my ideas and hypotheses, and to build up diverse collaborations with other people. Looking back now, I realize that his inspiration, motivation and zeal for science are really contagious! I have learned a lot from working with him, both personally and professionally.
I have also been honored to collaborate with great people whose contribution to my work has been very valuable. Especially, I have to thank Andela (*UC London*) for kindly being a constant source of support, encouragement and ideas through our endless Skype meetings to challenge myself in my work. I must also thank Daniela and Casper (*Leiden University*) for the fruitful discussions we had, and for being excellent collaborators. Finally, I extend my thanks to Benoit, Sebastian and Qian (*ETH Zurich*) for their significant experimental inputs and being great collaborators.
I would also like to thank Marileen Dogterom for being my promoter and for her continuous support. My sincere gratitude to all of the members of my defence committee: Marie-Eve Aubin-Tam, Frank Redig, Kees Storm, Andela Saric and Bela Mulder for taking the time to review this thesis.
I have also been very fortunate to have day-to-day contact with awesome people in the theoretical biophysics group. A very special gratitude goes to Martin whose enjoyable discussions and advices were of great value. Many thanks to Ruben, Aafke, Behrouz, Misha, Marc, Esmee, Teun, Duco, Daniel and Steven for being remarkable friends and colleagues. It was also a very delightful experience to work with and learn from Rachel, Kees, Jasper and Roel during their projects with me – due to time constraints, unfortunately, I could not include their interesting and novel results here, they will be published very soon!
Living far away from home and family has its own challenges and difficulties, but when I just joined BN, it soon became apparent that it's going to make an unforgettable and enjoyable period of my life. All the foosbal games(!), Mondays' football matches, Christmas parties, defenses, winter retreats, Kavli days and daily interactions indeed made it such an unforgettable experience. Being a part of BN community has enriched me not only scientifically but also as a person. In the fear of forgetting somebody, I would like to thank the entire bionanoscience department that supported me with advice and friendship.
A big thank to my lovely friends Hamed, Yoones, Hamid, Mojde, Amirhossein and Saeid for their support and company during my stay in Delft.
Last but definitely not least, my debt of gratitude goes to my beloved parents and siblings

for all of their support, encouragement and of course their patience during my absence.

Afshin Vahid (Delft, February 2018)

Afshin Vahid

Master of Science in Mechanical Engineering

Department of Mechanical Engineering, Sharif
University of Technology, Iran

Thesis: Three dimensional simulation of morphology of nanodroplets near and on structured substrates

Supervisor: Prof. dr. A. Moosavi

Ph.D. Biophysics

Department of Bionanoscience, Delft University of
Technology, The Netherlands

Thesis: Assembly of membrane deforming objects in tubular and vesicular membranes: theory & simulation

Promoter: Prof. dr. M. Dogterom
Supervisor: Dr. T. Idema

List of Publications

8. **A. Vahid** and T. Idema, *Pattern formation of intercalated molecules in tubular membranes*, in preparation.

7. **A. Vahid**, A. Šarić and T. Idema, *Collective interactions between Janus-like objects on fluid vesicles*, in preparation

6. **A. Vahid** and T. Idema, *Interaction between microtubule-driven protrusions in a vesicle*, submitted.

5. S. C. J. Helle, Q. Feng, M. J. Aebersold, L. Hirt, R. R. Grüter, **A. Vahid**, A. Sirianni, S. Mostowy, J. G. Snedeker, et al., *Mechanical force induces mitochondrial fission*, eLife **6** (2017).

4. **A. Vahid**, A. Šarić and T. Idema, *Curvature variation controls particle aggregation on fluid vesicles*, Soft Matter **13**, 4924-4930 (2017).

3. C. Van der Wel, **A. Vahid**, A. Šarić, T. Idema, D Heinrich and D. J. Kraft, *Lipid membrane-mediated attraction between curvature inducing objects*, Scientific reports **6**, 32825 (2016).

2. **A. Vahid** and T. Idema, *Pointlike inclusion interactions in tubular membrane*, Phys. Rev. Lett. **117**,138102 (2016).

1. **A. Vahid** and A. Moosavi, *Morphology of nanodroplets on structured surfaces*, Journal of Physics D: Applied Physics **46**, 215302 (2013)

Casimir PhD series 2018-36
ISBN: 978-90-8593-365-6